Forschungszentrum Karlsruhe
Technik und Umwelt
Wissenschaftliche Berichte
FZKA 5914

Results on Hydrogen Behaviour and Mitigation in Severe PWR Accidents

Annual Report 1996 of the Forschungszentrum Karlsruhe Hydrogen Program

W. Breitung, P. Royl, A. Veser

Institut für Neutronenphysik und Reaktortechnik
Institut für Reaktorsicherheit
Projekt Nukleare Sicherheitsforschung

Juni 1997

Forschungszentrum Karlsruhe
Technik und Umwelt
Wissenschaftliche Berichte
FZKA 5914

Results on Hydrogen Behaviour and Mitigation in Severe PWR Accidents

Annual Report 1996 of the
Forschungszentrum Karlsruhe Hydrogen Program

W. Breitung, P. Royl, A. Veser

Institut für Neutronenphysik und Reaktortechnik
Institut für Reaktorsicherheit
Projekt Nukleare Sicherheitsforschung

Forschungszentrum Karlsruhe GmbH, Karlsruhe
1997

The following organizations and individuals contributed to the results of the FZK research program in 1996

- Forschungszentrum Karlsruhe
  W. Breitung, G. Engel, A. Kotchourko, H. Massier, G. Necker, A. Miassoedov, R. Redlinger, H. Rochholz, P. Royl, P. Schmuck, J. Spore, J.R. Travis, H. Wilkening, J. Wolff, A. Veser

- Kurchatov Institute Moscow:
  S.B. Dorofeev, V.P. Sidorov, A. Efimenko, A. Dvoinishnikov, A. Lelyakin, A. Denkevits, I.D. Matsukov, M.S. Kuznetsov, V.I. Alekseev, A.V. Bezmelnitsin and RUT operational crew

- Russian Academy of Sciences, Moscow:
  B.E. Gelfand, S.P. Medvedev, O.V. Popov, A.M. Bartenev, S.V. Khomik, G.L. Agafonov, A.Y. Kusharin, A.N. Polenov

- University of Aachen, ITM (Inst. für Techn. Mechanik):
  V. Moser, R. Klein

Als Manuskript gedruckt
Für diesen Bericht behalten wir uns alle Rechte vor

Forschungszentrum Karlsruhe GmbH
Postfach 3640, 76021 Karlsruhe

ISSN 0947-8620

ABSTRACT

This report describes the activities and the main results of the FZK hydrogen program in 1996. The goals of the program are to

- develop verified numerical tools for the description of the main hydrogen related processes during severe PWR accidents,
- investigate the full spectrum of hydrogen mitigation options including catalytic recombiners, spark igniters, CO_2 dilution, increased strength of local or global containment structures,
- derive defence-in-depth solutions for the H_2-problem in future and existing power plants, satisfying the specific regulatory, economic and licensing requirements.

The results in 1996 for the following research fields are described

- hydrogen production,
- hydrogen distribution,
- hydrogen combustion including code development, experiments and code verification,
- deflagration-to-detonation transition,
- missile generation,
- hydrogen mitigation,
- reactor applications, and
- next generation program studies.

These results will be used to reduce or eliminate the risk of early containment failure during severe accidents due to hydrogen combustion loads.

Ergebnisse zum Wasserstoffverhalten und zu Gegenmaßnahmen bei schweren DWR-Unfällen (Jahresbericht 1996)

ZUSAMMENFASSUNG

Dieser Bericht beschreibt die wesentlichen Ergebnisse des FZK-Wasserstoffprogramms das innerhalb des Projekts Nukleare Sicherheit (PSF) durchgeführt wird. Die Ziele des Arbeitsvorhabens sind:

- die Entwicklung von verifizierten numerischen Programmen zur Beschreibung des Wasserstoffverhaltens bei schweren LWR-Unfällen,
- die Untersuchung des gesamten Spektrums möglicher Gegenmaßnahmen, insbesondere von katalytischen Rekombinatoren, Funkenzündern, CO_2-Verdünnung und verstärkte Strukturen,
- die Erarbeitung von gestaffelten Sicherheitskonzepten zur Lösung des H_2-Problems in zukünftigen und bestehenden Reaktoranlagen.

Der Bericht faßt die 1996 erzielten Ergebnisse in folgenden Forschungsbereichen zusammen:

- Wasserstoffproduktion
- Wasserstoffverteilung
- Wasserstoffverbrennung mit den Unterpunkten Programmentwicklung, Experimente und Programmverifikation
- Deflagrations-Detonations-Übergänge
- Geschoßbildung
- Wasserstoffgegenmaßnahmen mit CO_2
- Reaktoranwendungsrechnungen
- Studien zu zukünftigen Simulationstechniken.

Die Ergebnisse werden dazu benutzt werden das Risiko für frühes Containmentversagen durch H_2-Verbrennungslasten bei schweren LWR-Unfällen stark zu reduzieren oder ganz auszuschließen

CONTENTS

SUMMARY OF RESULTS

Hydrogen production was analysed for two accident scenarios in the future European Pressurised Reactor (EPR):

- small break LOCA (50 cm^2) in the cold led, and a
- station black-out sequence.

The MELCOR data set was updated using the newest information from Siemens/ KWU. Comparison with respective MAAP predictions showed that the H_2 and steam production is sensitive to the modelling of the accumulator behaviour.

A new theoretical model was completed to describe the rapid H_2 generation during CORA reflood tests. The main new hypothesis is that a reflood event reduces the radiation heat losses from the CORA bundle due to the largely increased steam partial pressure. The radiation treatment in SCDAP/RELAP-5 and MELCOR seems not adequate for a sufficiently precise description of the steam isolation effect. For reactor applications additional models need to be implemented. A corresponding cooperation with Siemens/KWU was started.

For investigation of the **hydrogen distribution** the GASFLOW code was further developed. The code was transformed from Fortran 77 to Fortran 90. The FZK version 1.4.3 was merged with the LANL version 2.0 to a new unified version GASFLOW 2.1. Test calculations were started and will be continuing in 1997. FZK participated in a blind He - air distribution benchmark in the Battelle Model Containment (Hyjet test). The GASFLOW calculation resulted in very good blind predictions for the observed He - stratification, the He - concentration along and across the jet axis. The blind analysis is an important proof for the predictive capabilities of GASFLOW. A dynamic H_2 - injection test in the large scale Russian RUT facility was also simulated with GASFLOW. The calculation showed a reasonable prediction of the general trends, but locally considerable differences were observed, which are probably due to some uncertain initial and boundary conditions in this highly dynamic test.

The work on **hydrogen combustion** included code development, experiments, code verification and reactor applications. The following results were obtained in these areas.

The **code development** concerns fast tubulent deflagrations (COM3D-code) and the slower flamelet regime (ERCO-code) .

The COM3D program was vectorized and parallelized. It runs now routinely on a dedicated 8 - processor Cray computer (J916). The turbulence modelling was extended to a RNG k-ε model. The two component formulation for burned and unburned gas was replaced by a more flexible multi - component model for e.g. H_2, O_2, N_2 and H_2O.

The 2-d ERCO-code development was completed. The program describes the flame as a discontinuity, seperating burned and unburned gas. The code contains no free parameters once the turbulent burning law is chosen. This provides important predictive capabilities.

The following **combustion experiments** were performed on different scales to provide data for code verification:

- turbulent combustion in lean H_2 - air mixtures in the FZK-12 m-tube,
- inert experiments with He-air shock waves in complex geometry (FZK-tube),
- large scale tests on turbulent combustion and DDT in H_2-air-steam mixtures at elevatad temperatures (RUT facility, 100°C, 480 m^3),
- test on turbulent H_2-air combustion in reactor-relevant H_2-gradients,
- interaction between a turbulent H_2-air flame and a vortex,
- influence of fog from steam condensation on the turbulent combustion in H_2-air - steam mixtures,
- laminar and turbulent deflagration in H_2-air-CO_2 mixtures at accident typical pressures and temperatures.

All experiments have provided new data for the evaluation of theoretical models. The most important results are summarised in the report.

The main goal of the **program verification** in 1996 was to evaluate individual COM3D models in test calculations of increasing complexity. The following cases were investigated:

- supersonic flow against a forward facing step (test of hydro-and thermodynamic models),
- simulation of a He-air turbulence experiment in the FZK-tube (test of turbulence model),
- simulation of a flame-vortex interaction (test for turbulence and chemistry model in simple geometry and small scale),
- calculation of seven RUT combustion experiments with homogeneous H_2-air and H_2-air-steam mixtures (test for turbulence and chemistry in complex geometry and for large scale).

The two-dimensional ERCO-code was tested on six RUT H_2-air combustion experiments. There was general agreement with the COM3D results and the experiments, in terms of pressures and flame speeds.

A **DDT criterion** for the evaluation of the detonation potential in severe accidents was further verified against experimental data and extended to different types of room geometry. For the detonation cell size, which appears in the criterion, new analytical fit functions were derived from the available literature data. These functions for λ=f(% H_2, % steam, p_0,T_0) allow now the best possible evaluation of the DDT criterion during a containment evaluation. A theoretical model was used to calculate detonation cell sizes λ for hot, partially N_2-or steam-inerted mixtures. Such mixtures were predicted in GASFLOW simulations for the EPR.

The program developed for the calculation of **detonation loads** on complex 3-d geometry (DET3D) was further developed by improving the chemistry modell. It is now possible to simulate also H_2-air-steam mixtures.

Fast combustion modes in a severe accident can generate **missiles** by dragging objects with the flow or by fracturing walls and then accelerating the wall fragments. A 3-d code describing the drag problem was written in 1995. Calculations suggested that relatively long flight paths are needed to accelerate free bodies to containment threatening velocities. In 1996 the wall problem was investigated with a new 2-d model. Neglecting the fracture process itself, wall fragments can reach velocities in the 100 m/s range within few meters of flight path. The damage potential increases with the area of the fragment because the velocitiy is area independent. Hydrogen mitigation systems should exclude fast combustion modes with high reliability.

The possibilities for **hydrogen mitigation** analysis were extended by adding a model for Siemens recombiners to the GASFLOW code. The model was verified extensively on the Battelle Gx test serie. Good results were obtained for the hydrogen distribution in case of nearly homogenous tests (Gx4 and Gx6) and in case of strongly stratified conditions (Gx7). Togeter with the model for the NIS granulate recombiner, GASFLOW contains now verified models for all relevant recombiner types. The very successfull simulation of test Gx7 has demonstrated that GASFLOW can now be applied to analyze hydrogen and steam distributions under severe accident situations involving mitigation by recombiners and igniters (dual concept).

Reactor application studies in 1996 investigated EPR release scenarios via the IRWST, in which a relatively dry H_2-steam mixture is released into the containment. The GASFLOW simulation assumed a quite conservative H_2-release scenario with two main release phases of 600 kg H_2 each. Without hydrogen mitigation measures a high detonation potential was predicted throughout the containment, including the possibility of a late global detonation. Calculations with spark igniters at different locations showed that it is possible to ignite the hydrogen close to the source without significant pressure development. It seems possible to control even very severe dry H_2 release scenarios with spark igniters if, as in the EPR case, the release location is known.

The development of a **next generation program** for 3-d containment analysis was started in 1996 (INCA-code). The INCA code, will be used in the near future as a test bed for advenced numerical techniques, mainly adaptive mesh refinement on

structured grids, parallel and vectorised computing, as well as distributed processing on different platforms. An adaptive grid library of Lawrence Livermore National Laborating (LLNL) was successfully implemented at FZK and tested with a LLNL problem. The next step will be incoporation of the DET3D program.

The current **status** of numerical simulations for hydrogen behaviour and control in severe PWR accidents can be summerised with the list of calculations which are possible now:

- H_2 and steam source terms (MELCOR),
- 3-d transport and mixing on full containment scale (GASFLOW 1.4),
- pressure load estimates from premixed H_2-air-steam combustion in complex 3-d geometry (COM3D),
- loads from local detonations in 3-d enclosures
    - pressure, impulse (DET3D, D3D),
    - missile velocity (BO2),
- design and qualification of H_2 mitigation systems for full reactor containments (GASFLOW, COM3D, DET3D)
    - recombiners (NIS, Siemens),
    - spark igniters,
    - CO_2 dilution,
    - strong local structures,
    - strong containment shell.

To allow a mechanistic and fully integrated containment simulation the completion of the following main tasks need to be addressed in the future:

- prediction of H_2-generation in reflood situations (REFLOX-code),

- final testing and documentation of the consolidated GASFLOW version 2.1,
- development of verified turbulence and chemistry models for standing diffusion flames and fast freely propagating flames,
- derivation of criteria for flame acceleration limits and stability of diffusion flames,
- adaption of COM3D models into GASFLOW 2.1,
- development of adaptive grid and parallel processing capabilities.

1. INTRODUCTION

The FZK research program on hydrogen behaviour in severe PWR accidents addresses the three main phases of severe accident sequences in pressurised water reactors

- hydrogen production,
- hydrogen distribution, and
- hydrogen combustion (**Fig. 1.1**).

These phases are investigated on three levels

- module development and verification by experiments,
- current reactor applications, and
- development of a next generation program.

This report describes the main results obtained in these R+D areas during 1996.

2. HYDROGEN PRODUCTION

The hydrogen production in the EPR was investigated with the MELCOR code for two scenarios without reflood. The REFLOX code was developed to describe the rapid H_2-generation in CORA-experiments with reflood.

2.1 MELCOR calculations for EPR

The MELCOR input deck for description of the EPR primary and secondary system was up-dated using new EPR design data. Details are given in the section by P. Schmuck et al. This section summarises the results for hydrogen and steam sources which provide the initial conditions for distribution calculations.

2.1.1 SB-LOCA sequence

A 50 cm^2 leak in the cold leg was analysed with MELCOR 1.8.3. The schematic EPR representation is shown in **Fig. 2.1**. Three of the four EPR loops are lumped together into one combined loop. The core is subdivided into three radial rings and eleven

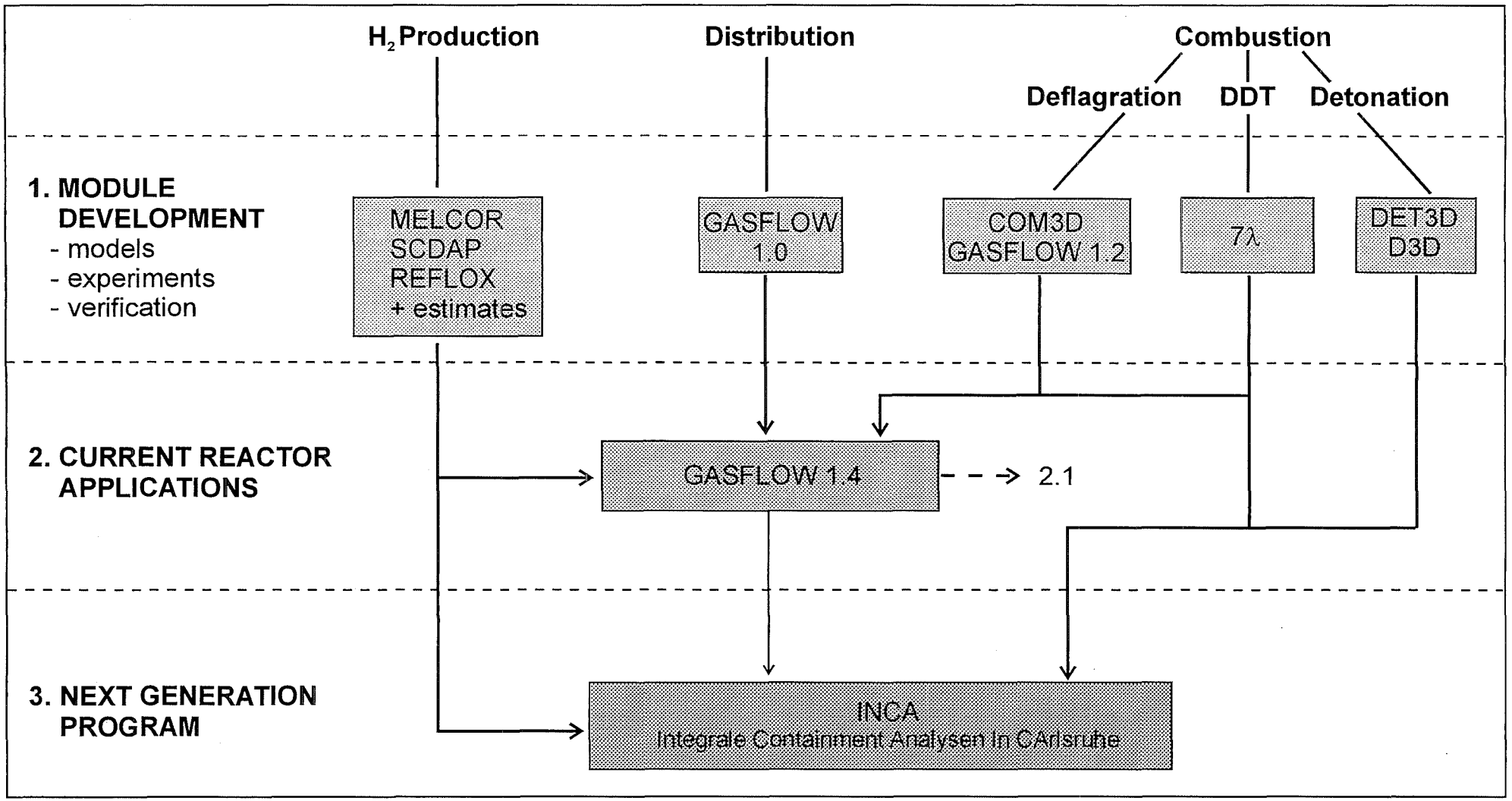

Fig. 1.1: Structure of FZK research program on hydrogen behaviour and control in severe accidents.

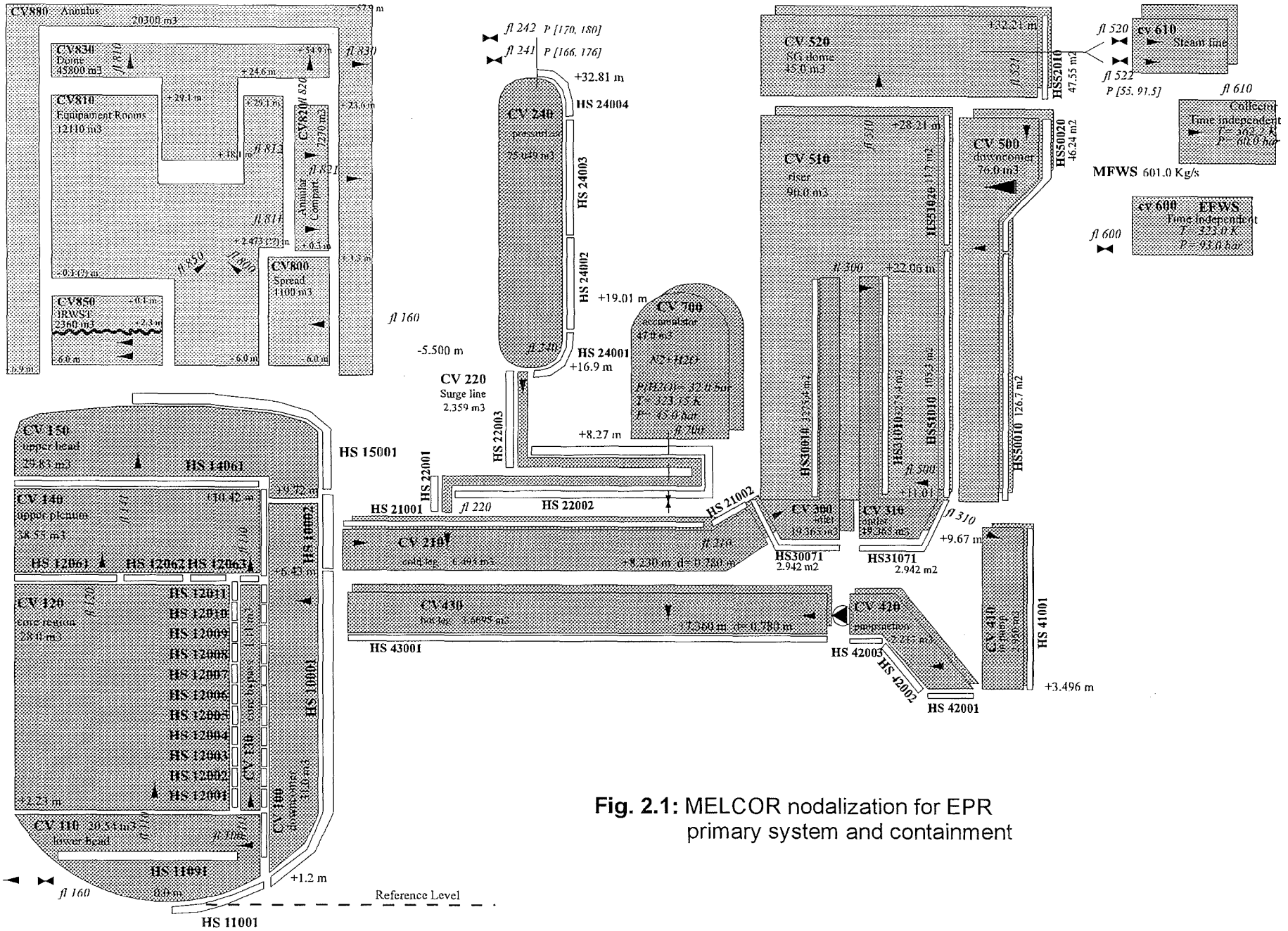

Fig. 2.1: MELCOR nodalization for EPR primary system and containment

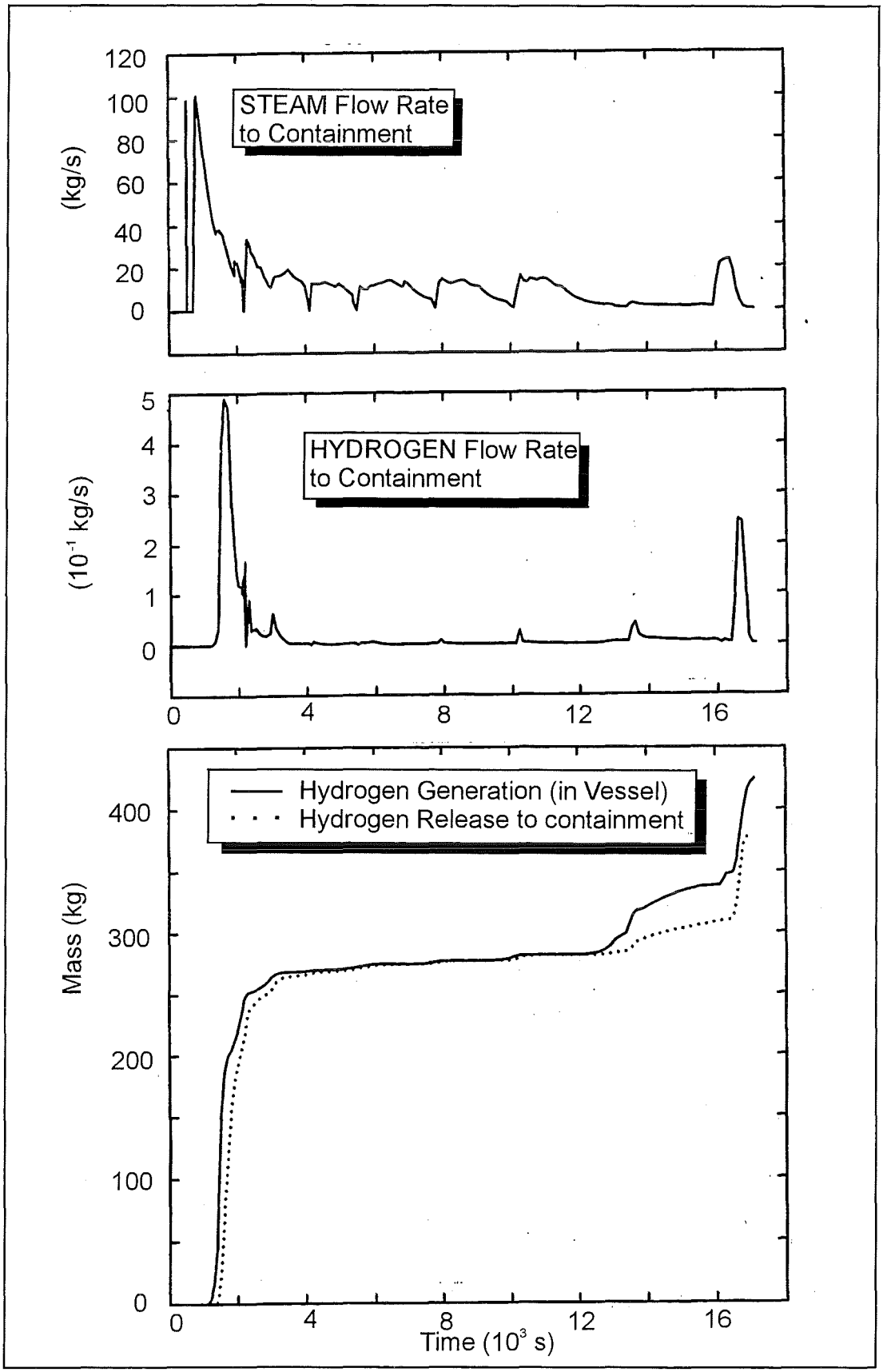

Fig. 2.2: MELCOR results for hydrogen and steam production during a small - break LOCA sequence in the EPR (50 cm^2 leak)

axial segments. The sequence was modelled up to failure of the reactor pressure vessel. The results are presented in **Fig. 2.2.**

The first hydrogen is generated about 1200 seconds after accident initiation. The accumulator injections produce small individual H_2-peaks. The last two peaks in the H_2 production are related to the failure of the core support plate (≈14000 s) and the reactor pressure vessel (≈17000 s). The total in-vessel H_2-production in this base case calculation amounts to about 420 kg. Sensitivity calculations are underway to investigate the influence of model parameters (e.g. debris characteristics) on the resulting hydrogen and steam production.

2.1.2 Station-black-out sequence

Due to the small steam leak rate in this scenario core dry-out occurs much later than in the previous case (**Fig. 2.3**). The first significant H_2 production period between 10.000 and 15.000 s results from accumulator injections. The core is refilled with water to about 70 %. Shortly after 20.000 s the core dries out finally and large scale oxidation takes place with about 0.4 kg H_2/s maximum rate. The vessel is predicted to fail after 32.000 seconds. The total hydrogen generation is about 450 kg.

Additional sensitivity studies are currently performed for this accident scenario. The described base case included opening of all pressurise values (200 cm^2) and shut down of the secondary side.

2.2 REFLOX code development

In all severe accident sequences the primary goal of the operators will be to cover the overheated core with water as soon as possible. This measure is prescribed in most accident hand books. The core flooding can also occur automatically; e.g. from the accumulators during pressure decrease, of from re-activated emergency pumps at the end of a station-black-out sequence.

Since very high hydrogen generation rates were observed in a number of severe core damage tests, a model was developed at FZK to predict hydrogen production

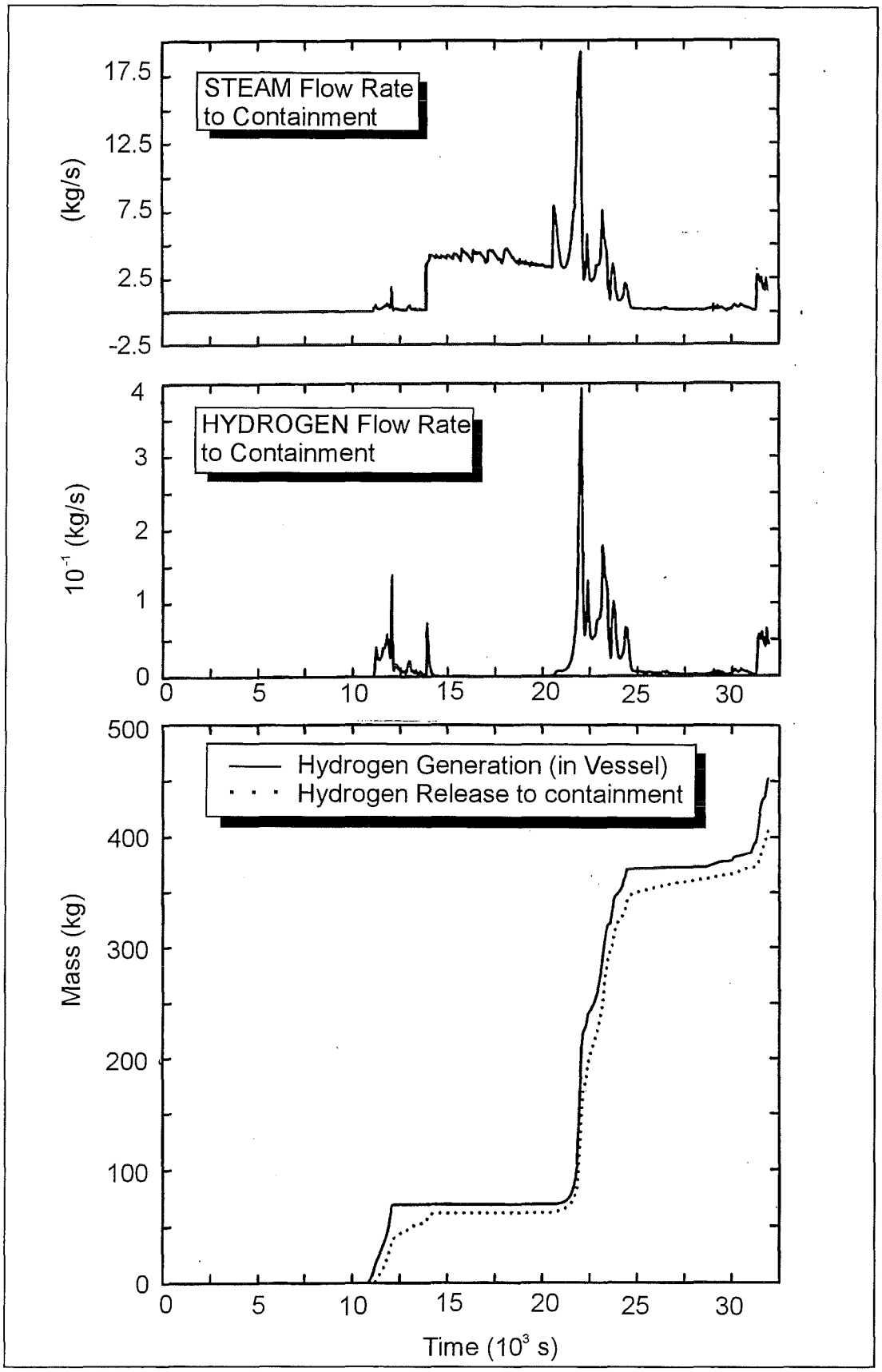

Fig. 2.3: MELCOR results for hydrogen and steam production during a station - black - out sequence in the EPR.

during reflood events. The model currently describes the CORA experiments. In a second step additional models will be added for full-size reactor predictions.

The program simulates the following set of coupled physical phenomena for a representative fuel pin [1]:

- Oxygen diffusion in the Zircalloy cladding and growth of the various O-Zr-reaction layers,
- heat conduction and heat generation in the fuel pin (nuclear decay heat, heat of reaction from Zr-oxidation at the metal/oxide interface),
- radiation transport through the steam containing atmosphere around the bundle.

The model is based on intact fuel rod geometry, melt relocation is neglected. Convective heat transfer is only implicitly modelled in the energy balance, no mass convection is included. The main new hypothesis for explanation of the observed high H_2-production rates during reflood (e.g. CORA and LOFT tests) is that flooding suddenly increases the steam partial pressure in the test bundle, which reduces the radiation heat losses to the cold environment and results in a sudden temperature excursion. The temperature increase triggers elevated oxygen-diffusion rates and H_2-production. The model was validated on the large CORA-data basis existing at FZK.

A major result from the CORA-simulations was, that the sudden high hydrogen release rates from a reflood event do not create immediately dangerous gas compositions because they are mitigated by an even stronger steam production. E.g. in CORA-13 the H_2: steam ratio dropped from about 1:3 before the reflood, to less than 1:10 during the reflood. When air is added to such mixtures inert or weakly flammable gases are generated. Sensitive H_2-air-steam mixtures can only develop later in time if significant steam condensation should occur. The hydrogen risk from flooding an overheated core is more related to the integral H_2-mass than to the high H_2 release rate.

3. HYDROGEN DISTRIBUTION

3.1 GASFLOW model development and code maintenance

A model for sump vaporization and condensation has been added to the code. Vaporization from a sump surface is simulated when the steam density in the adjacent fluid node is below the saturation steam density on the sump surface. The vaporization rate is proportional to the density difference and is calculated from the Reynolds analogy in the same way as the film vaporization and condensation.

A new model was implemented into GASFLOW for the Siemens plate recombiner. It determines a volume flow rate through the recombiner in dependence of the hydrogen concentration at the recombiner inlet and applies this as a velocity boundary condition like an active ventilator. The model uses measured performance data for the recombiner efficiency and the recombination rate from the Battelle Gx tests as function of the hydrogen concentration (see **Fig. 3.1**). Least square fits were made to the experimentally derived correlations for the recombination rate in dependence of the hydrogen concentration and for the recombiner efficiency in dependence of the recombination rate. The model reflects the reduction of the recombiner efficiency for hydrogen concentrations above 7% . It covers a range of hydrogen concentrations up to 10 Vol%. An asymptotic velocity vo through the recombiner is determined so that the amount of hydrogen for the measured recombination rate actually gets to the recombiner plates. Close to the steam inertization we plausibly limit the flow and recombination rate by the oxygen concentration. Like in the model for the NIS granulate recombiner we approach the asymptotic velocity with a time constant. For the Siemens plate recombiner this constant is selected two orders of magnitude smaller (10s) than for the NIS granulate recombiner. The model calculates the hydrogen recombination and its effect on the convection processes in all analyzed Gx tests quite well.

The diffusion terms in the transport equations of GASFLOW were corrected to remove non physical pressure changes from numerical errors during the diffusion of two different gases from adjacent meshes. The molar diffusion fluxes are now exactly balanced to zero. The correction particularly improves the simulation of diffusion flames.

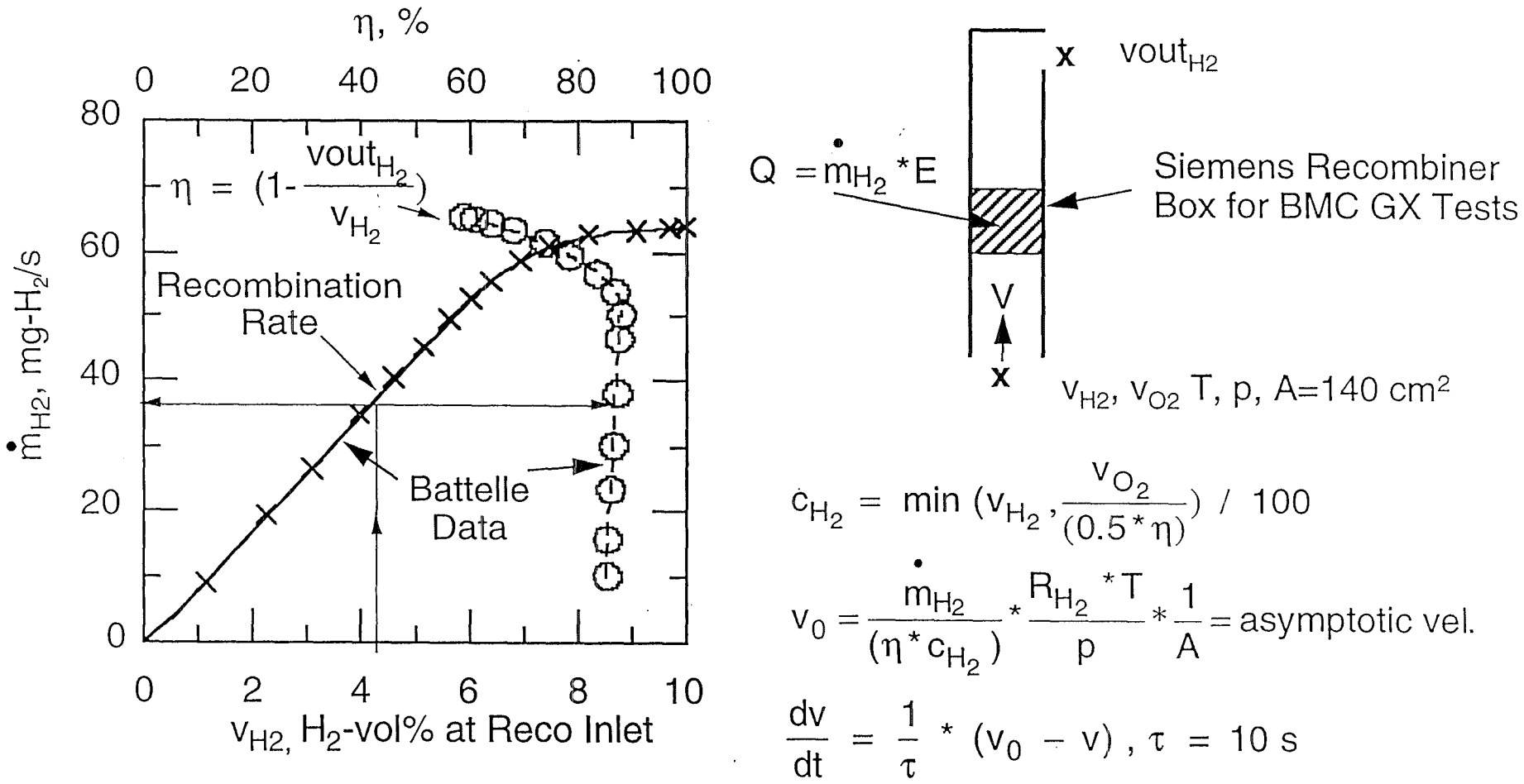

Fig.3.1: GASFLOW model for the Siemens recombiner.

The variable area option that allows to simulate fractional areas on the mesh boundaries instead of the full geometrical size was extended to allow for the simulation of leakage pathes with small hydraulic diameters. The higher velocities at strongly reduced flow areas can significantly reduce the time step due to Courant conditions, however.

All code extensions were consolidated into a new GASFLOW version 1.4.3. We are now documenting the new models and code additions relative to the released base version GASFLOW 1.0 from 1994. Since September we are combining the consolidated GASFLOW version 1.4.3 with the multiblock version 2.0 of GASFLOW developed at Los Alamos National Laboratory (LANL) to a new code version GASFLOW 2.1. We rewrote the code from FORTRAN 77 to FORTRAN 90 during this merging process and we switched our update method from Historian (CMP) to a new update procedure RCS (Revision Control System), which allows the automatic generation of code versions from different development stages of the code. This major revision of GASFLOW is done as a joint activity between FZK and LANL and also supported by US-NRC. The new GASFLOW version 2.1 will allow to change meshes between different rooms that are connected through 1 dimensional ducts. Besides it includes an aerosol model which allows simulation of aerosol transport in the gas field which can also be coupled to volumetric decay heat sources.

The switching to FORTRAN 90 makes the code more platform independent. The new GASFLOW code runs on the Cray J90, on the new Siemens Fujitsu machine VPP and on Risc and Solaris workstations without major changes. But the use of FORTRAN 90 lead to some difficulties with the vectorization of GASFLOW on the VPP and Cray J90, that are related to the use of pointers. We attribute this to compiler errors and hope that the coming up improved FORTRAN 90 compilers for these machines will vectorize better.

3.2 Overview over new GASFLOW simulations

Our important new GASFLOW simulations have been included in the updated overview of the GASFLOW simulations for steam/hydrogen transport without and with inclusion of mitigation effects (**Fig.3.2**). New transport simulations without mitigation effects were performed for the Biblis A reactor containment. We

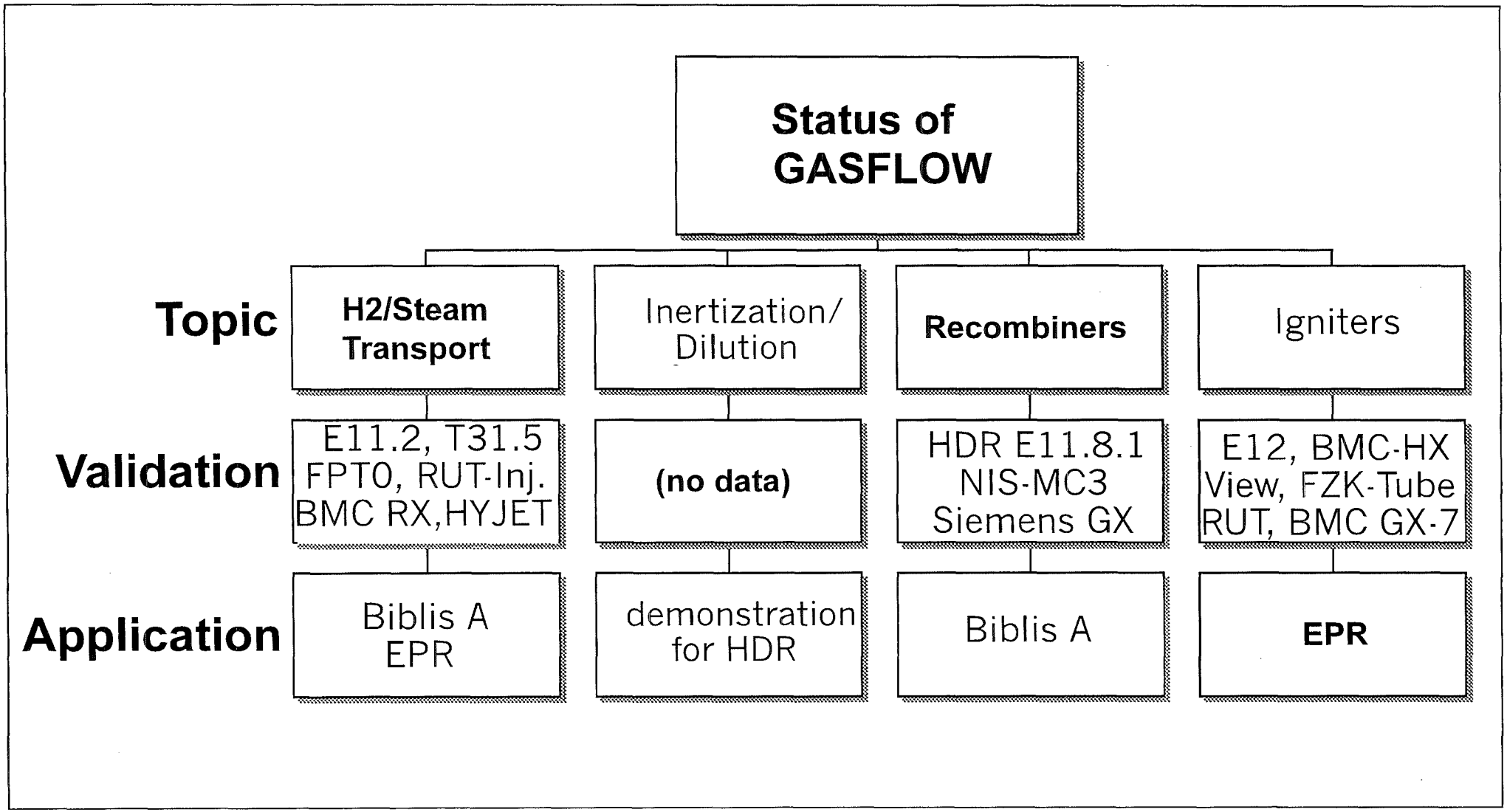

Fig. 3.2: FZK activities on hydrogen transport and mitigation.

developed a complex 3D geometry model for this containment and analysed stratification and mixing of the steam-hydrogen release from a loss of coolant accident under simplified design basis accident conditions. Steam vaporization from a heated sump provides an important mechanism for mixing the initially stratified steam/hydrogen mixture. GASFLOW calculated the initial stratification phase and the transition to homogeneous conditions from the sump vaporization. The applied sump model was succesfully validated with the specific sump tests RX4 and RX5 that were performed in the Battelle model containment. This work was done outside the Siemens/EVU contract with direct support from RWE and is published in [2]. We have started to study the hydrogen distribution during the dynamic injection tests in the Russian RUT facility using GASFLOW, this work is still in progress. GASFLOW could succesfully predict Helium stratification in a recent blind posttest analysis of the Battelle Hyjet test JX7. This progress report will summarize these results.

Steam/hydrogen transport simulations with mitigation measures include the effects of inertization for instance by CO_2 release, the catalytic hydrogen combustion in recombiner modules and the local hydrogen deflagration at igniters. We will report here about our analysis of the Battelle Gx tests which simulated steam hydrogen distribution together with a plate recombiner of the Siemens type. Test Gx7 also simulated mitigation by the so-called "dual concept" with a plate recombiner and a series of spark igniters that were positionned in different rooms of the Battelle Model Containment. The GASFLOW combustion model was further tested in the analysis hydrogen combustion in some FZK tube tests. Besides we analyzed hydrogen combustion in the test RUT 23. We will briefly report about these new combustion calculations also.

3.2.1 Hyjet test JX7

Recently we participated with GASFLOW in a blind benchmark set up by Battelle for the test JX7. The blind benchmark was also analyzed with the field code FLOW3D and with the lumped parameter codes RALOC, WAVCO, and Gothic.

Test JX7 involved the full Battelle containment with a total gas volume of 600 m^3. Helium with a total mass of 10 kg was injected in 200 s near the bottom of the banana room R6 (**Fig. 3.3**). The injection velocity was 42 m/s. The nozzle was

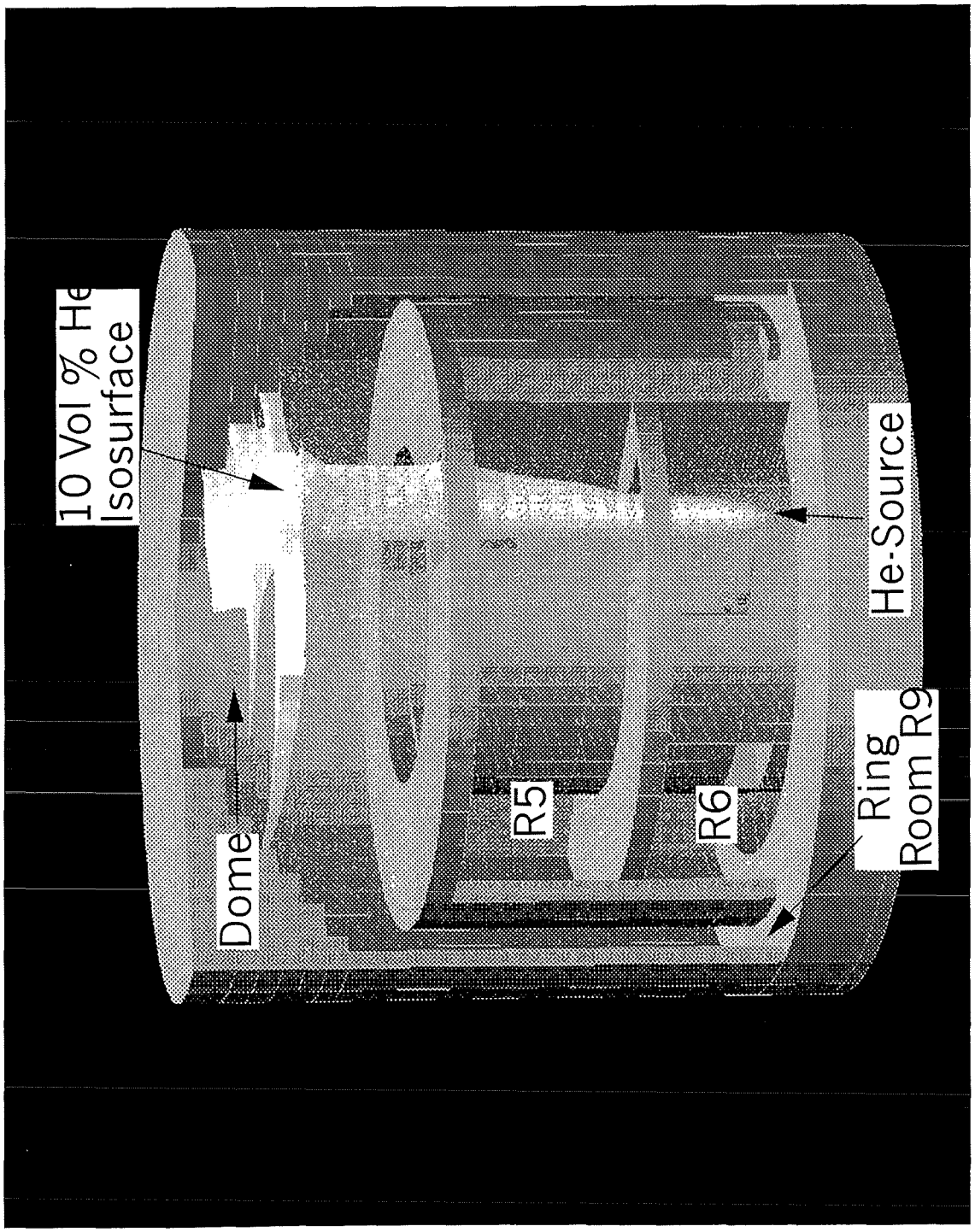

Fig.3.3: Jet in Battelle model containment during Hyjet test Jx7 at 50s (GASFLOW-Kismet visualization)

positionned underneath vertically aligned overflow openings in the ceilings of the banana rooms. A jet formed that extended all the way from the source location into the dome region. The jet is displayed in **Fig. 3.3** into the actual containment model at 50 s after the start of helium injection as the isosurface for 10 Vol% helium. The helium stratifies in a cloud in the containment dome. The geometrical model for GASFLOW applies 50000 computational cells. It models the jet well but requires quite long running times (10 d for 800s) mainly due to the Courant limitation for the time step. A preceding analysis with a coarser mesh of only 5000 cells did not resolve the jet with the same detail, but it could capture the plume behavior in the dome quite well also. The analysis of the 800s problem time took only 80 min with this coarser model.

The plots in **Fig. 3.4** compare the results from the GASFLOW simulation with the fine mesh to the test data and to the other code predictions at four sensor locations in the dome, near the bottom of the central room, and in the upper and lower part of the ring room. Compared to the test data the GASFLOW concentrations are 18% instead of measured 16% at the top of the dome and 9% instead of measured 11% in the upper region of the ring room. Good agreement is obtained at the bottom of the central room and in the lower ring room where the lumped parameter codes significantly overestimated the helium concentration. GASFLOW simulates turbulent diffusion based on the algebraic turbulence model with a prespecified turbulent length scale. The overprediction of the helium concentration in the dome region can be attributed to insufficient air entrainment along the jet surface. The helium concentration profile across the jet shows good agreement with the test data near the source location.

FLOW3D results are in better agreement with the test data in the dome but not as good as GASFLOW in the lower containment regions. Overall the blind benchmark demonstrated that field code predictions are in better agreement with the test data than the results from lumped parameter codes. The predictions of the two field codes GASFLOW and FLOW3D for this Hyjet test are of a comparable quality when one includes all sensor locations in the comparison.

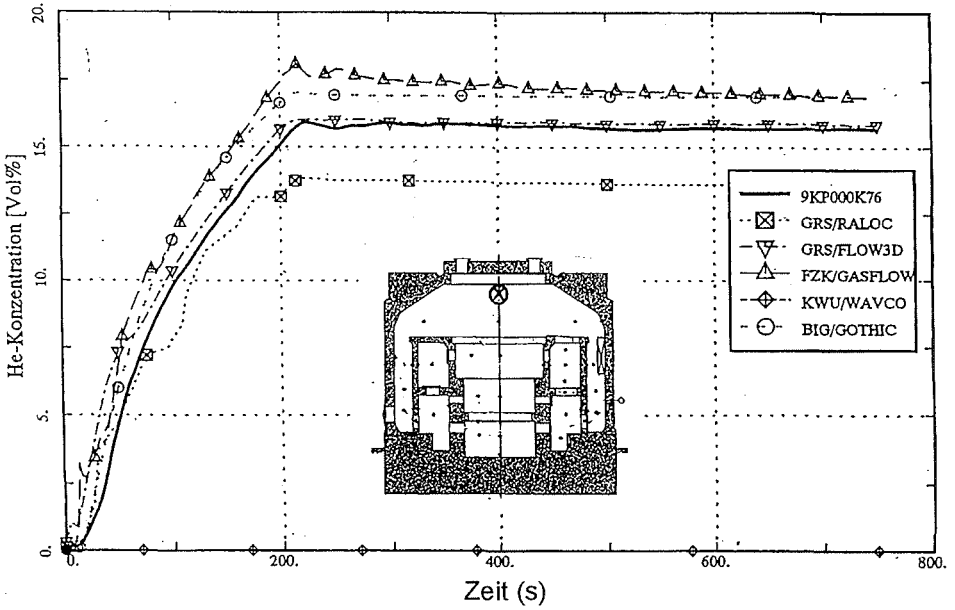

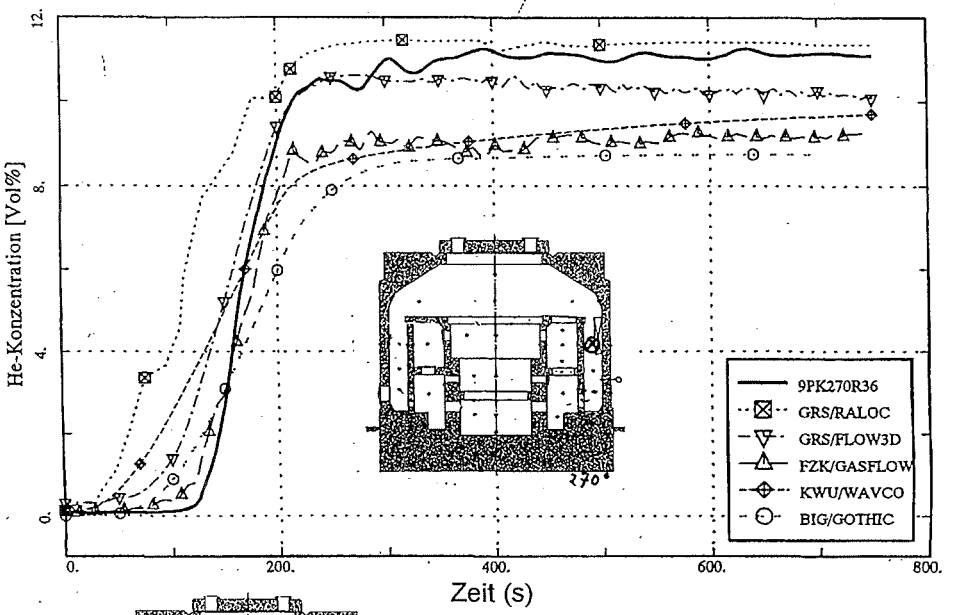

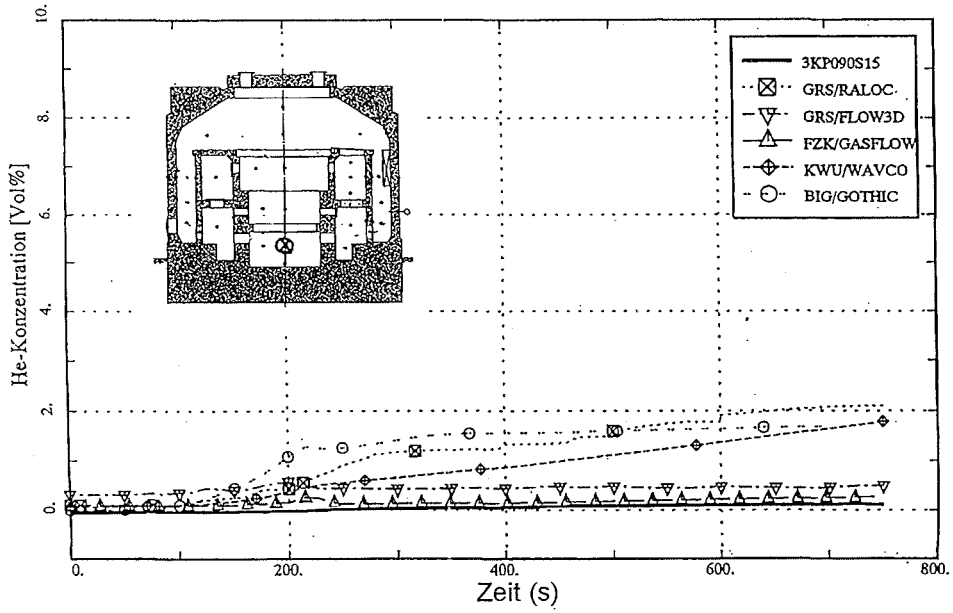

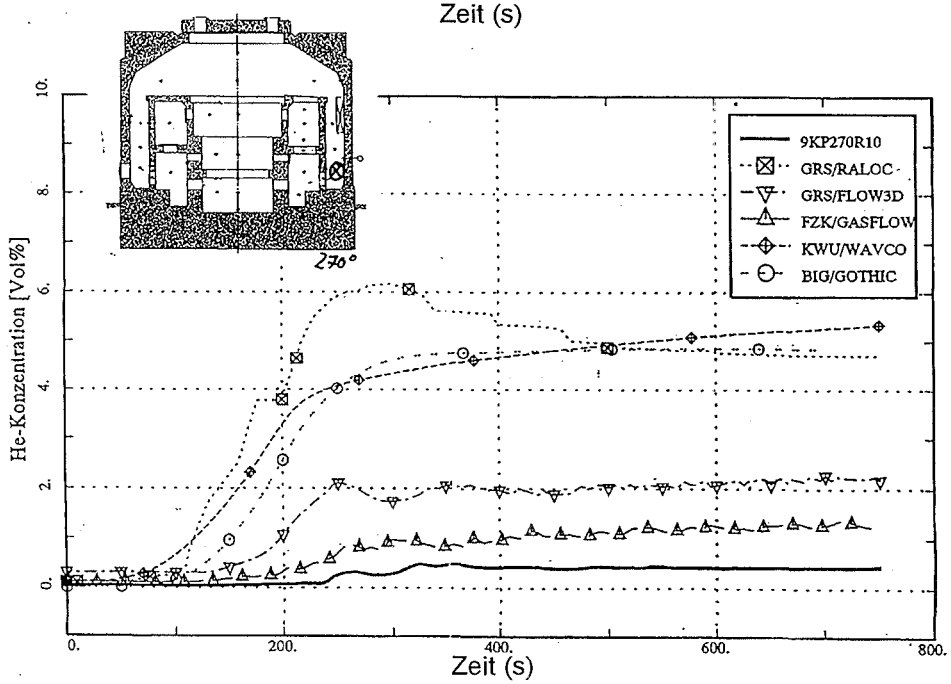

Fig.3.4: Results of the Jx7 distribution benchmark.

3.2.2 RUT Injection test

Experiment RUT-29 was selected for a simulation of the hydrogen distribution during a dynamic injection because this test provided more extended data than other dynamic RUT injection tests. In the dynamic injection tests only the canyon (16.6x3x2.5m) and the second part of the channel (13.4x2.3x2.5m) have been used. The injection was performed under an angle of 45° downwards with a flow rate of 0.59kg/s. After 7.98s injection time there was a time delay of 26.3s until ignition occurred. During this time delay hydrogen concentrations had been monitored at 8 positions (5 in upper part of the test facility and 3 in the lower part of the canyon).

For the simulation GASFLOW was used. The RUT-geometry was modelled in a 3-D mesh with 155x50x21 grid points. An inflow velocity of 700 m/s was assumed, because the thermodynamic state was not measured. The calculation time was 29 days on one CPU of a CRAY-J90 computer.

Fig. 3.5 shows a comparison of measured and calculated hydrogen concentrations. The experiment as well as the calculation shows a hydrogen wave transported by convection from the source (S1) to the igniter (I2). The maximum concentration of about 40 % hydrogen is predicted well by the simulation. In the simulation the hydrogen wave travels faster towards the igniter than in the experiment. In the lower part of the canyon the calculated hydrogen concentrations are slightly higher, they are too low nearby the igniter.

Differences between simulation and experiment are due to several effects: Only the experimental mass flow rate has been defined, but not the inflow conditions (temperature and velocity, no adiabatic flow from the hydrogen storage tank to the injection nozzle). To test the experimental reproducibility test RUT-27 was performed. The measured hydrogen distribution time history of RUT-27 showed significant differences compared to RUT-29. This indicates a strong sensitivity to boundary conditions such as e.g. initial temperature distribution in the test facility and weather conditions.

This simulation has shown the principle capability of GASFLOW to calculate hydrogen distributions even under situations where hydrogen distribution processes are difficult to predict e.g. high velocity jets against gravity, but further investigation

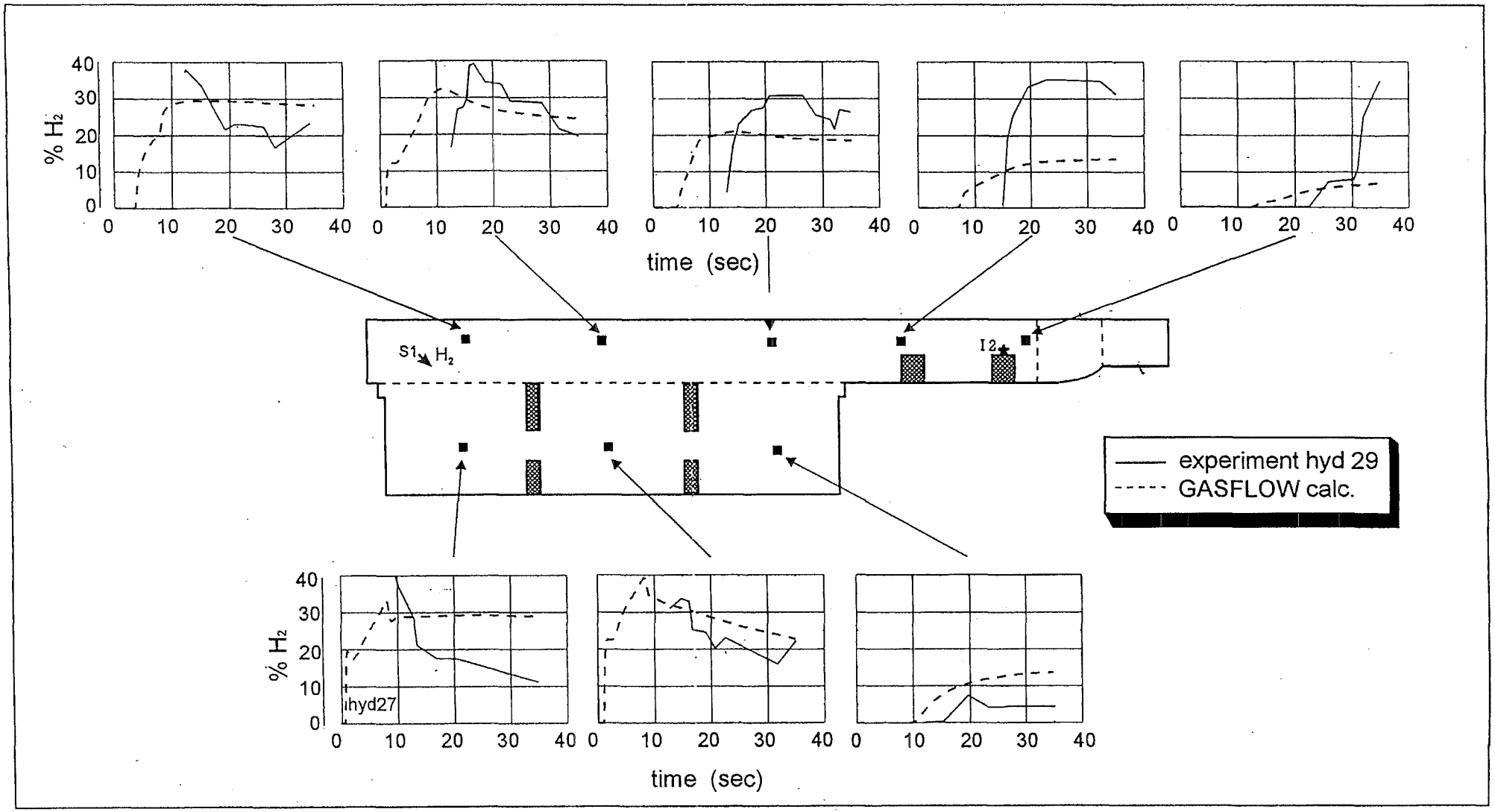

Fig. 3.5: GASFLOW simulation of a dynamic H_2 - injection test in the RUT facility (experiment hyd 29, injection rate 0.59 kg H_2 / s)

is needed. This will be possible with new improved experimental data performed in the next RUT test series.

3.2.3 Validation of mitigating measures with Battelle Gx experiments

The EPR calculations reported about last year [3] and the analysis of steam/hydrogen distribution in the Biblis A containment under LOCA conditions documented well the ability of GASFLOW to simulate such transport phenomena in quite complex geometries. We continue to include the major mitigation effects into such analyses based on validated models. We developed and validated a model for the NIS granulate recombiner already last year [3]. This year we extended our mitigation modeling to also include the Siemens plate recombiner and validated it succesfully with the analysis of the Battelle Gx tests. We consider this a further important strengthening of our basis for integral containment analysis of severe accident sequences. Test Gx7 with a Siemens plate recombiner and with spark igniters in the various rooms was the first integral performance test for the "dual concept" which is currently in discussion for hydrogen mitigation both in the EPR and in the operating PWR plants. So far the GASFLOW analysis of test Gx7 is the only available 3D field code analysis of this complex performance test.

The Gx tests were done in the inner containment region of the Battelle model containment with the banana rooms R5, R6, R7, and R8 that are arranged in two axial planes and with the central rooms R1 and R3. A large plug above room R1 and closed openings in the ceilings of R5 and R7 separate these rooms from the remainder of the containment with the dome and ring rooms. The total gas volume of the test rooms was 209 m^3. We simulated the inner containment region with GASFLOW in a 3D cylindrical model with 5800 computational cells.

The scheme in **Fig. 3.6** shows a radial cut through the central room with the concrete plug on the top and and through the banana rooms outside. The right hand side gives an unwrapped scheme of the four banana rooms. The recombiner box is a scaled Siemens plate recombiner module with a cross section of 11.6 by 16 cm^2 and a prototypical height of 1.6 m. It is positionned at the inside wall of room R5 not far from the overflow opening to room R6 underneath. The recombiner box has a vertical inlet at the bottom and a horizontal outlet at the top. With the small

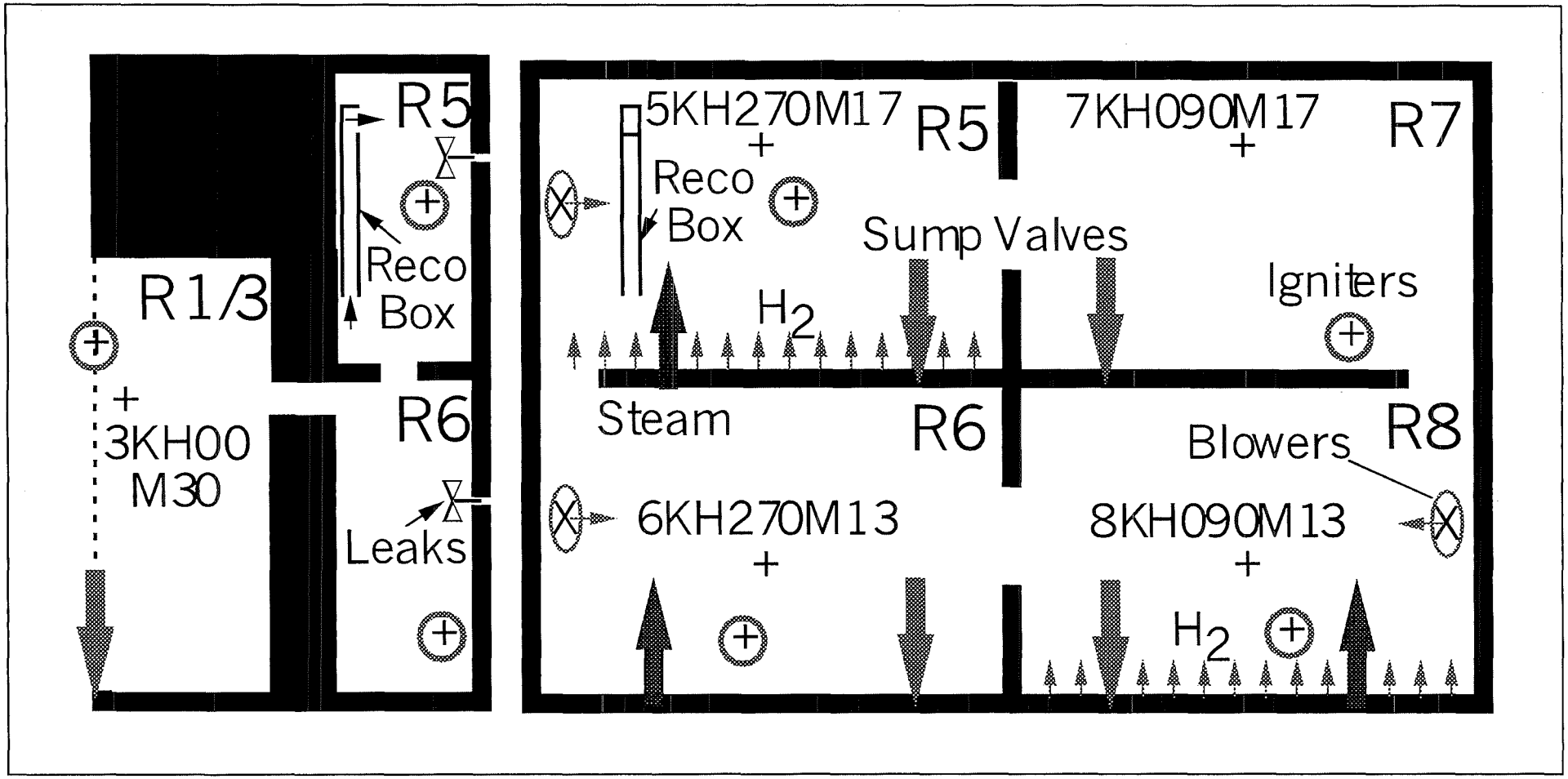

Fig. 3.6: Scheme of the Battelle model containment for the Battelle Gx tests, radial cut and unwrapped geometry of banana rooms.

recombiner box the wall effects became quite important in this test which was different from our earlier analysis of test MC3 with the full size NIS granulate recombiner [3].

Test Gx4 had 2 periods of hydrogen injection, first from a line source in room R5 and then from a line source at the bottom of R8. Steam was injected into R5, R6, and R8 prior to the hydrogen release and in between the two release periods. Test Gx6 had only one hydrogen injection period into the lower room R8. Test Gx7 was run with a higher steam concentration and stronger hydrogen sources. Hydrogen was injected into R5 and R8 again in two periods. Spark igniters were positionned in each room. They were all activated during the first period of hydrogen injection. In the second injection period only the igniters in R6 and R7 away from the source room were active. The igniters operated with a frequency of 7s during the activation periods.
The boundary conditions for all these tests were quite complex. Sump valves and blowers that are open and active during the pre-conditionning phase and in between the hydrogen injection periods control the composition of the atmosphere and relieve the pressure during the steam injection. The containment was also not leak tight after valve closure. Leakage effects were found in the analysis of tests Gx4 and Gx6. In tests Gx7 these had so much impact on the concentration that we included in our model 14 known leakage pathes with 1mm hydraulic diameter and 3.1 cm^2 surface at the locations where the instrument guide tubes penetrated the outer walls of the banana rooms. Although they were quite small these leaks relieved the pressure on a fast enough time scale. The steam and hydrogen injection rates and their interplay with the valve opening and the fan operation, also the activation times of the igniters in test Gx7 are shown in **Fig. 3.7**. The figures only plot the integral steam release from all three injection points as it was recorded in the test. The actual distribution of the steam source over the three rooms R5, R6, and R8 was estimated on basis of the relative valve openings. We applied the original estimates from Kanzleiter for this distribution. However, significant overpredictions of the gas temperature resulted in room R5 during the preconditionning of test Gx7 with Kanzleiter's specified original steam distribution which lead to a too high steam content and nearly steam inerted conditions at the recombiner box. This was

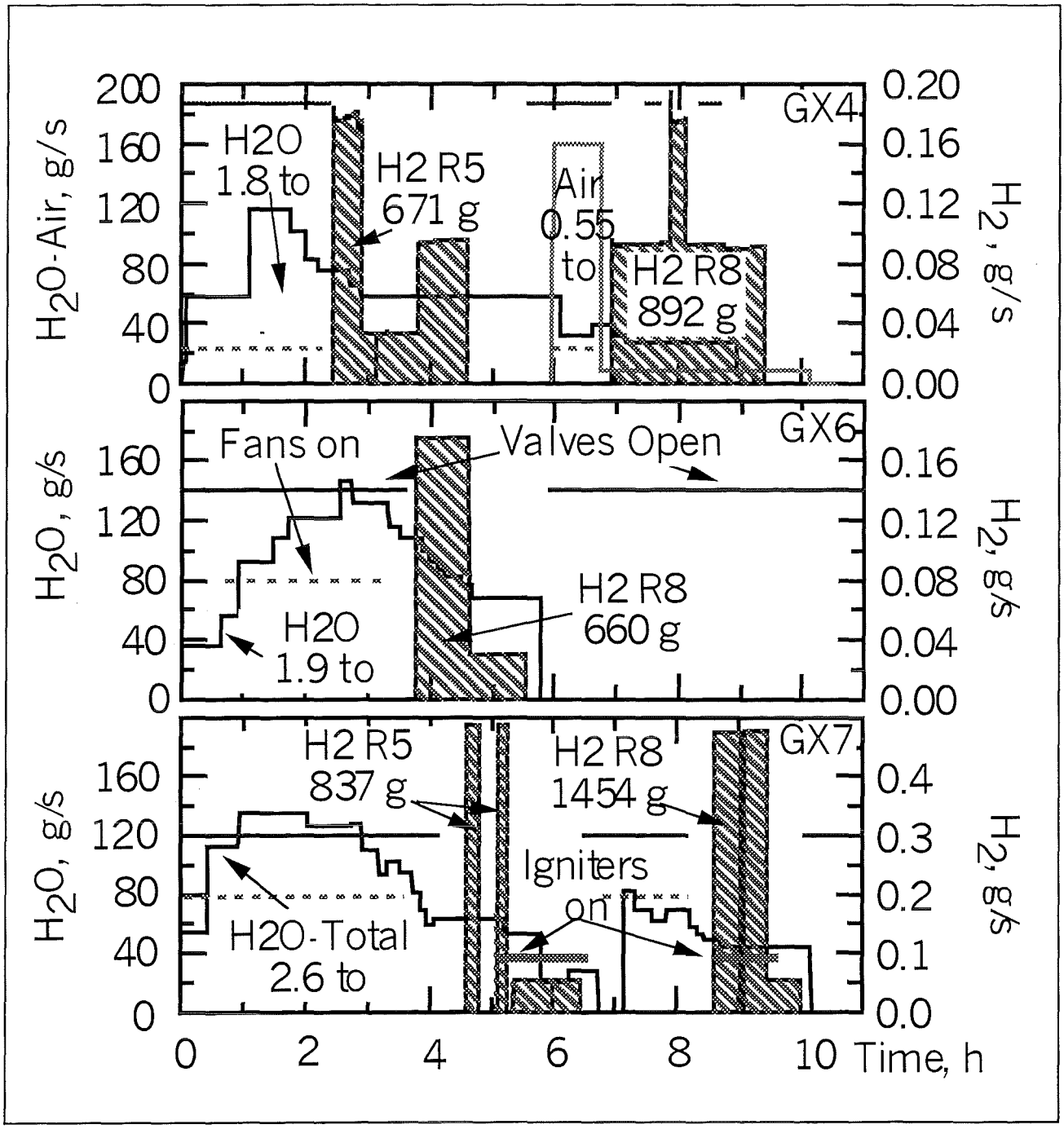

Fig. 3.7: GASFLOW conditions for Battelle Gx tests with a Siemens recombiner and spark igniter.

independently found also in a RALOC simulation of this phase for test Gx7. We then used an adjusted steam distribution GRS had estimated from their analysis of the preconditionning phase and like GRS got a much better agreement with the measured gas temperatures and steam concentrations prior to the hydrogen injection. Because the high steam volume fraction in room R5 makes the recombiner operate near the limit of steam inertization this adjustment of the steam distribution in test Gx7 was quite important. The collection of all details from these tests was not easy and only possible with the help of Dr. Kanzleiter from Battelle and Mr. Klein-Heßling from GRS.

3.2.3.1 Results for tests Gx4 and Gx6

The measured and calculated hydrogen volume fractions for tests Gx4 and Gx6 are compared in **Fig. 3.8**. The upper two plots are for the high banana rooms R5 and R7, below are the data for the two low banana rooms R6 and R8 and at the bottom a characteristic hydrogen concentration is displayed for the central room R3. We have analyzed a problem time of 20h for test Gx4 and 10h for test Gx6. The two hydrogen peaks for test Gx4 reflect the two periods of hydrogen injection. Hydrogen concentration never exceeds 4% in both tests and the hydrogen distributes fairly homogeneous over the different containment rooms. Agreement with the test data is quite good for both tests.

There is a slight overprediction of hydrogen concentration in the upper rooms during the second injection period in test Gx4. Responsible for this is an increase of the steam concentration in the upper rooms after a strong reduction of the steam source which increases the hydrogen volume fraction while reducing the pressure. The local underpressure due to the condensation sucks additional gas from the lower source room R8 which in turn reduces the calculated hydrogen concentrations in the source room R8 relative to the test data. We attribute the fact that this behavior is not seen in the test data to the containment leakage which doesn't allow such an evacuation after loss of the steam source and which replaces the condensed steam by the air sucked in through the leaks instead of increasing the hydrogen volume fraction.

Condensation is also overpredicted after shutting off the steam source in test Gx6. In this case the resulting underpressure increases the hydrogen volume fraction only

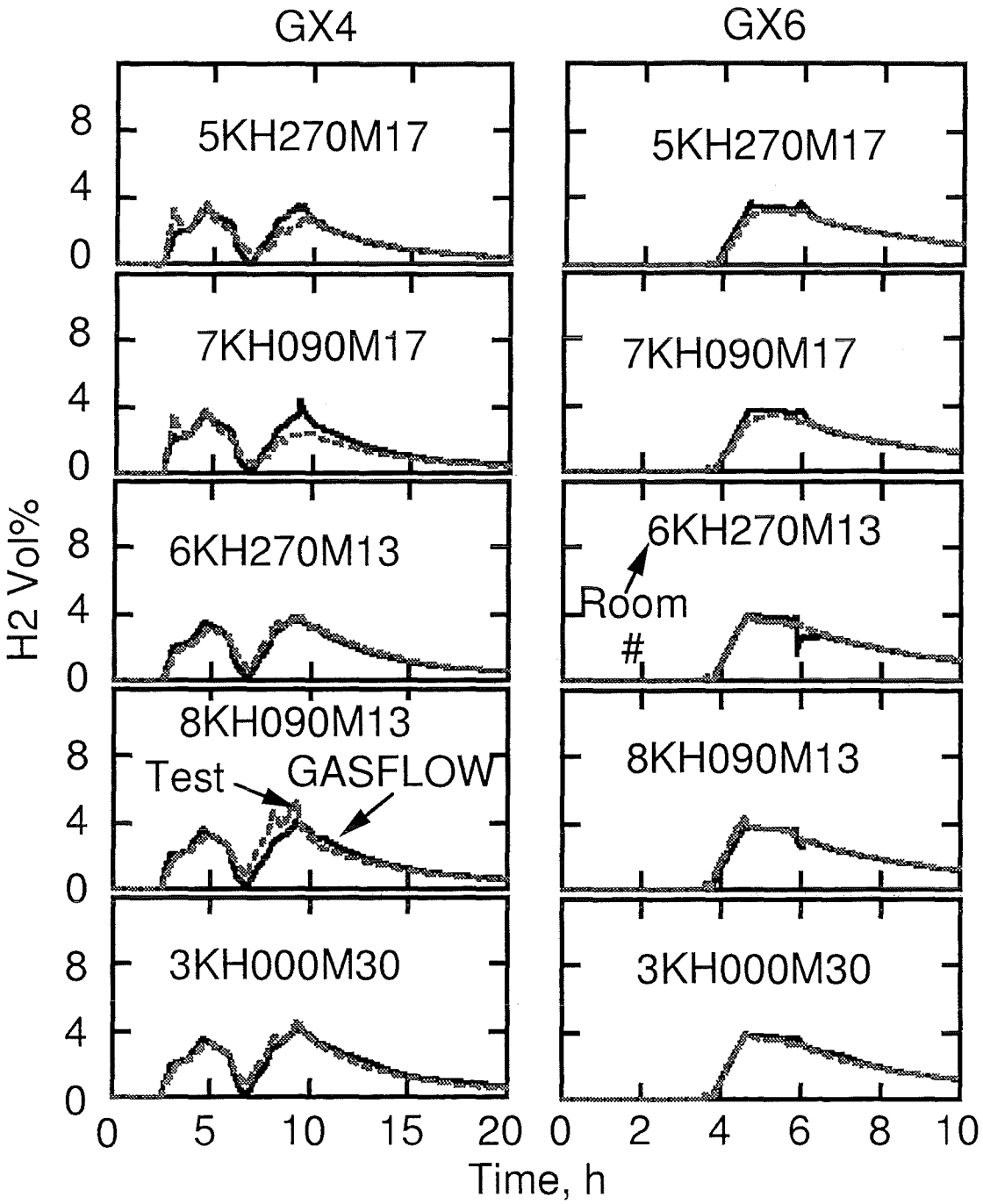

Fig:3.8: Hydrogen volume fractions in Battelle tests Gx4 and Gx6 with Siemens recombiners. GASFLOW results vs. test data for all containment rooms.

for a short time, an effect which shows up to a certain degree also in the test data (Gx6 results around 6h). Then the sump valves open in R6 and bring in air which causes a local temporary hydrogen dilution in R6. The nearly 0.1 bar underpressure that develops in the leak tight GASFLOW model after stopping the steam injection makes this dilution stronger than in reality, but it is a local effect only and mixing brings the hydrogen concentrations back to the experimental data quite fast.

3.2.3.2 Results for test Gx7

The calculated and measured hydrogen concentrations for test Gx7 in **Fig. 3.9** also show quite good agreement with the test data. Steam and hydrogen injection are significantly stronger in Gx7 than in the previous tests Gx4 and Gx6.

First injection period of hydrogen

The upper banana rooms R5 and R7 have steam volume fractions above 65% at onset of hydrogen injection.The hydrogen release in room R5 causes a rather strong stratification with peak hydrogen volume fractions of 8% in the upper rooms and values below 3% in the lower rooms. GASFLOW captures this stratification quite well. Catalytic combustion in the recombiner box gradually removes the released hydrogen from the first injection period. The solid bars in each graph indicate the activation times of the igniters in each room. Igniters were sparking in each containment room during the first hydrogen injection period with a frequency of 7s. But the hydrogen concentrations never exceeded the flammability limit at any location during the first activation period of the igniters. This flammability limit for the burnable hydrogen concentration in a steam/hydrogen mixture was determined from the lean combustion limit in the Shapiro diagram and is evaluated in dependence of the steam volume fraction at the igniter position in each room from the correlation

$$H_{Burn} = 0.04 + \min\left(0, \frac{(v_{f_{H_2O}} - 0.3)}{(v_{flam} - 0.3)} * 0.08\right)$$

which has also been implemented into GASFLOW. In this correlation

v_{fh2o} = steam volume fraction

v_{flam} = 0.65 = steam volume fraction threshold for inertization

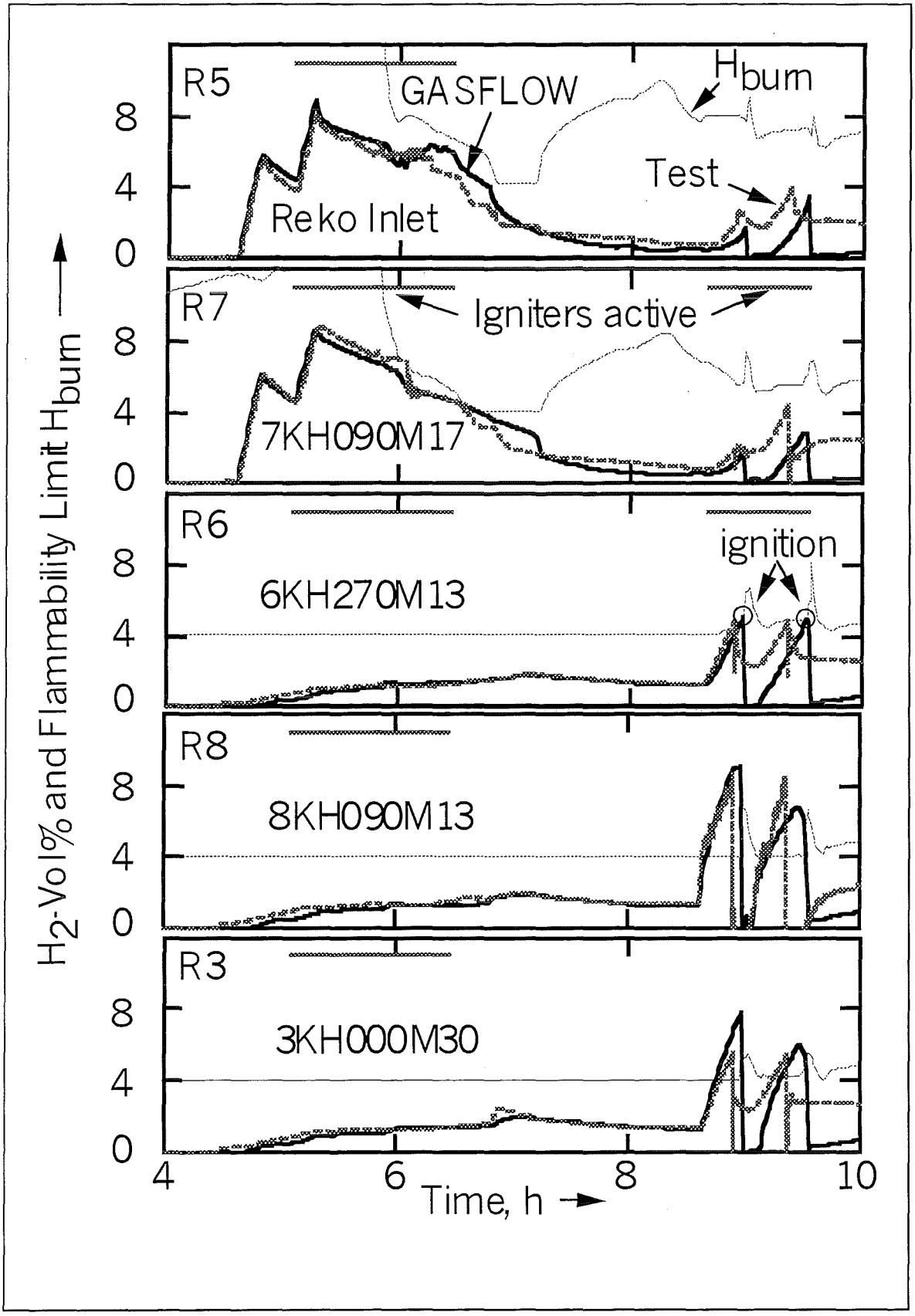

Fig. 3.9: Calculated H_2 concentration in BMC test Gx7 with Siemens recombiner and igniters. H_{burn} is the flammability limit for the calculated steam concentration.

To trigger a combustion in a lean hydrogen/steam/air mixture the hydrogen concentration must exceed 4% for steam volume fractions below 30%. This threshold increases to 12% with increasing steam content. No combustions are triggered above steam volume fractions of 65%.

In test Gx7 the regions with high hydrogen volume fractions initially are fully steam inerted. The recombiner continues to operate above the limit of steam inertization but with a reduced efficiency and a reduced flow rate during the lack of oxygen. Steam concentrations in the lower rooms are much smaller. The flammability limit never exceeds 4% there, but not enough hydrogen gets there for an ignition during the first injection period. As the steam release goes down the flammability drops nearly to the hydrogen concentration in particular in room R7. But when the mixture becomes burnable for a short time in R7 the igniters have already been deactivated. The recombination rate increases during the reduction of the steam injection. Most hydrogen is gone in the upper rooms after 8 hours. The hydrogen concentrations in the lower rooms even exceed the values in the upper rooms then.

Second injection period of hydrogen

In the second phase, that starts at 8.5 h, hydrogen gets injected into the lower room R8. Hydrogen concentration there rapidly exceeds the flammability limit, but the igniters are only activated in the adjacent rooms R6 and R7 then. The relative increase of the hydrogen concentration and the changes of the flammability limit in these two rooms controls the progression of the experiment in this second phase. The hydrogen distribution becomes quite sensitive to the distribution of the steam release.

With the estimated distribution of the steam injection into the three rooms R6, R8 and R5 from Kanzleiter the hydrogen concentration in R7 increased faster than in R6. Combustion in the second period of hydrogen release was triggered in R7 then. It brought about a change in the circulation that kept the concentration in R6 from exceeding the flammability limit. The hydrogen concentration in R7 remained too low for a backflash into the source room R8 and cyclic combustions in R7 with

continued hydrogen supply from the room R8 below gradually removed the hydrogen in the second period. The experiment did not show such behavior.

Without changing the measured overall steam source we reduced the steam release in the lower rooms R6 and R8 by 5% each and enhanced it correspondingly in the upper room R5. This slight redistribution of the steam injection caused the initiation of hydrogen combustion in R6 when the hydrogen concentration there exceeded the flammability limit (**Fig.3.9**). After some time for enthalpy accumulation the flame propagated horizontally into the source room R8 which is in good agreement with the test data. GASFLOW calculates a nearly complete combustion then.

The test data indicate a complete combustion only in the source room R8 and leave behind a residual hydrogen concentration in the other rooms. The GASFLOW mesh size was primarily set to simulate hydrogen transport with recombination. To maintain the combustion process in the coarse mesh we had to increase the sparking duration (it was increased from the specified value of 1 ms to 0.5 s) in order to get enough enthalpy into the coarse mesh for a flame propagation. We also reduced the temperature threshold for the use of the Arrhenius law from the recommended value of 800K to 500K to be able to propagate the combustion into the adjacent nodes and prevent it from extinguishing when the convected enthalpy is not sufficient to raise the temperature to a high enough value in the coarse mesh of the adjacent nodes. Running the whole transport sequence with a rather fine mesh for the combustion would be rather time consuming and not be feasible for large containment systems. A local mesh refinement at the onset of the combustion would certainly be more appropriate. The INKA code that is currently under development at FZK is designed for such dynamic mesh refinements during the hydrogen transport phase. It will also apply a more detailed turbulence model for the combustion simulation than the simple algebraic model that was applied in this analysis. When we analyze steam hydrogen distribution in GASFLOW with the dual mitigation concept of recombiners and igniters we must be aware that the combustion results currently cannot have the same accuracy as the results from the transport analysis.

We do conserve the enthalpy, however, which should be sufficient to account for the effect of local combustions on the overall convection behavior.

As seen in **Fig. 3.9**, the ongoing hydrogen injection after the first burnout again builds up combustible mixtures, that are ignited in room R6. The residual hydrogen inventory after the first burnout in GASFLOW is rather low compared to the test data. The development of a new flammable mixture takes longer and the second hydrogen ignition in room R6 starts more delayed relative to the test data. GASFLOW again calculates a complete burnout in all rooms while in the test complete burnout is seen only in the source room.

The first full burnout leads to a narrow pressure peak of 1.9 b in GASFLOW which is above the recorded peak of 1.2 b from the pressure sensor. In the second combustion a wider pressure pulse with a peak value of 1.2 b results which is nearly at the same level as the sensor reading. Not only the earlier flame extinction in the test but also differences in the kinectis of the flame propagation contribute to the value of the pressure peak. For instance in another analysis with an even stronger shift of the steam release from the lower rooms into the upper room R5 (20% instead of 5%) the combustion with a similar hydrogen inventory only caused a pressure peak of 1.25 b. In this case only one flame controls the combustion in the source room while in the before discussed case two flame fronts meet in the source room coherently, one coming from R6 by an azimuthal flame propagation, the other from a propagation through a central shortcut in R3.

The GASFLOW simulation does include convective and condensation heat transfer with cut off of wall condensation at structure surface temperatures above the critical point of steam. It does not account for radiative cooling. The calculated gas temperatures peak at nearly 1000K in room R8 during the first and 600K during the second combustion. Steam condensation brings these temperatures back to saturation values for the steam vapor pressure quite fast. The recorded temperature readings never exceed 500K but they stay at an elevated level for a longer time.

Representative configurations for recombination and combustion

The Kismet plots in **Fig.3.10** show two snap shots from the GASFLOW simulations during the first hydrogen release phase and at the onset of the ignition in R6 in the second hydrogen release phase. To allow a better view we removed the ceiling and the outer walls of the banana rooms in these snap shots.

The left configuration shows the two banana rooms R5 and R6 with the Siemens recombiner box at 5.26 h when the hydrogen concentration peaks in R5 (Fig. 3.9). Hydrogen is released from a line source on the floor of R5. A cloud which contains more than 9 Vol% hydrogen has been determined from the calculated hydrogen concentrations (the surface is marked by the superimposed wire frame). It builds up above the line source. It doesn't extend high into R5 and is consumed near the recombiner from the ongoing catalytic hydrogen combustion. The 400K isosurface of the gas temperature has also been entered and documents the hot plume above the recombiner box that spreads under the ceiling of R5 and reflects the released recombination energy. The downward extension of this isosurface along the recombiner box documents hot temperatures within this box. Its appearance on the outside of the box reflects the limitation of the interpolation procedure for the isosurfaces from the concentration field which doesn't account for walls and obstacles. A transparent cloud in moiree extends from the roof of R5 to near the upper surface of the hydrogen cloud. It marks the region where the steam volume fraction is above 72%. Only recombination but no hydrogen combustion is possible inside this cloud, it fully inertizes the igniter in room R5. Similar steam only somewhat smaller hydrogen concentrations are found in R7 which is also fully inertized at this time (see Fig. 3.9). Burnable conditions may exist closed to the floor in room R5, provided that the vaporization of the collected sump with hot condensate there doesn't inertize this region also. The picture documents the importance of igniter positionning. Had the igniter been placed away from the recombiner near the bottom of R5 it would have triggered a combustion also during the first hydrogen injection phase.

The right configuration in Fig.3.10 shows the conditions at the point of hydrogen ignition in room R6 during the second phase of hydrogen release. The hydrogen

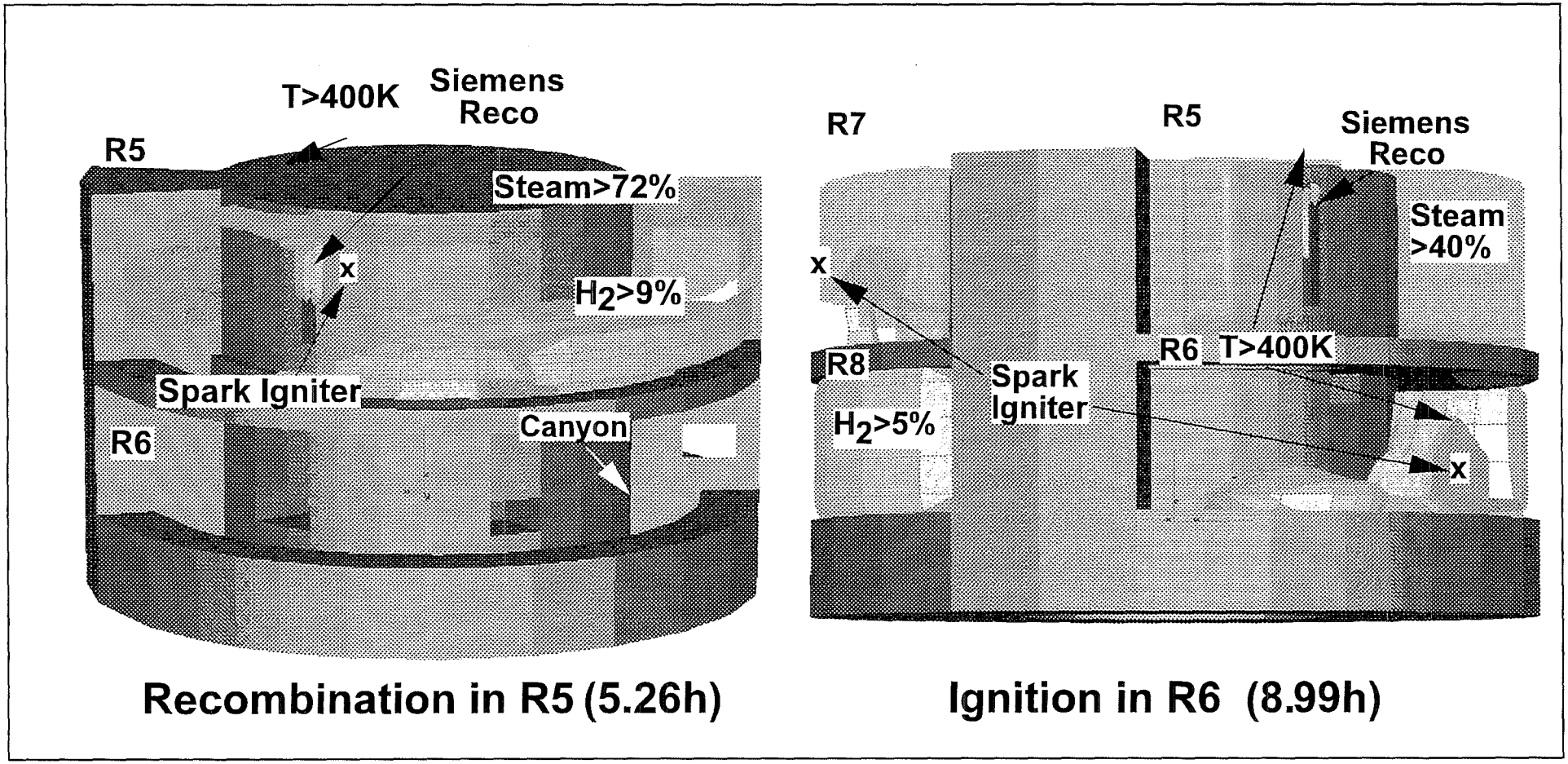

Fig. 3.10: GASFLOW results for BMC "Dual Concept" test Gx7 (Kismet plots).

comes from a line source near the bottom of room R8 (inside wall of the canyon). A burnable hydrogen cloud (>5Vol%) fills the whole source room (surface marked by superimposed wire frame). It spreads circumferentially and extends partially also into the adjacent banana room R6. It also makes a shortcut radially inward through overflow openings into the central room R3 where the hydrogen concentration grows faster than in R6 (Fig.3.9). Some hydrogen then enters room R6 through openings from the central room R3 via the shortcut through the center. It forms the secondary hydrogen cloud around the lower overflow opening above the canyon at the far end of room R6. The location of the igniter in R6 is near the floor and next to the outside wall. It falls in between the clouds from the two transport pathes. The picture also includes the 400K isosurface of the gas temperature. The early combustion builds up a hot plume locally above the igniter, the plume around the recombiner box is small at this time because the hydrogen concentration there is low. Some hydrogen also enters the room R7 through the overflow opening in the ceiling of R8. A finger of the 5% hydrogen cloud is visible in room R7 that spreads mostly upward, it cannot reach the other igniter. With less shifting of the steam release into room R5 when using Kanzleiter's estimate for the distribution of the steam release this cloud would have spread circumferentially. The flammability limit would have first been reached in R7 thus completely changing the combustion sequence. The finger from the hydrogen cloud in room R7 pushes away some steam which can be seen from the shadows in the transparent cloud that bounds the region with a steam volume fraction above 40%. The atmosphere is no longer steam inerted during this second phase of hydrogen injection. We have visualized the flame propagation in a sequence of 100 snap shots after the ignition in R6. Combustion starts with a flickering period of nearly 40 s. Only then the flame accelerates. It spreads out circumferentially and enters room R8 from the side. In parallel a propagation occurs through overflow openings to the central room R3. It triggers a second flame front in the source room R8 which superimposes with the azimuthally propagated flame. This strongly amplifies the pressure and is the principal reason for the much higher than measured pressure peak in the first combustion.

Conclusions from analysis of test Gx7

The GASFLOW analysis of test Gx7 shows that in principle it is possible to describe the steam/hydrogen transport with the combined mitigation from recombiners and igniters. The GASFLOW results allow the precise control of when and where the hydrogen/steam/air mixture becomes burnable. We found out that the transport phase with the recombination superimposed is described quite accurately. The combustion simulation in the coarse transport mesh requires to use longer than the physical sparking durations and to reduce the temperature threshold for simulating the combustion rate with the Arrhenius correlation. GASFLOW then propagates the flame well from the barely combustible ignition point into the highly combustible region. But compared with the test more hydrogen burns out in the regions with low hydrogen concentrations. In the test flame extinctions occur in the rooms adjacent to the source rooms and leave behind higher unburnt hydrogen inventories. Local mesh refinements and improved turbulence modeling may eventually give better interpretations also for such combustion/extinction processes. There are also considerable sensitivities in the interpretation of this test that come from uncertainties in the distribution of the steam injection over the three banana rooms. The code does of course conserve the combustion enthalpy. In a large containment geometry this should be sufficient to account for the effect of local combustions on the overall convection process as long as local ignitions don't progress into a global combustion process.

4. HYDROGEN COMBUSTION

The combustion related work addresses code development, experiments and code validation based on the test results.

4.1 Code development for turbulent deflagration

The development of numerical models for description of premixed turbulent ´v9*-air-steam deflagration was continued. According to the different regimes of turbulent combustion two different modelling approaches are pursued:

- ERCO-code for the flamelet regime (Ka=reaction time scale/Kolmogorov eddy timescale < 1), and
- COM3D-Code for distributed reaction zones (Da=turbulent time scale/reaction time scale >1) and well stirred reactor (Da <1).

4.1.1 COM3D-code

The turbulence modelling in the COM3D code was extended. The code now offers the choice between two different turbulence models:

- a standard κ-ε, and
- a RNG κ-ε (Renormalization Group Theory).

The RNG model is a modern development of the traditional κ-ε model. An additional term has been added in the ε-equation, which changes dynamically with the rate of strain of the turbulent flow, providing more accurate predictions for flows with rapid distortions and large eddies (**Fig. 4.1**). The RNG model appears attractive for a number of reasons:

- it is applicable to compressible flow,
- the model constants result from a closed theory, not from empirical experiment data,
- it covers low Reynolds numbers, and
- the additional computational costs compared to κ-ε are low (+3%).

Test calculations with the new RNG model are presented in Section 4.3 of this report.

In the field of turbulent combustion modelling the COM3D code now offers an Eddy Dissipation Model for Da>1 and an Arrhenius formulation for the well-stirred reactor (Da<1). This model approach corresponds to a jumping between two states, the actual evolution of the mixing from unburned to burned gas is not treated.

The next logical extension of the combustion modelling is to treat the intermediate mixing states for each component with a presumed β-PDF model. If the joint probability density function (PDF) F is known as function of temperature T and mass fractions f_i, the mean reaction rate ϖ can be calculated from

$$(\rho k)_t + (\rho u_j k)_{x_j} = S - \rho\epsilon + (\frac{\mu_{tur}}{C_k} k_{x_j})_{x_j},$$

$$(\rho\epsilon)_t + (\rho u_j \epsilon)_{x_j} = \frac{\epsilon}{k}[(C_1 - C_\eta)S - C_2\rho\epsilon] + (\frac{\mu_{tur}}{C_\epsilon}\epsilon_{x_j})_{x_j} +$$
$$+[C_3 - \frac{2}{3}C_\eta(C_\mu\frac{k}{\epsilon}u_{j,x_j} + 1)]\rho u_{j,x_j}\epsilon.$$

Here C_η is defined by

$$C_\eta = \frac{\eta(1 - \eta/\eta_0)}{1 + \beta\eta^3}, \qquad \eta_0 = 4.38$$

$$\eta = \frac{k}{\epsilon}\left(\frac{1}{2}(u_{i,x_j} + u_{j,x_i})(u_{i,x_j} + u_{j,x_i})\right)^{1/2},$$

and

$$C_3 = \frac{-1 + 2C_1 - 3m(\gamma - 1) + (-1)^\delta\sqrt{6}C_\mu C_\eta\eta}{3}.$$

Turbulence model constants

	C_μ	C_1	C_2	C_k	C_ϵ	β
RNG k-ϵ	0.0845	1.42	1.68	0.719	0.719	0.012
Standard k-ϵ	0.09	1.44	1.92	1.0	1.3	-

Fig. 4.1: Equations and model constants of the RNG k - ε model as implemented in the COM3D code.

$$\varpi = \iint\ldots\int\omega(T,f_i)\bullet F(f_i)dTdf_i \qquad (4.1)$$

where ω is the real reaction rate of the mixture for given mass distribution f_i and temperature T.

The implementation of such an PDF model into COM3D was started. Compared to the Eddy Dissipation Model only one more transport equation needs to be solved, e.g. for a 4-component system 11 instead of 10 equations. The main difficulty in evaluating Eq. 4.1 at each time step and in each computational node is to develop a fast and still precise numerical scheme for solving the multidimensional integral, which contains singularities at the end points (f_i = 0 or 1).

A major advantage of the presumed β-PDF approach is that it allows also to treat non-premixed combustion, e.g. a hydrogen diffusion flame in a steam-air environment. This is the desired combustion mode which is obtained in a successful (non-energetic) hydrogen control with spark igniters. A β-PDF model would also allow a more mechanistic description of the quench and extinction phenomena in turbulent flames, which are important for flame acceleration predictions.

4.1.2 ERCO-Code

A two-dimensional version of the ERCO-code was completed and tested against RUT-experiments [4]. The numerical scheme models the turbulent flame zone as a reactive discontinuity (no reaction before, complete reaction behind the interface). The laminar burning velocity is calculated from detailed chemistry models and used as input data to ERCO. The effect of turbulence on the burning velocity is modelled with single relations using the local velocity fluctuation. Turbulence is calculated with a standard κ–ε model. Ignition of unburned gas is described with a two-step induction model, fitted to detailed chemistry calculations. Details of the numerical scheme can be found in [4].

The verification calculations performed with ERCO are described in Section 4.4. Since the code contains no free input parameters the comparison to experimental data provides a thorough test of its predictive capabilities.

4.2 Experiments

A large variety of experiments was performed in 1996 to provide test data for different models developed in the combustion codes COM3D and ERCO.

4.2.1 FZK „3 m-tube“

A rectangular test tube (10 cm x 10 cm) was designed and constructed for the visual observation of turbulent H_2-air combustion around flow obstacles. The tube is a scaled-down model of the existing FZK 12m-tube.

The tube was instrumented and tested with a 15% H_2-air mixture and rectangular obstacles blocking 30% of the flow cross section. The tube was damaged at the end from high reflected pressures of the fast turbulent flame. Additional tube extensions without optical access were fabricated and installed, thus avoiding high reflected pressure loads on windows.

The tube was now modified and prepared for testing of Laser Doppler Anemometers (LDA) to measure flow velocities and turbulence generation ahead of a fast turbulent flame.

4.2.2 FZK „12 m-tube“

In 1996 two different types of experiments have been performed in the FZK 12 m-tube:

- experiments on turbulence generation and dissipation in obstructed geometry (inert He/air).
- experiments on turbulent combustion in lean H_2-air mixtures.

The intention of the two test series is to decouple the turbulence and the combustion model development into two sequential steps:

1) verification of turbulence models alone for the relevant flow conditions under inert conditions (He+air), and
2) investigation of turbulence with chemical reaction (H_2+air).

4.2.2.1 He-air turbulence tests

The 12 m-tube was modified to allow inert tests in a shock tube mode, where a 3m long section can be pressurised **(Fig. 4.2)**. After bursting of the membrane a shock wave travels into the remaining section which is initially at low pressure (e.g. 1 bar) and contains circular orifices as obstacles.

The shock wave looses velocity and pressure amplitude by partial reflection and turbulence generation. The measured pressure signals at different locations can then be compared to numerical simulations using different turbulence models. These data allow to verity the turbulence modelling under inert conditions, without interference from a combustion process.

Four experiments were performed in the inert shock-tube mode. **Fig. 4.2** shows one example for the measured pressure decay as the wave proceeds into the obstacle region. These results are compared to COM3D calculations in section 4.3.

4.2.2.2 H_2-air combustion tests

New germanium photodiodes with higher infrared sensitivity were tested and installed. They allow to register flame fronts in lean H_2-air mixtures with high resolution.

A new sampling unit for analysis of the hydrogen concentration in test gases was constructed, tested and applied to the experiments. The principle is to measure the mole change in the test gas due to H_2-air mixtures with high resolution. The results agree well with the H_2 concentration values devived from the mass flow meter readings during the filling.

15 experiments have been performed in the 12 m-tube with different obstacle configurations (blockage ratio 30 to 90 %), initial pressures (1-2 bars) and with lean hydrogen concentrations (8-11% H_2). The test parameters are summarised in **Fig. 4.3.**

Fig. 4.4 shows the data from experiment R0796-02 as an example. In this test the flame accelerated to a terminal velocity of about 170 m/s. COM3D calculations are

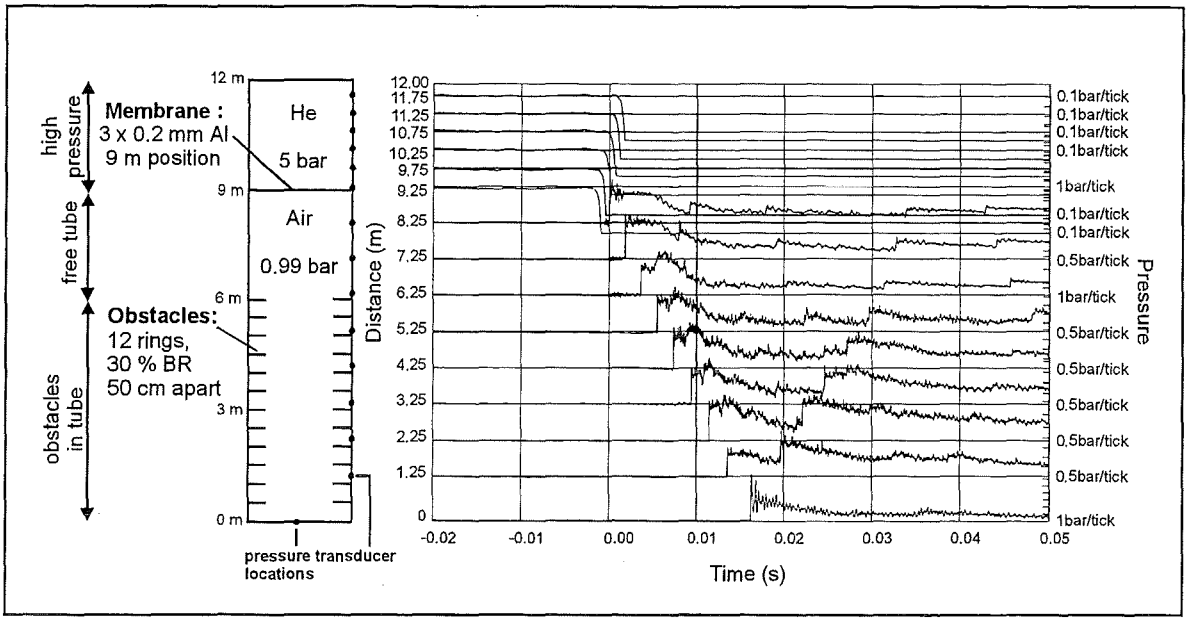

Fig. 4.2: Inert shock tube experiments in FZK " 12 m tube ". The measured pressure data contain information about turbulence generation and dissipation without combustion.

Experiment	BR (%)	p_o (bar)	H_2 (%)
R0696_00	60	1	10
R0696_01	60	2	10
R0696_02	60	1	8
R0696_02a	60	2	8
R0696_03	60	1	11
R0696_04	60	1,4	11
R0796_01	90	1	10
R0796_02	90	1	10
R0796_03	90	2	10
R0796_04	90	1	9
R0796_05	30	1	11
R0796_06	30	1	10
R0796_07	30	1	9
R0796_08	30	1	8,5
R0796_09	30	1	8,5

Fig. 4.3: Combustion experiments performed in 1996 in the FZK " 12 m tube " with lean H_2 - air mixtures, different obstacles and pressure.

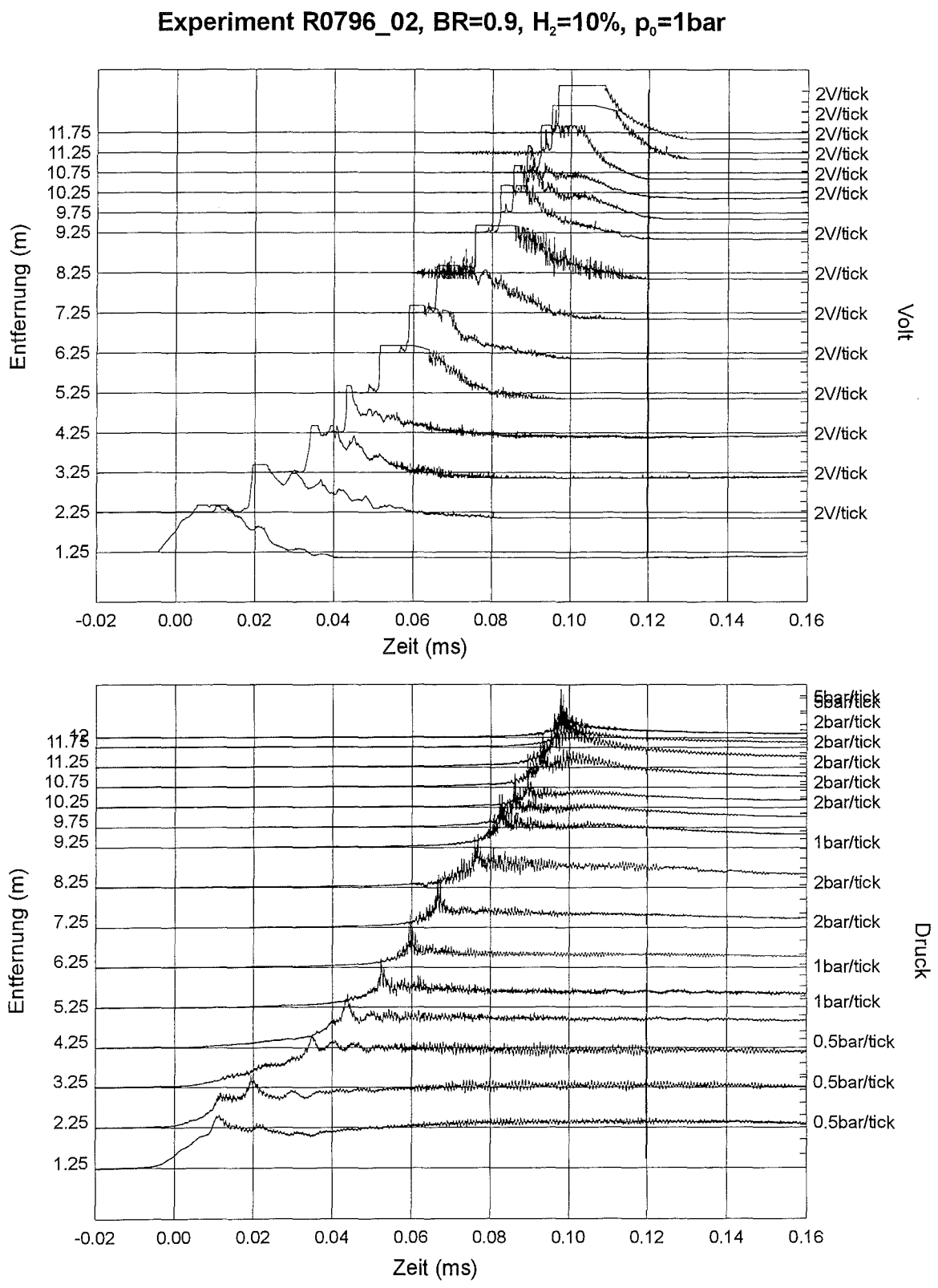

Fig. 4.4: Turbulent combustion experiment in the FZK 12 m - tube with a lean H_2 - air mixture, flow blockage 90 %, photodiode signals in upper figure, pressure signals in lower picture.

currently underway to determine the performance of the eddy-break-up model for lean mixtures and different flow restrictions.

4.2.3 RUT tests with H_2-air-steam mixtures

In 1996 eight large scale tests were performed in the Russian RUT facility to study the critical conditions in hydrogen-air-steam mixtures at elevated temperatures for a deflagration-to-detonation-transition (DDT).

The experimental parameters were

- temperature 80 - 100°C, pressure 1 bar,
- total test volume 480 m^3,
- steam concentration 6.6, 15, and 34-45%,
- hydrogen concentration (dry) 10.5, 18.5, and 29-32%,
- ignition by a weak electric spark.

The test serie was jointly sponsored by FZK, IPSN and NRC, and performed by Kurchatov Institute Moscow in the RUT facility.

Fig. 4.5 summaries the test parameters and the observed combustion regime. **Fig. 4.6** shows the dependence of the combustion mode from the gas composition (hydrogen and steam concentration). The figure includes the results of the first test series in 1995 (denoted 1 to 7). The experiments have shown a clear limit between deflagration and detonation modes. This experimental limit is close to the theoretical prediction using cell size scaling (critical size $\approx$ 7 x detonation cell width), which results in λ about 1 m.

Four types of combustion process were registered in the tests:

- slow deflagration (tests sth4, sth9)
- fast turbulent deflagration (sth6, sth7)
- DDT in the large cavity (sth1, sth2, sth3)
- DDT in the channel (sth8).

An example for a slow deflagration case is shown in **Fig. 4.7**. The flame reached a maximum speed of 200 m/s at the entrance to the large cavity. The evolution of the flame front within the cavity was computed from measured photodiode signals.

File name	Average hydrogen concentration (dry) % vol	Average steam concentration % vol	Minimum steam concentration % vol	Comments
sth1	32.7	34.6	33.4	DDT
sth2	29.0	36-38 ?	30.5-37.5 ?	DDT Uncertain steam concentration
sth3	29.2	39.5	37.7	DDT
sth4	30 ± 1	44	41.2	Deflagration ignition from operating fan
sth6	29.6	45	43.3	Deflagration
sth7	28.8	40.6	38.1	Deflagration
sth8	18.5	15.5	14.0	DDT in 1st channel
sth9	10.1	6.6	4.2	deflagration

Fig. 4.5: RUT combustion experiments with H_2 - air - steam at elevated temperatures

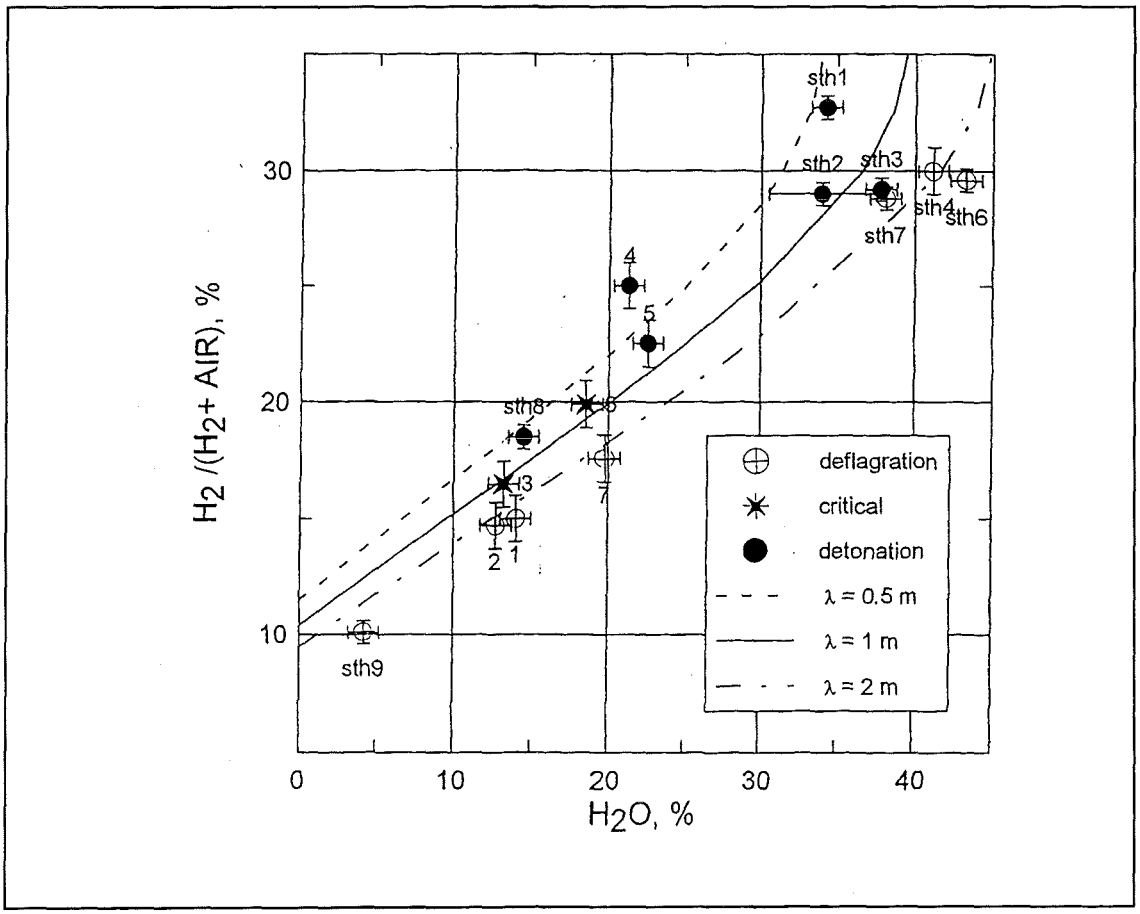

Fig. 4.6: Observed combustion regimes in large scale RUT experiments as function of mixture composition (temperature ≈ 100°C). Experiments 1 to 7 refer to the test series in 1995.

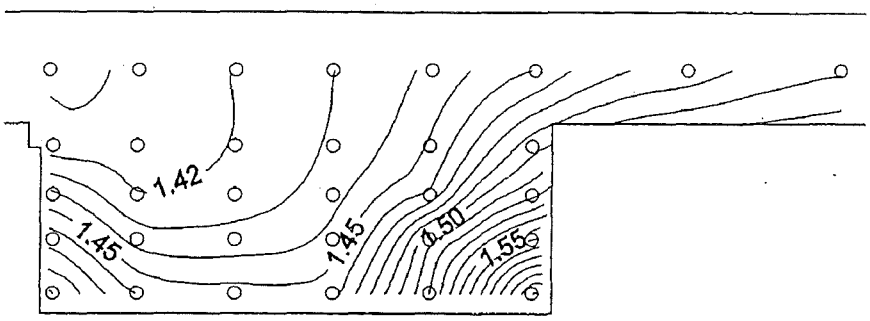

sth9, dt=10 ms

Flame front shape evolution in test sth9. Numbers show time after mixture ignition (s).

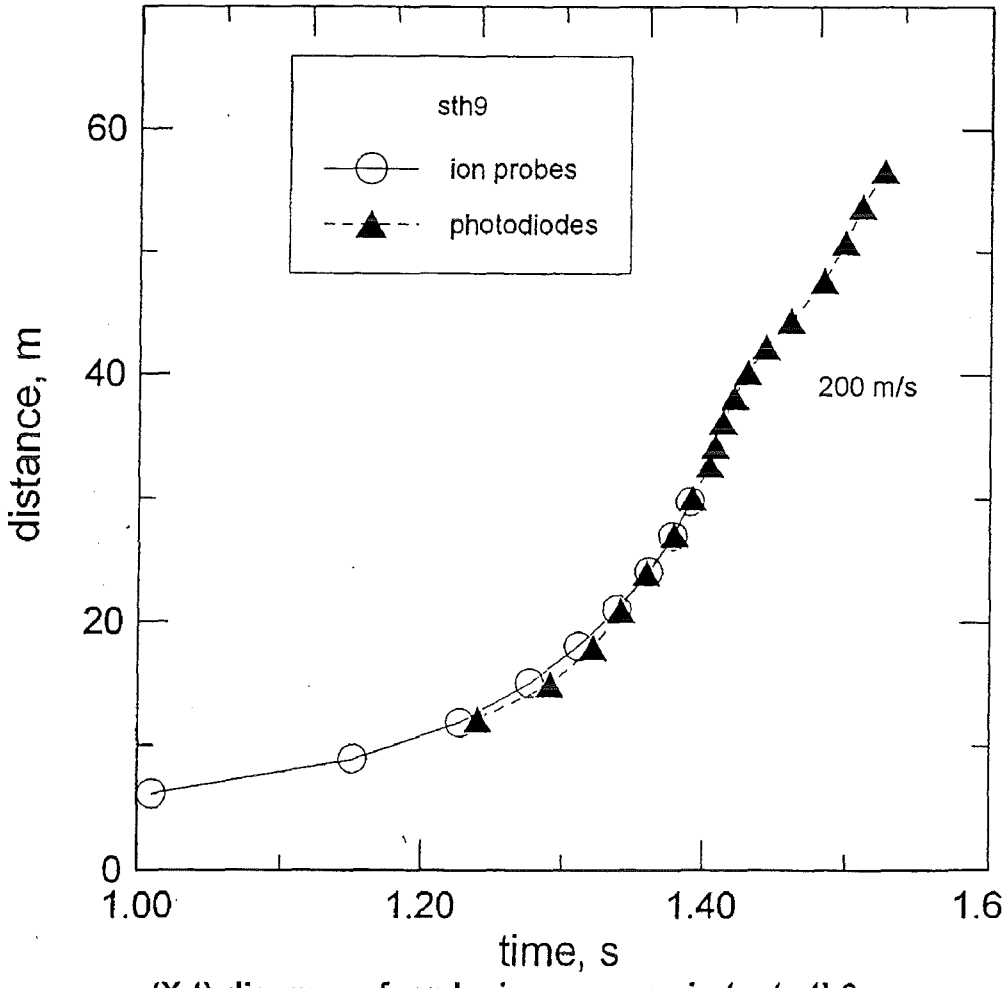

(X-t) diagram of explosion process in test sth9.

Fig. 4.7: Example for a slow deflagration test in RUT facility, 10.1 % H_2 dry, 6.6 % steam. The maximum flame speed was about 200 m/s after a travel of about 40 m.

The opposite extreme in combustion speed is represented by test sth8, in which a DDT occurred already in the first channel after about 25 m flame path (**Fig. 4.8).** The detonation propagated in a stable manner throughout the remainder of the system with the theoretically predicted CJ-detonation velocity (1550m/s).

The RUT tests with steam have confirmed the 7 λ-DDT criterion on large scale for steam containing mixtures at elevated temperatures. They have also provided large scale test data on different combustion modes in H_2-air-steam mixtures which will be used for the verification of numerical models and programs (COM3D, GASFLOW, ERCO).

4.2.4 Quenching in non-uniform H_2-air mixtures

For a realistic simulation of hydrogen combustion in severe accidents the phenomenon of flame quenching must be modelled. Flame quenching can occur e.g. if the flame burns into regions rich in steam or lean in hydrogen. Also the development of high turbulence levels can extinguish the combustion process locally or even globally. Experiments were performed at the Russian Research Center „Kurchatov Institute" which investigated both of these quenching mechanisms. The data will be used for verification of quenching models in numerical codes (COM3D, GASFLOW).

The experimental set-up is shown in **Fig. 4.9**. It consist of a 11.5 m long shock tube equipped with annular orifice obstacles to generate turbulence during the flow. The blockage ratios of the obstacles were BR = 0.3, 0.6, 0.75 and 0.9, where BR = $1-(d/D)^2$, with tube diameter D = 174 mm.

A hydrogen gradient in the tube was generated by inserting a certain amount of pure H_2 into the air filled tube at one end of the tube and by diffusional transport towards the opposite tube end. In a pre-test serie the hydrogen concentration profile along the tube was measured as function of injected H_2-mass and diffusion time. **Fig. 4.10** shows an example. In this case a nearly linear concentration gradient had developed after 16 minutes, ranging from 30 % down to 4 % H_2 in air. By varying the amount of H_2 injected and the diffusion time different gradients could be generated in the tube.

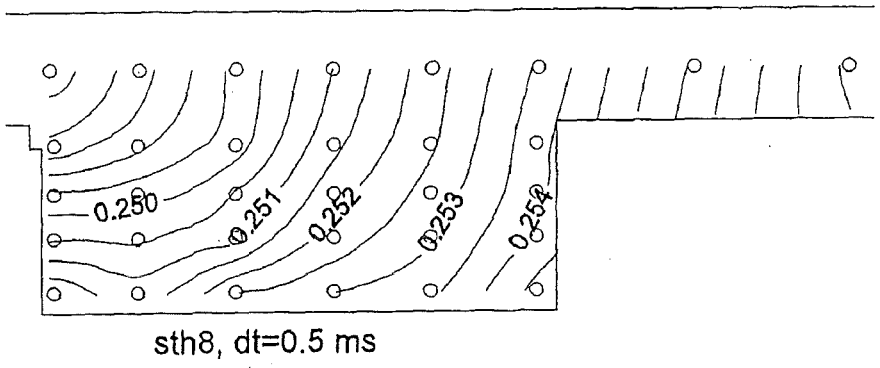

Detonation front shape evolution in test sth8. Numbers show time after mixture ignition (s).

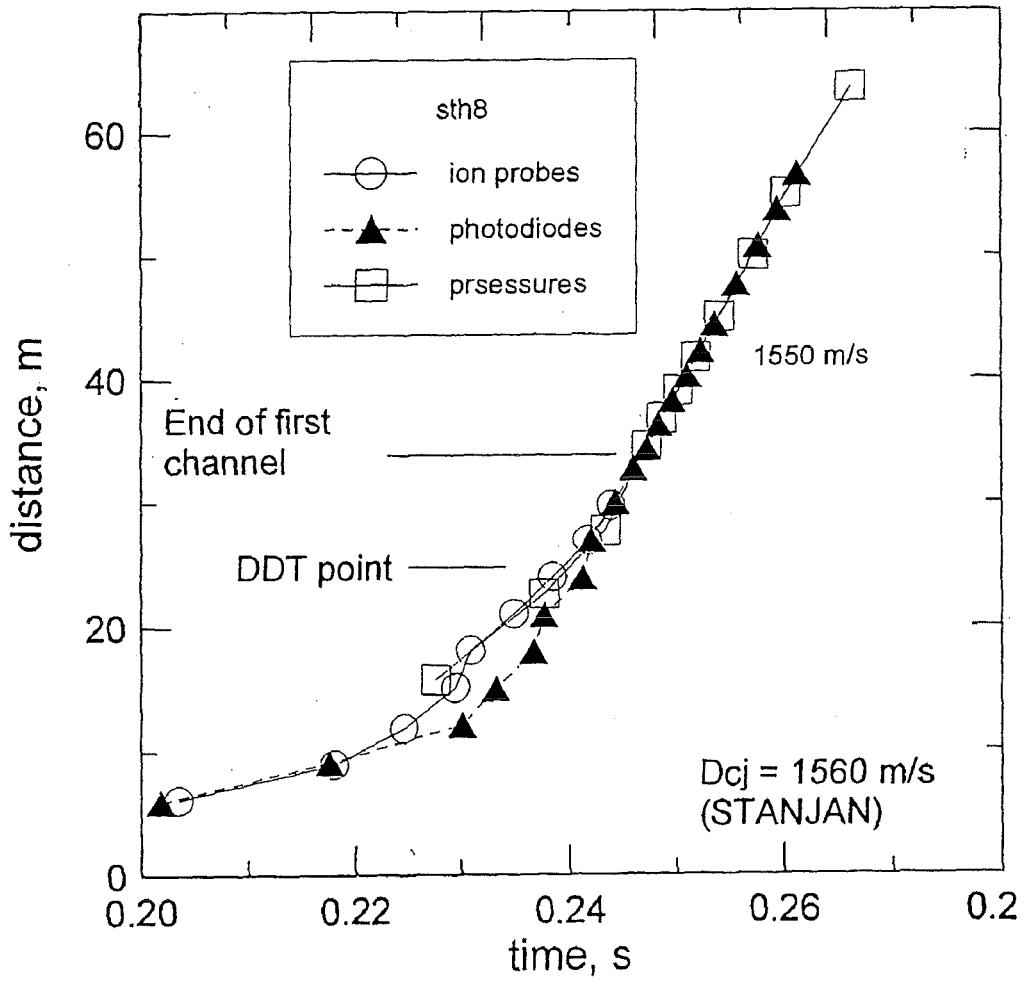

(X-t) diagram of explosion process in test sth8.

Fig. 4.8: Example for a DDT in a large scale H_2 - air - steam mixture at about 100°C, RUT test sth 8, 18.5 % H_2 dry, 15.5 % steam. After DDT a stable detonation propagates throughout the remainder of the facility.

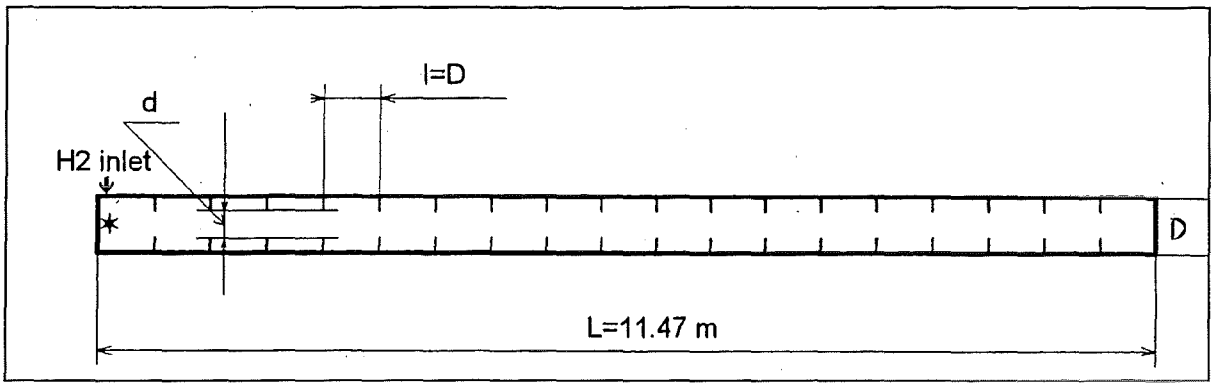

Fig. 4.9: Experiment tube for investigation of quench mechanisms in non - uniform H_2 - air mixtures [5].

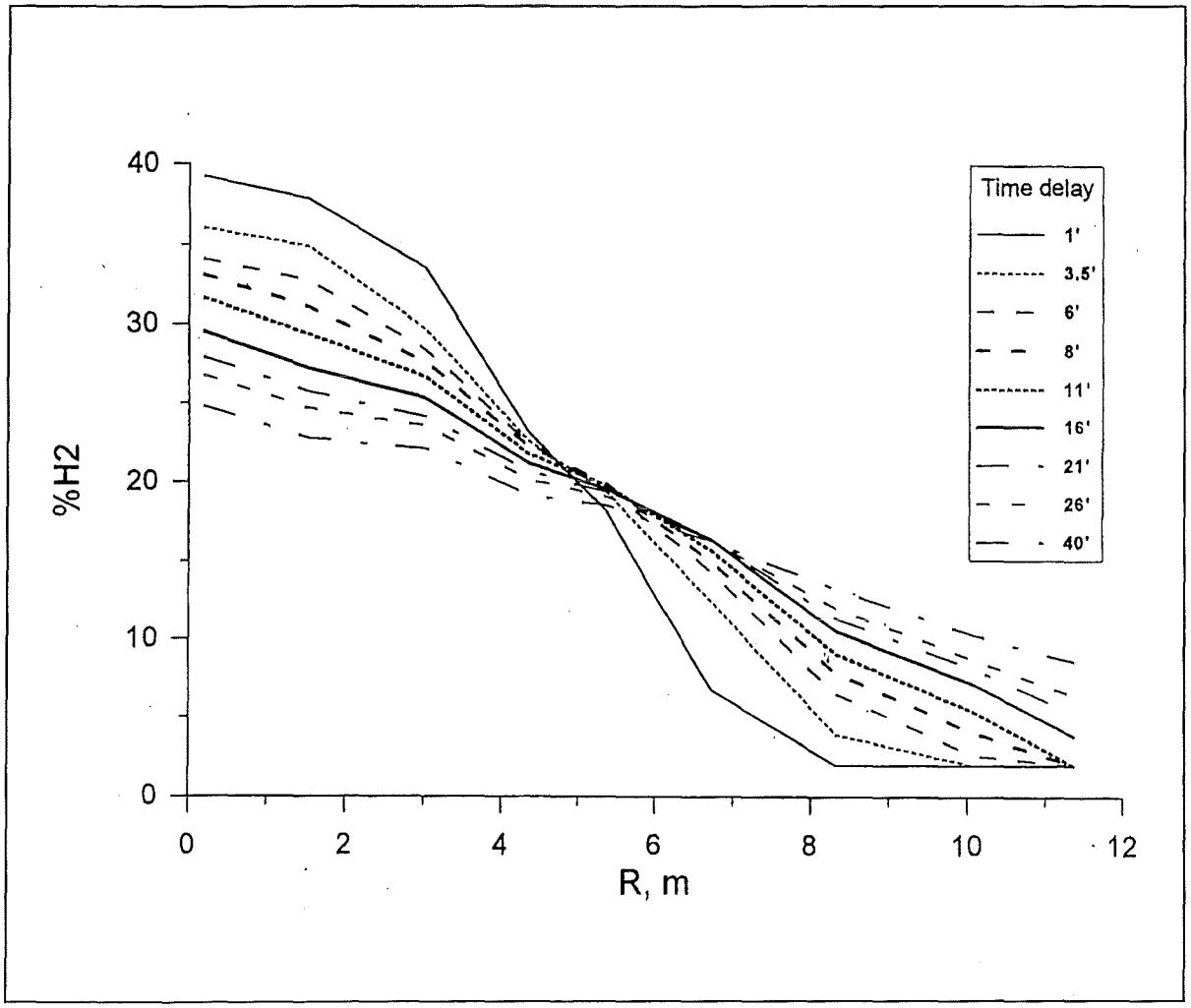

Fig. 4.10: Evolution of the axial H_2 - concentration in the test tube as function of diffusion time [5].

Test variables in the main experiment serie were blockage ratio and average hydrogen concentration. The minimum hydrogen concentration at the end of the tube, opposite to the rich ignition location, was kept constant at about 5 % H_2. The steepness of the H_2-gradient was determined by the amount of H_2 injected. Tests with homogeneous H_2-distribution were also performed for comparison. Photodiodes and pressure transducers were used to resolve the flame and pressure wave propagation. After each test the total mass fraction of H_2 burned was determined from the measured final pressure in the tube at ambient temperature. A total of 30 experiments were performed.

Fig. 4.11 shows as example a test with a hydrogen concentration gradient from 19 to 4.5 % H_2 in air (test GRD54). The combustion was ignited at the rich end (R=0). The flame accelerated to about 500 m/s maximum speed and quenched completely near the 8 m position. These and other test results will be used for the verification of quench models.

In summary the experiments have shown that global quenching can easily occur when a turbulent flame propagates through obstructed channels. Quenching is more distinct in case of a concentration gradient from rich to lean when compared to the homogeneous condition. In the gradient case the flame accelerates very fast at the beginning of the tube, generating high turbulence levels ahead of the flame and resulting in faster quenching. Quenching is increased by the blockage ratio and by a decrease in H_2-concentration.

4.2.5 Flame-vortex interaction

The interaction of an isolated vortex with a flame is a fundamental phenomena of reactive flow which involves all important effects like strain, curvature and quenching. It provides a serious test case for all numerical combustion models. Experiments were therefore performed which investigate the interaction between a single laminar vortex and an initially laminar premixed flame. The experimental data will be simulated with the COM3D code.

The experimental apparatus consists basically of a quasi two-dimensional test chamber, equipped with a fast Schlieren system and an array of photodiodes **(Fig.**

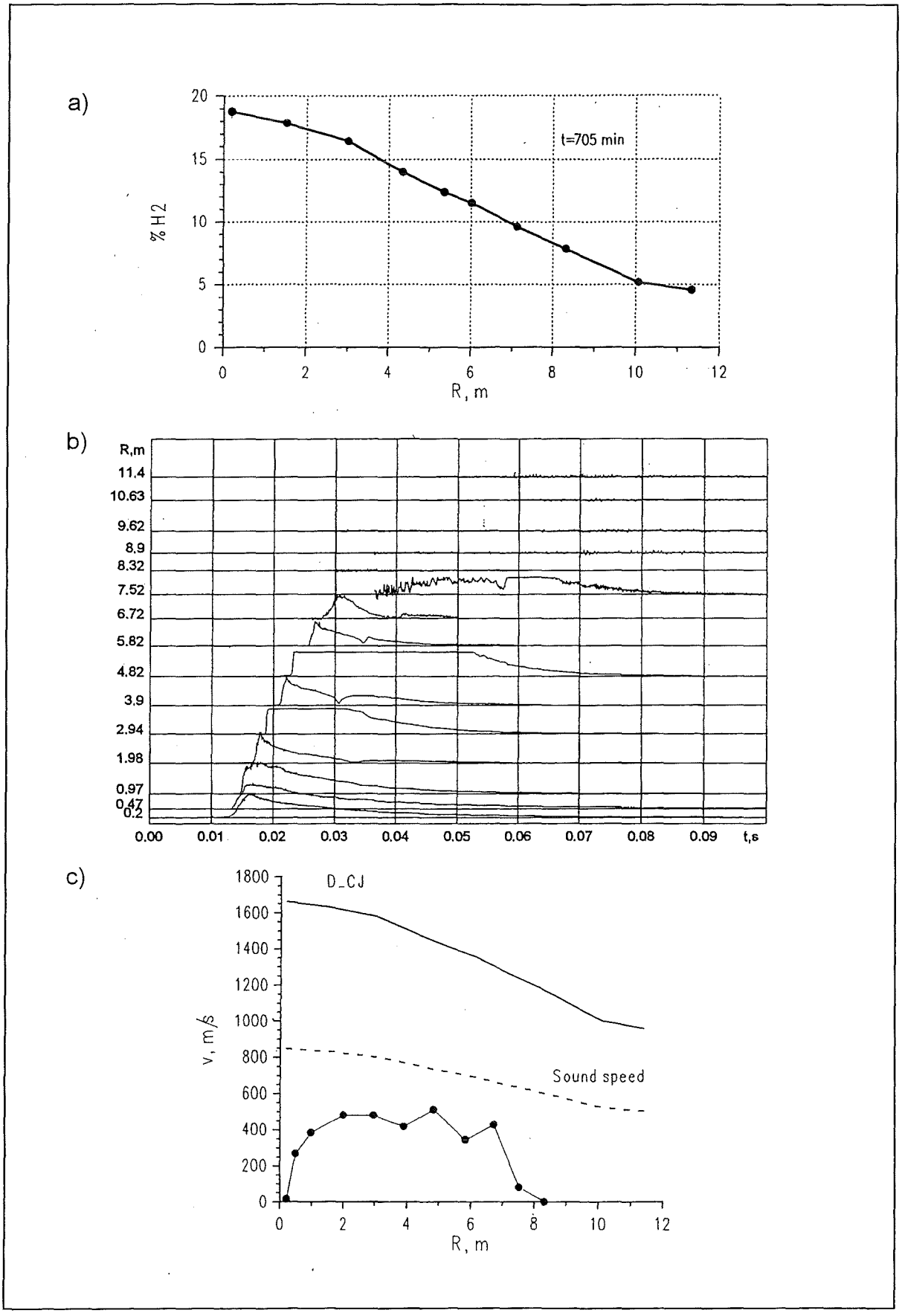

Fig. 4.11: Tube experiment on turbulent combustion in a H_2 gradient:
a) hydrogen concentration gradient (19 - 4.5 % H_2),
b) photodiode signals and
c) resulting flame speed in test GRD 54 [5]. Quenching occurred near the 8 m position. The data will be used for validation of quench models.

4.12). The vortex ring was formed by transmitting a shock wave through a circular orifice. The vortex velocity was in the range of 80 ±10 m/s. The experiments were conducted in lean H_2-air mixtures (8-15% H_2) in which quenching effects can be expected.

Three different arrangements of flame and vortex were investigated:

- vortex of unburned mixture moves towards the flame **(Fig. 4.12a)**,
- the vortex of unburned mixture moves through flame kernel **(Fig. 4.12b)**,
- a burning vortex moves through unburned mixture (**Fig. 4.12c)**.

The experiments require careful synchronisation of all events: mixture ignition, electromagnetic release of the membrane piercer, light flash time marker, high speed camera starting, recorder triggering and illuminating laser flash. **Fig. 4.13** shows an example from the first test series. The vortex of unburned gas compresses the flame front in the first frame, then enters the flame and burns out rapidly in the last two frames. The signals of the installed photodiodes show distinct transient reductions in light during this interaction, which is due to quench effects.

The experiments can be summarised as follows:

- For a vortex moving towards a flame front, the character of the interaction depends mainly on the hydrogen concentration. With concentrations of about 15% H_2 the flame easily penetrates into the vortex and very fast combustion is observed. With lower H_2 concentrations the flame is delayed and often quenched by the vortex flow.
- When a vortex moves through a flame kernel, the outcome depends on the size of the kernel. Small kernels ($\leq$ 6 cm in these tests) are partially or completely quenched, large kernels can penetrate into the vortex and cause complete burn-out.
- When a burning vortex enters unburned mixture the result depends strongly on the H_2-concentration. Varying the H_2-content from 10 to 12.5% changed the interaction from complete quench of the vortex, over partial quench, to intensive ignition of the mixture.

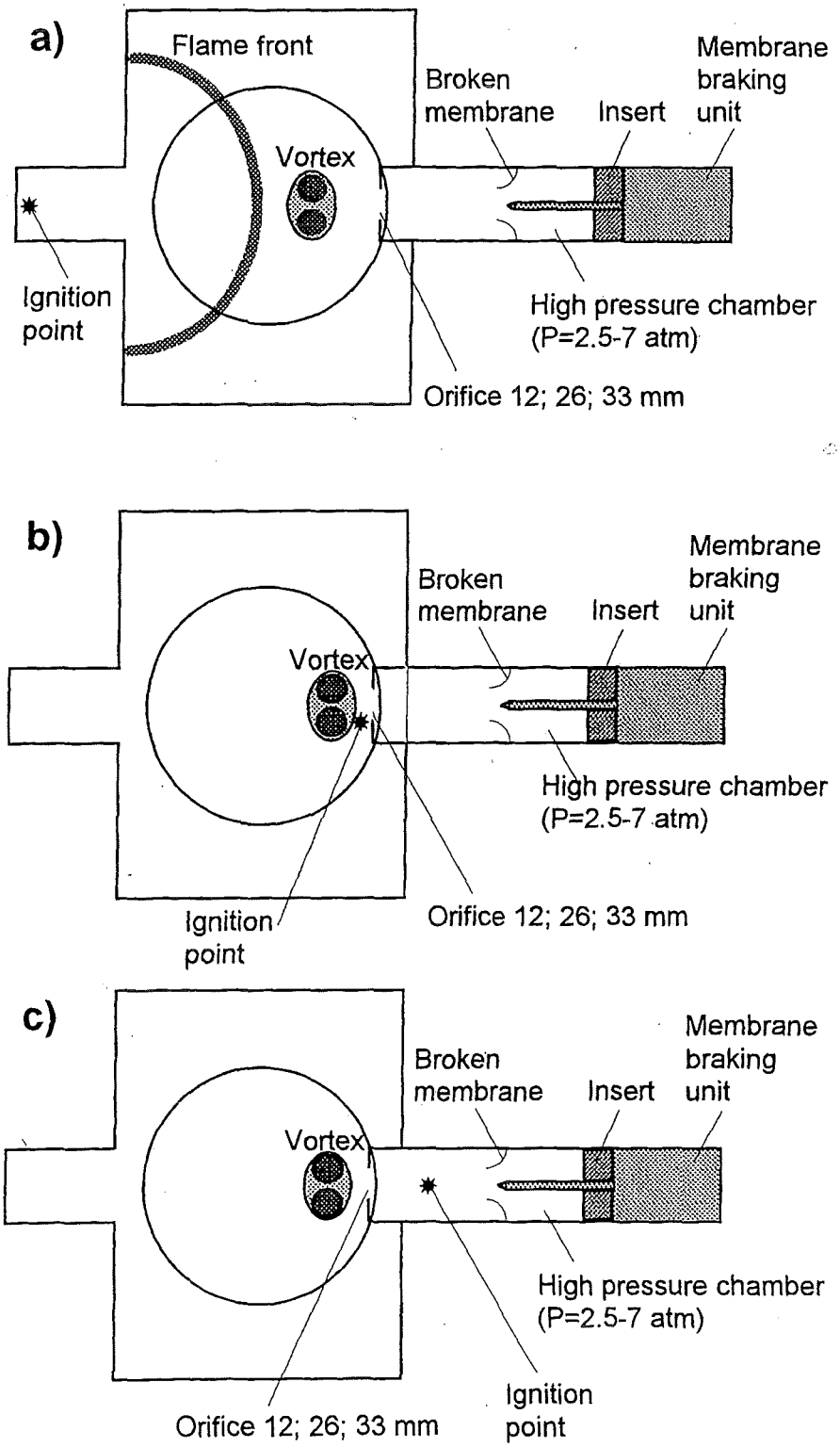

Fig. 4.12: Experimental set - up for flame - vortex interaction tests:
a.) unburned vortex moves towards flame,
b.) unburned vortex moves through flame kernel,
c.) burning vortex moves through unburned mixture [5].

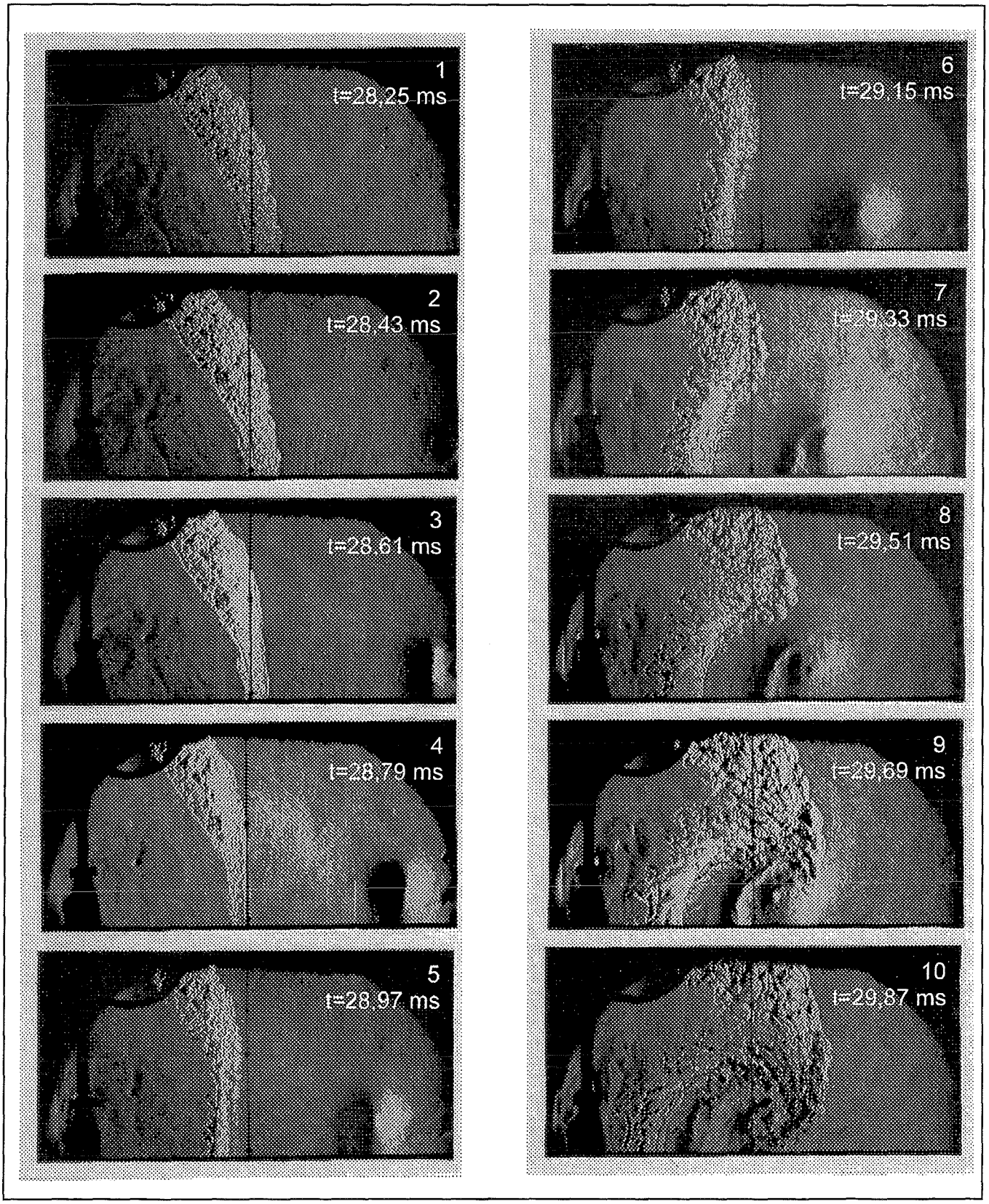

Fig. 4.13: Schlieren pictures of a vortex interacting with a turbulent flame front. The vortex approaches from the right, experiment st142, 15 % H_2 in air. Photodiode signals showed transient quenching of the flame [5].

The experiments will be modelled with turbulent combustion codes. An example is given in Section 4.3.

4.2.6 Turbulent deflagration in H_2-air-steam-fog systems

All severe accident sequences involve partial or complete discharge of hot primary coolant water/steam into the initially cold containment. Steam condensation will create air-steam-fog mixtures, where fog can be considered as nearly mono-dispersed microdroplets in a carrier gas (initially air and steam). Fog from condensation processes must be distinguished from spray, typical droplet diameters being 1-10 μm and > 100 μm, respectively. Fog droplets suspended in a H_2-air-steam mixture can act as a heat sink that absorbs a large amount of the combustion heat by vaporisation and heating of the additionally created steam. The flame may be inhibited or quenched, pressure and temperature development from H_2-combustion will be reduced. For a flame speed of 2-3 m/s the drop residence time inside the combustion zone is about 0.5 ms. Such times are sufficient to entirely vaporise fog of less than about 8 μm diameter.

The presence of fog may therefore be an inherent mechanism to mitigate hydrogen combustion effects in serve accidents.

Since up to now no systematic data on combustion in H_2-air-steam-fog systems were available, experiments were performed at the Russian Academy of Sciences in Moscow which use fog particle sizes, adequate to typical accident situations. A shock-tube method and bomb-type experiments with new types of nozzles were developed.

Fig. 4.14 gives a schematic view of the heated shock tube for studying flames in H_2-air-steam-fog systems. The high pressure section (HPS) was heated to 410-420 K. First a controlled mass of water was inserted into the HPS and vaporised. Then a hydrogen-air mixture was added through a preheated inlet until the membrane failed (4.2 and 11 bar with two different membranes). The adiabatic expansion cooled the gaseous H_2.air-steam mixture and fog formation occurred. After a preset delay time an exploding wire ignited the mixture, which contained 16 and 20 % H_2, respectively. Two different outflow cross sections were used to vary the flow velocity in the tests.

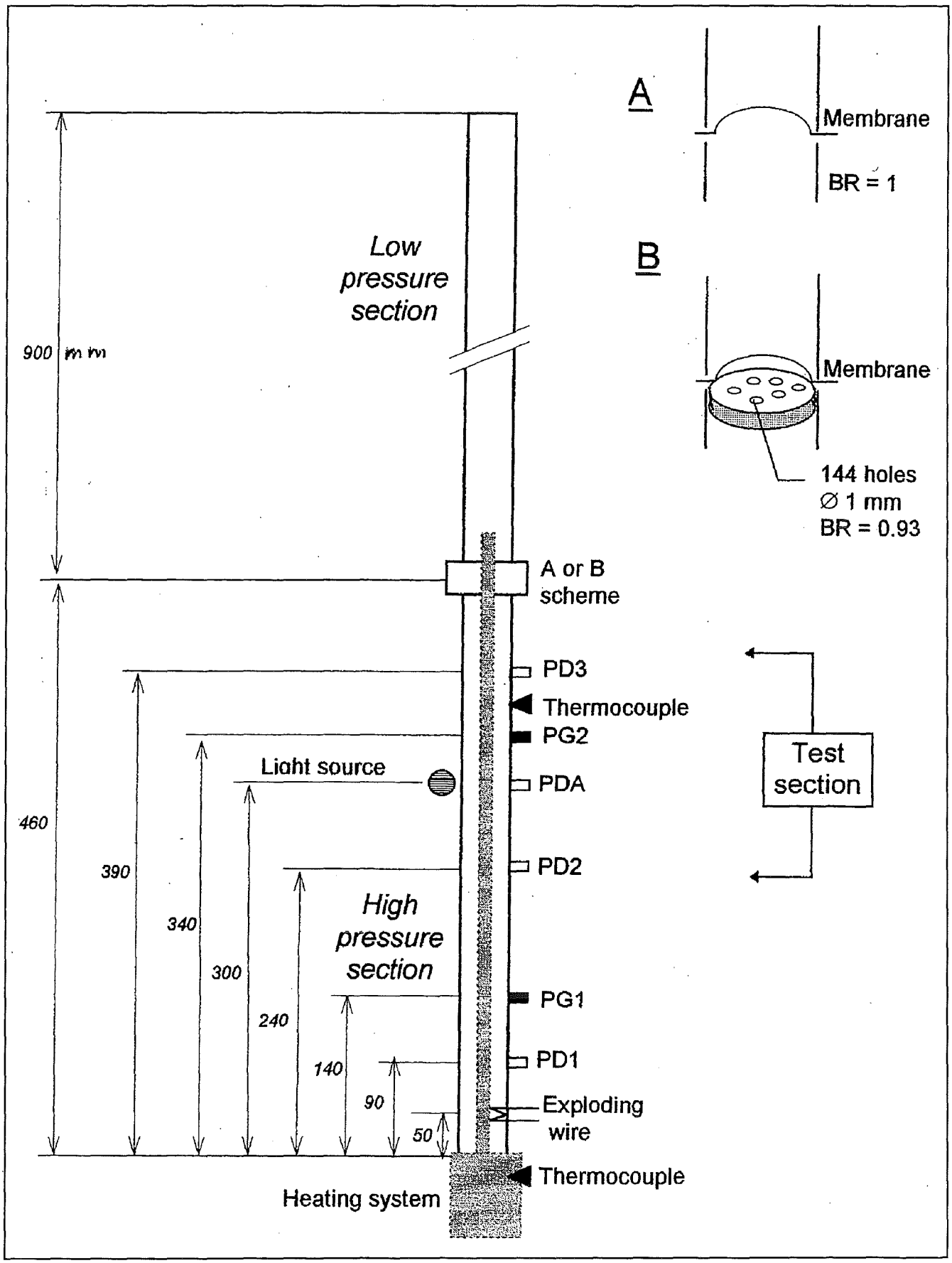

Fig. 4.14: Scheme of heated expansion / shock tube for studying H_2 - air - steam - fog systems. PG = pressure gauges, PD = photodiodes, PDA = extinction meter, A, B = membrane sections with different blockage ratios for fast and slow expansions.

The main results for the fast and slow expansion tests are summarised in **Fig. 4.15** and **4.16**, respectively. The data show that the presence of fog can have a strong mitigation effect on the combustion dynamics in lean H_2-air-steam mixtures (16-20 % H_2). The flame velocities, the peak pressures and the rate of pressure rise decrease all significantly with increasing fog concentration.

A second test series on the combustion in foggy H_2-air-steam mixtures was performed in a spherical explosion bomb (**Fig. 4.17**). The vessel is heated to 373-393 K. Fog was created in two ways:

a) by cooling and condensation of superheated water vapor,
b) by mechanical dispersal of a water jet passing through a specially designed nozzle.

The main results are presented in **Fig. 4.18**. The solid line is a thermodynamic calculation for a stoichiometric saturated H_2-air-steam mixture without fog. The dashed lines are calculations for mixtures containing fog. The given percentage refers to the fraction of fog, e.g. 20 % of the total water is present in so small droplets that they vaporise completely in the flame, 80 % of the water is present in the gaseous state.

The solid and open points are experimental data in mixtures containing 20-30 % of the total water in liquid form, produced in the two different ways described above.

The effect of liquid water increases rapidly with decreasing H_2-concentration because of the decreasing flame temperature in leaner mixtures. A very significant observation is that quenching occurred consistently below 14% H_2. According to the present experiments fog has a strong effect on the flammability limit, which has so far not be considered in severe accident analysis.

4.3 COM3D-code validation

A substantial effort was devoted in 1996 to verify the different models of the COM3D-code in a step-by-step procedure. **Fig. 4.19** summarises the main components of the code. Different sub-sets of these models were tested on increasingly complex problems.

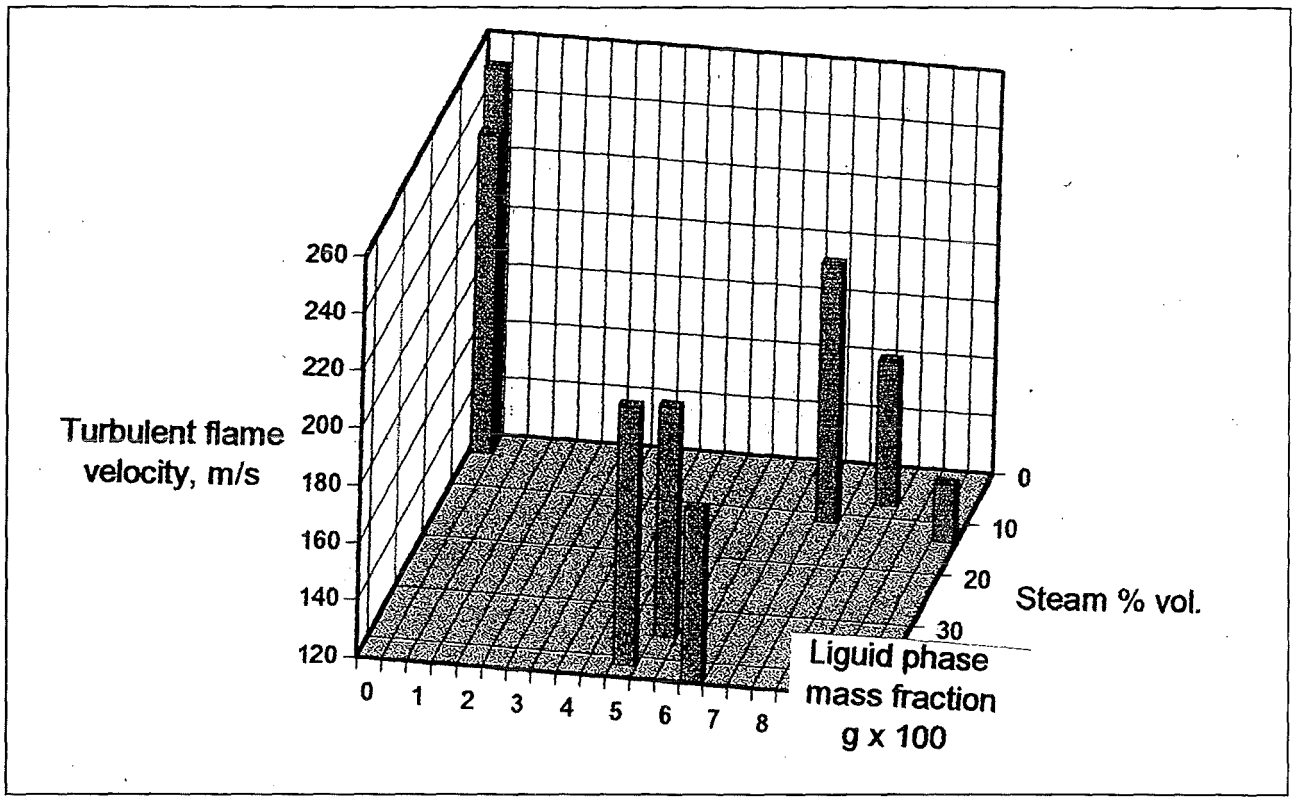

Fig. 4.15: Measured turbulent flame velocities in fast expansion tests as function of steam concentration and fog mass fraction [6]. The presence of fog can significantly mitigate H_2 combustion dynamics.

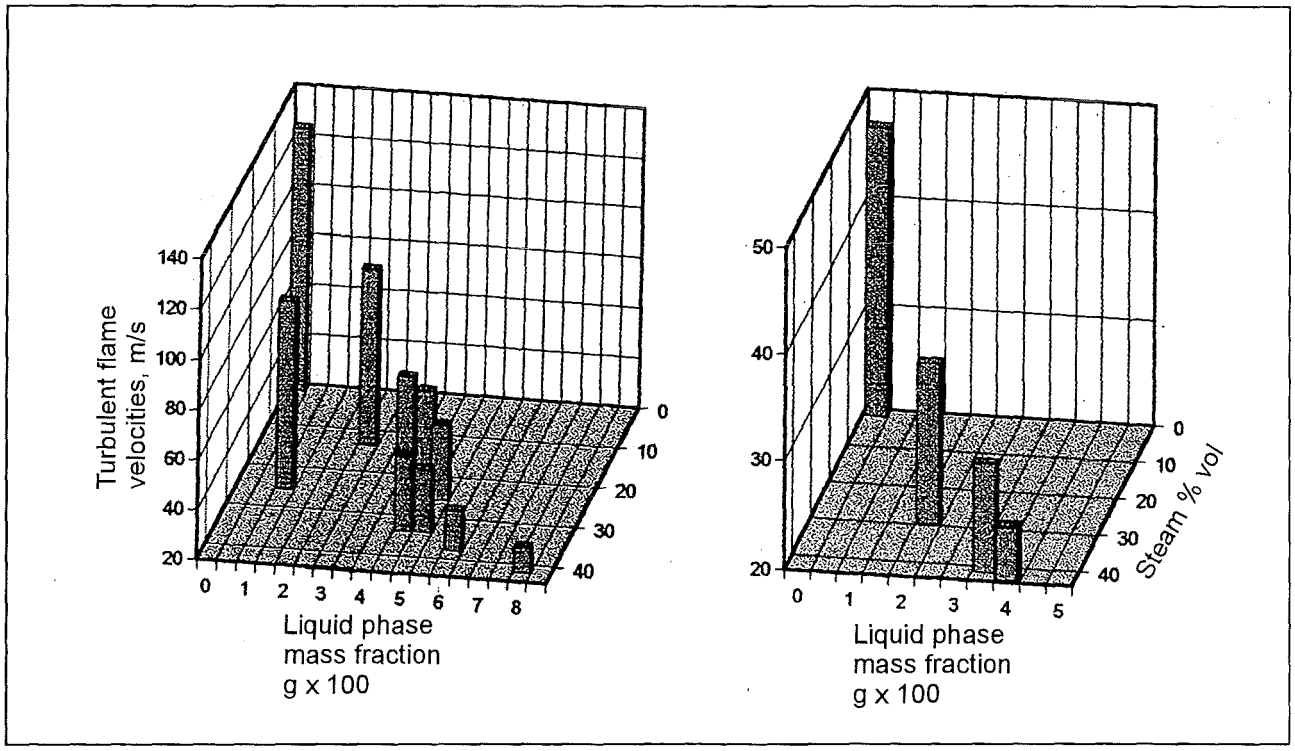

Fig. 4.16: Measured flame velocities in slow expansion experiments. The presence of fog reduces flame speeds significantly [6].

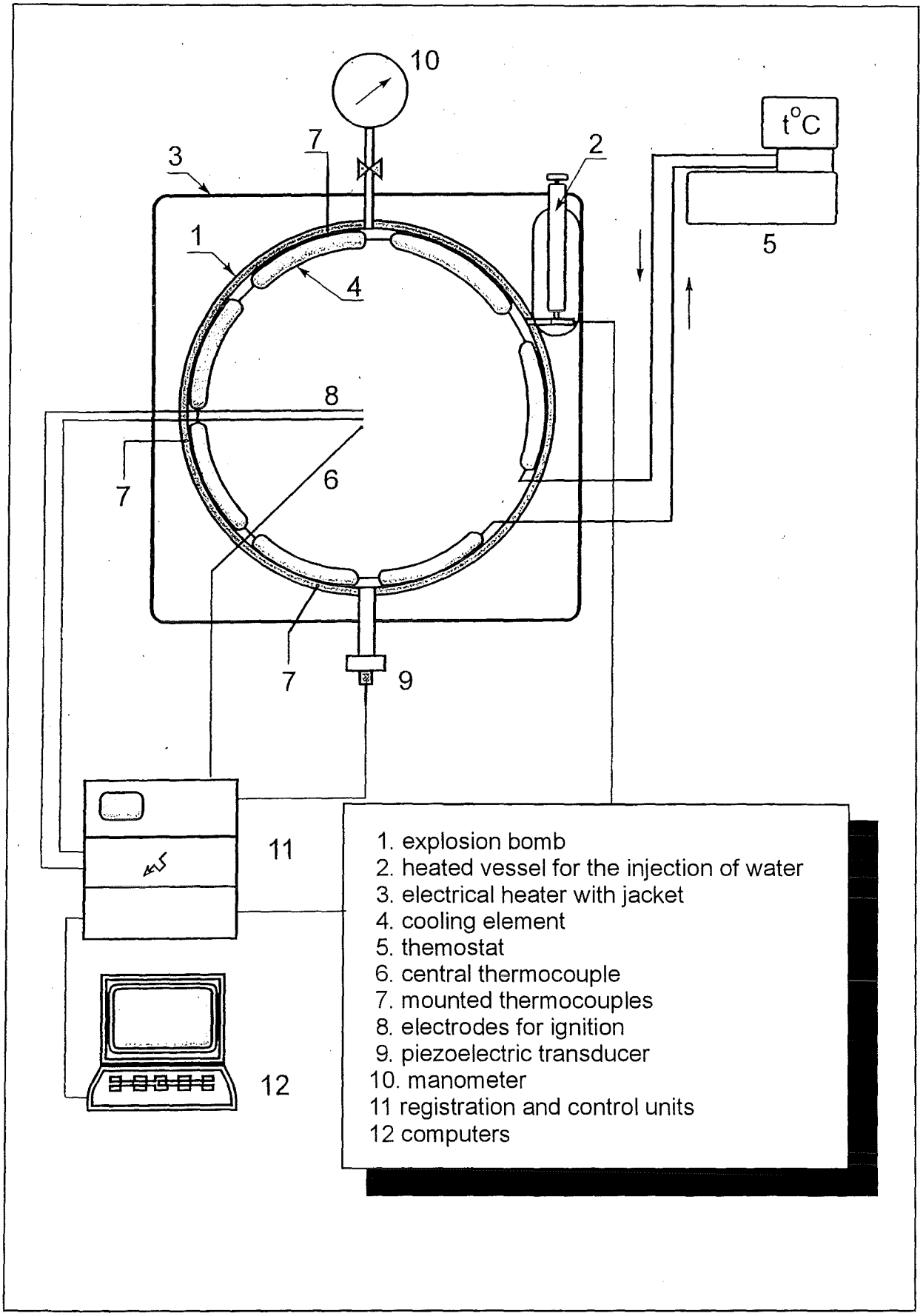

Fig. 4.17: Bomb experiments on combustion in foggy H_2 - air - mixtures [6].

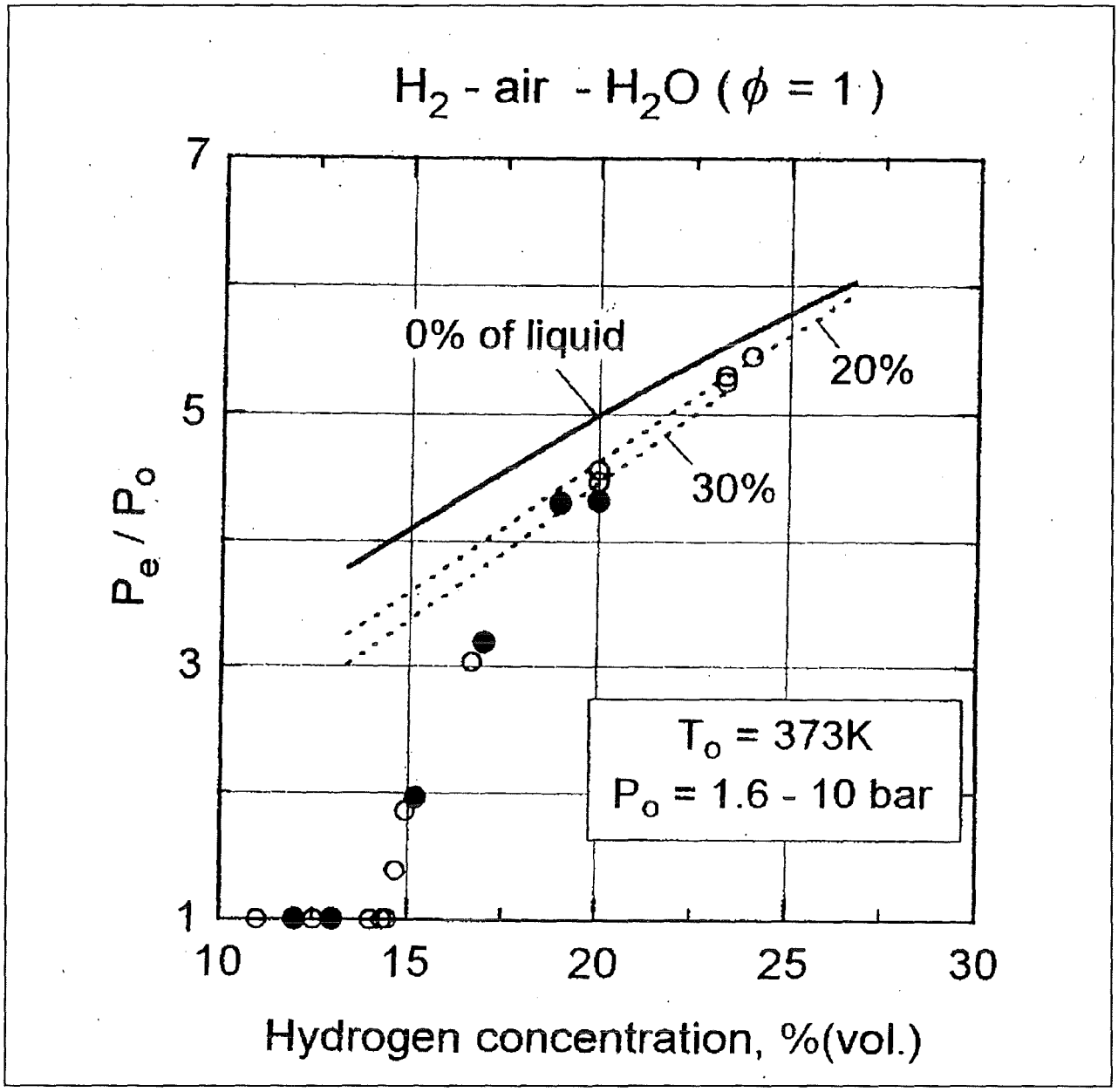

Fig. 4.18: Measured peak pressures in heterogeneous H_2 - air - steam -fog mixtures at elevated temperatures and pressures.

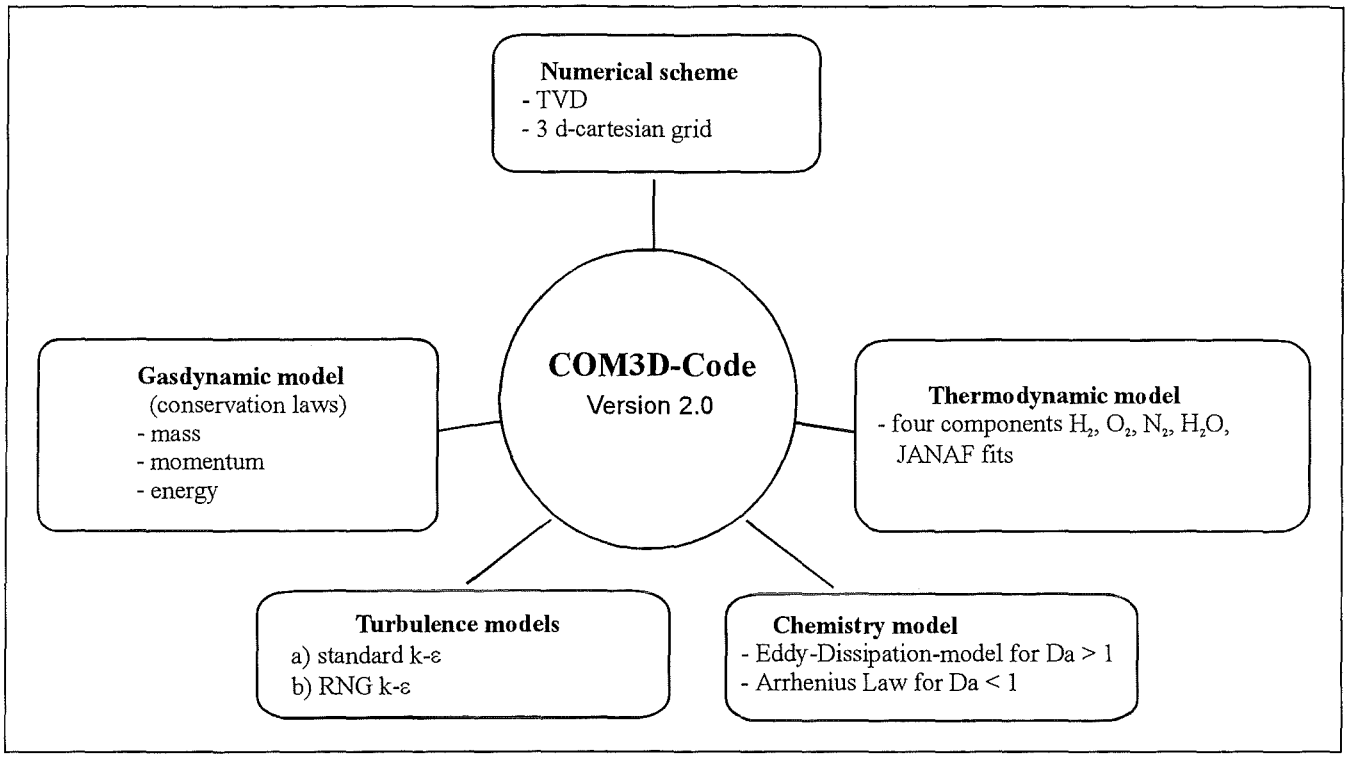

Fig. 4.19: Models of the COM3D code.

4.3.1 The forward facing step

The supersonic flow through a 2-d duct containing a forward facing step was analysed. This numerical test problem has been investigated by many authors using various codes and numerical methods. The correct solution is well known. The problem is a test for the numerical solution of the Euler equations and the thermodynamic data in the COM3D-code for a high velocity case.

The results obtained with three different grids are shown in **Fig. 4.20**. The calculated stagnation pressure, angle of the low shock, shear layer, and downstream shock pattern agree well with the known numerical solutions. The TVD scheme used in the COM3D code preserves shock fronts very well. Even in the coarse grid only about three meshes are needed to resolve a discontinuity.

4.3.2 He-air turbulence tests

The experiment on turbulence generation and dissipation in inert He-air (Section 4.2.2.1, **Fig. 4.2**) was simulated with COM3D using three different turbulence models:

- COM3D without turbulence model
- with κ-ε,
- with RNG κ-ε.

The calculation was performed with a 3-d cartesian grid using a space resolution of 1 cm in each direction. A total of 390000 cells were modelled. **Fig. 4.21** compares the measured pressure signals to the three COM3D calculations.

The calculation without turbulence model shows large deviations from the measured pressure data. These results are clearly inadequate.

Including a κ-ε model improves the agreement with the experiment significantly. The calculation matches the measured pressures associated with the incoming wave very well. The deviation in the 6.25 m-signal is due to the membrane rupture. In the calculation an ideal plane surface is assumed, whereas in the experiment the membrane was deformed to an almost hemispherical shape before rupture occurred. This results in a slightly curved shock wave.

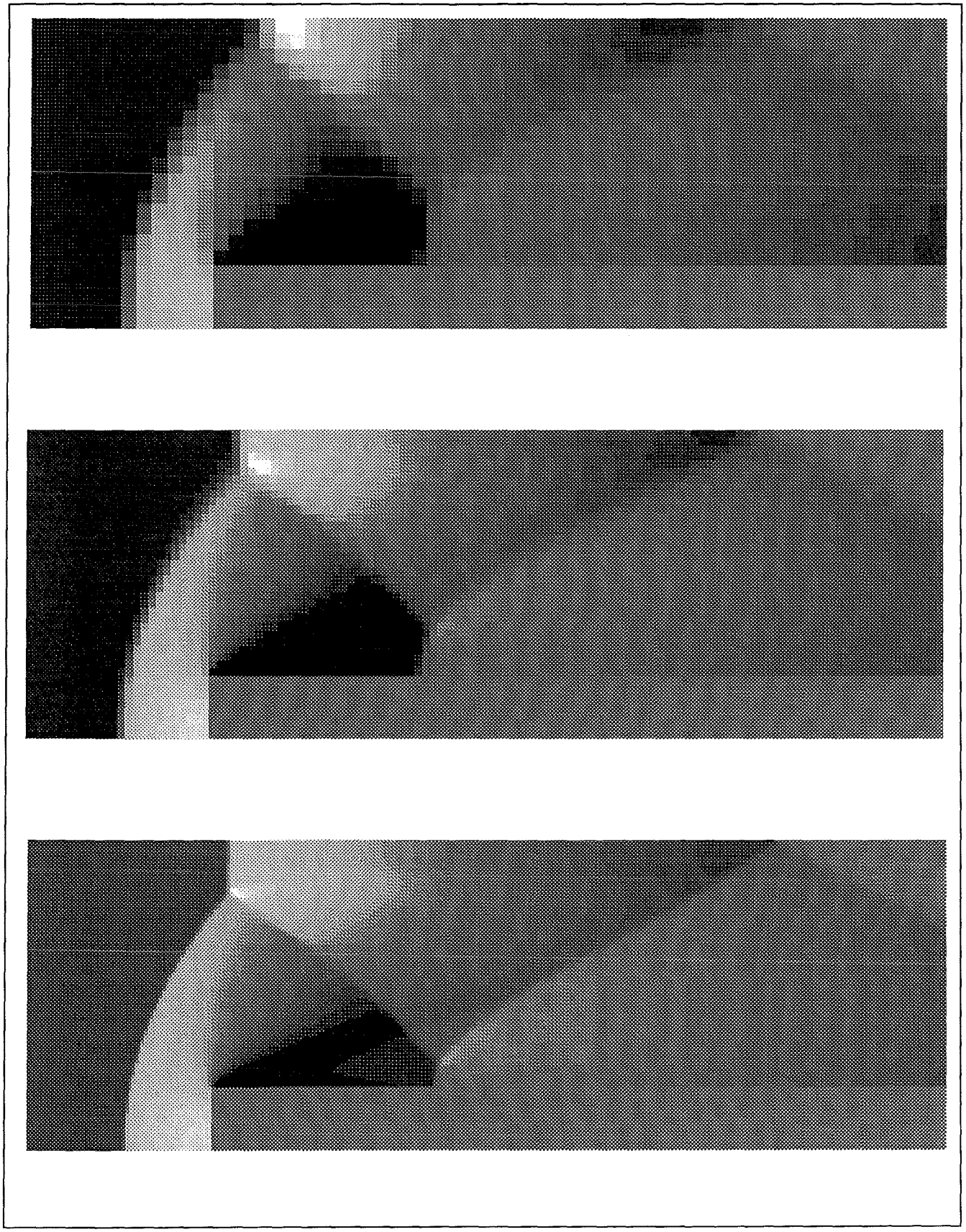

Fig. 4.20: COM3D verification on a hydrodynamic test problem. Supersonic flow through a duct containing a forward facing step: N_2, M =3, p_0=1 bar, T_0 = 298 K. Three grids are shown: 20 x 60, 40 x 120, 100 x 300 cells. The COM3D results agree well with the known solutions.

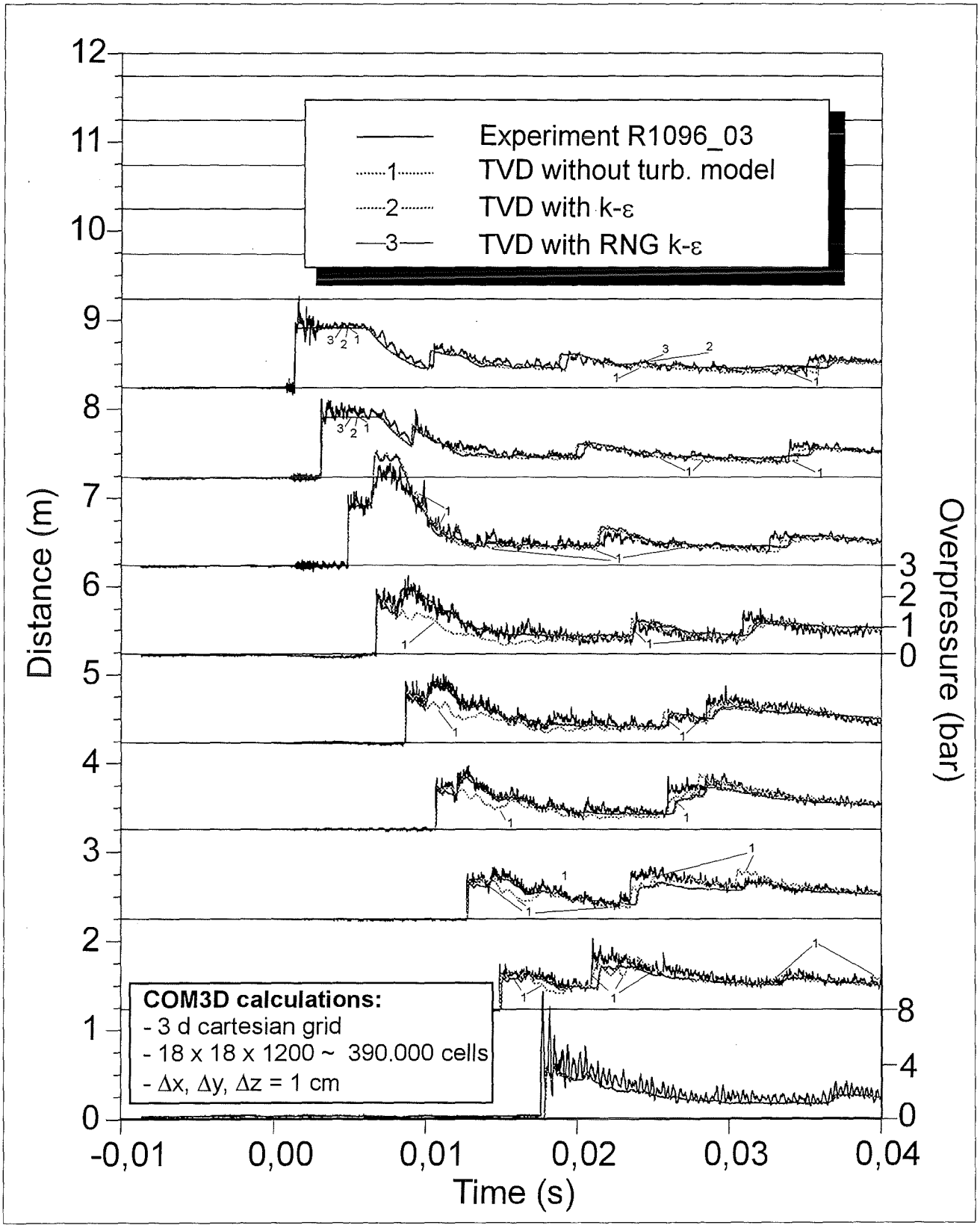

Fig. 4.21: Verification of turbulence models against shock tube experiments in obstructed geometry. Both the k - ε and the RNG k - ε model result in good agreement with the measured pressure data.

The calculation with an RNG κ-ε turbulence model resulted in pressures practically identical to the standard κ-ε model. Very good agreement is obtained for the incoming wave, and slightly too high dissipation is observed for the reflected wave. The last two calculations are indistinguishable on the plot.

The measured and calculated shock trajectories for this experiment are compared in **Fig. 4.22**. This plot allows to investigate velocity results. Shock tube theory for free flow results in 565 m/s velocity for the incoming wave. This agrees very well with the experimental and numerical data in the obstacles free tube section (6-9 m). The annular obstacles (0-6 m) generate turbulence and slow down the wave velocity.

The velocity of the leading shock in this very complex flow field is described well by the COM3D calculations. The simulations of the inert experiment on turbulence generation in an abstracted geometry have shown that the standard κ-ε and the RNG κ-ε turbulence models are both fully satisfactory for describing the turbulence effects on the macroscopic properties (pressures and wave velocities) of the flow.

4.3.3 Flame-vortex interaction

The third step in code verification is inclusion of chemistry into a turbulent flow problem. The flame-vortex experiments were selected as a test problem ([5], Section 4.2.5).

Figure 4.23 shows the interaction of a flame moving from left to right, with a vortex approaching from the opposite direction. The density gradient of the flow field is depicted, simulating in a Schlieren picture. The flame appears as dark curve moving into the unburned gas. The vortex of unburned gas emerges from the narrow channel in the third frame (left column, top to bottom). Pressure waves are visible as grey zones. The vortex and its associated turbulence penetrates into the flame zone and enhances the burning rate.

Fig. 4.23 was obtained with a standard κ-ε model. The calculation with a RNG κ-ε model showed no significant differences in flame propagation and vortex-flame interaction. A noticeable difference was more corrugation of the flame surface with

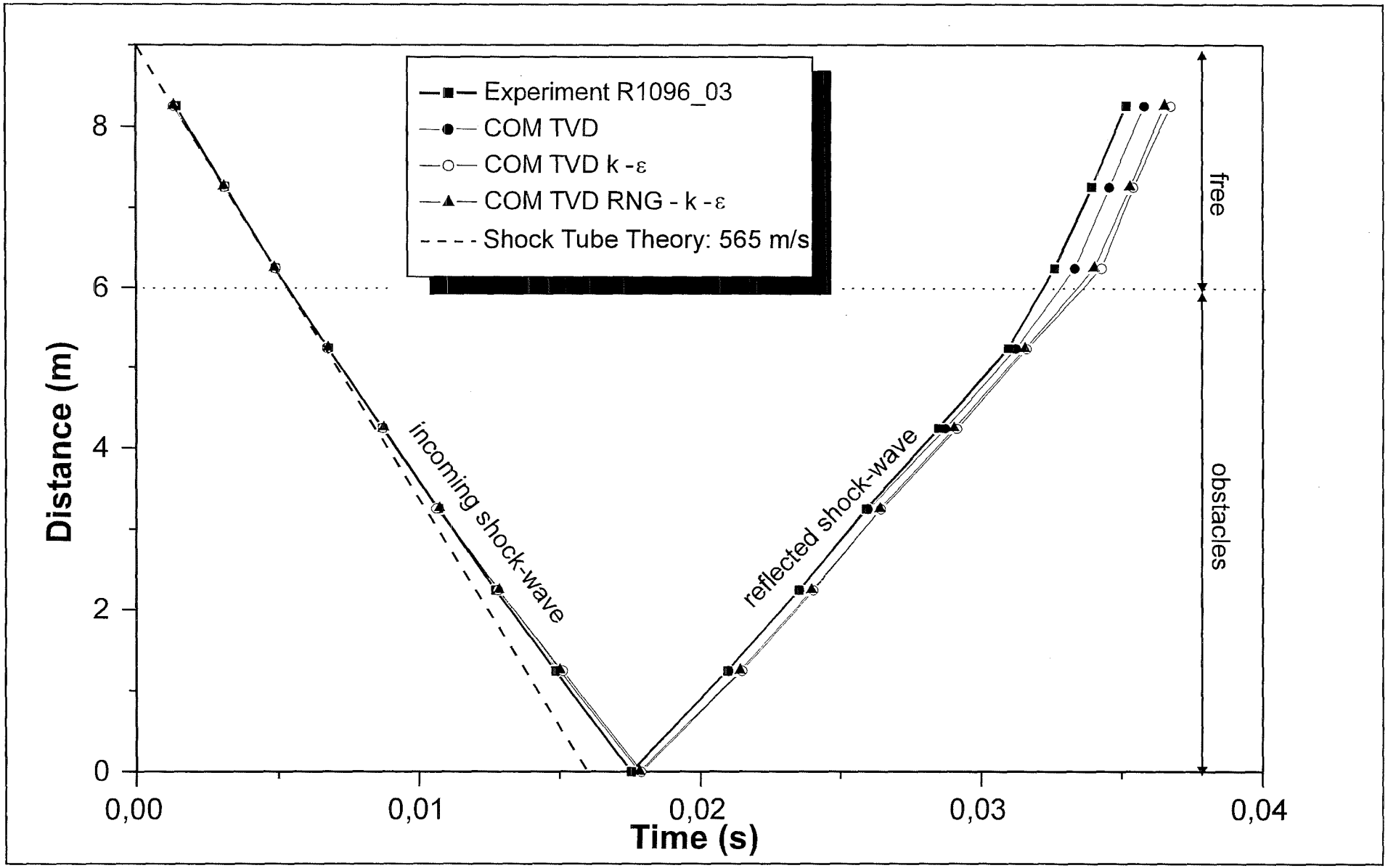

Fig. 4.22: Measured and calculated shock wave trajectories for tube experiment R1096_03.

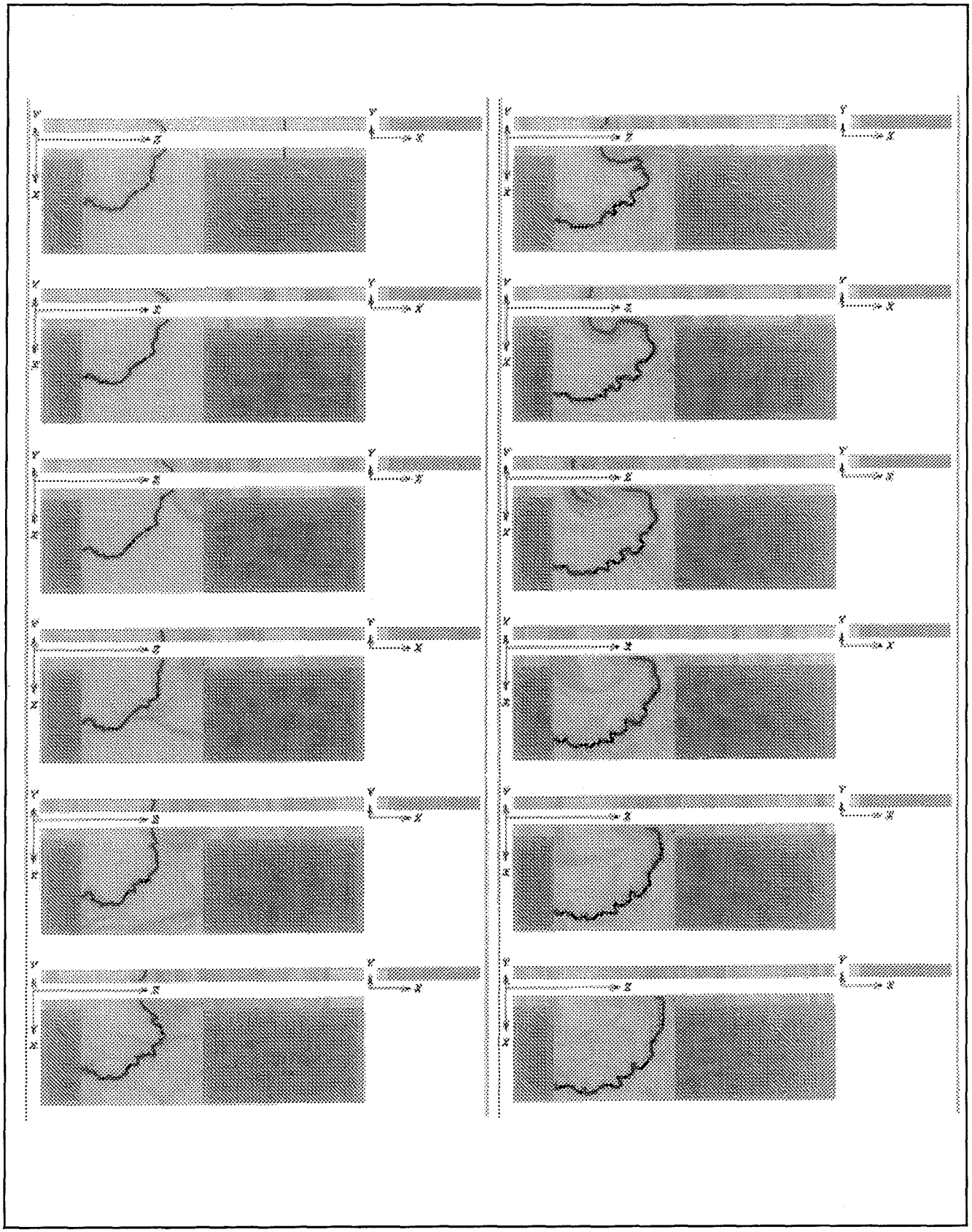

Fig. 4.23: Numerical simulation of a turbulent vortex - flame interaction in a H_2 - air mixture.Shown is the density gradient (Schlieren picture). The flame front moves from left to right (dark line), the vortex from right to left (gray). COM3D calculation with standard k - ε turbulence model.

RNG. The flame front velocity and consequently pressure wave amplitudes and positions were close in both calculations.

It is possible that significant differences could be observed in simulations of fast accelerating flames, producing strong pressure waves and shock waves. A possible conclusion from these investigations is that the turbulence model itself is less important than the chemistry model for predicting turbulent premixed flames.

4.3.4 RUT combustion experiments

The eddy-break up combustion model in the COM3D code contains a reaction rate constant c_f which must be determined empirically from experimental results. A previous series of calculations for turbulent combustion experiments in the 12 m-tube had shown that for quite different experiments a c_f-value of 7 ± 1 gave good agreement with the test data, provided the mixture burned completely in the test.

A second series of calculations was performed in 1996 simulating large scale RUT experiments (**Fig. 4.24**) in order to determine the optimum c_f-values for larger, more reactor typical geometrical scales. **Table 4.1** summarises the turbulent combustion tests for which COM3D calculations were performed, together with the optimum c_f-value, necessary to produce good agreement with the test results (flame speed, overpressures). These tests were selected because they resulted in turbulent flame propagation (no DDT) and because they provided the detailed measured data. The experimental parameters cover a wide range of initial conditions (p_o, T_o, % H_2, % steam), geometrical configurations (S_1=opening from first channel to canyon, S_2=vent opening of second channel, BR=blockage ratio of installed obstacles, and maximum flame speeds in the first channel (v_{max}).

Fig. 4.25 compares measured and calculated positions of the flame front as it accelerates along the obstructed first channel. Ignition was near the 1.4 m position by a weak spark. It is remarkable that despite of the quite different initial conditions (%H_2) and geometries (S_1, S_2, BR), the flame path can be modelled well with a nearly constant c_f-value (6 or 7). The maximum flame speeds varied significantly (factor 3). The calculations were done with a numerical grid size of 12.5 cm (44x50x 50 $\approx$ 1.100.000 grid cells).

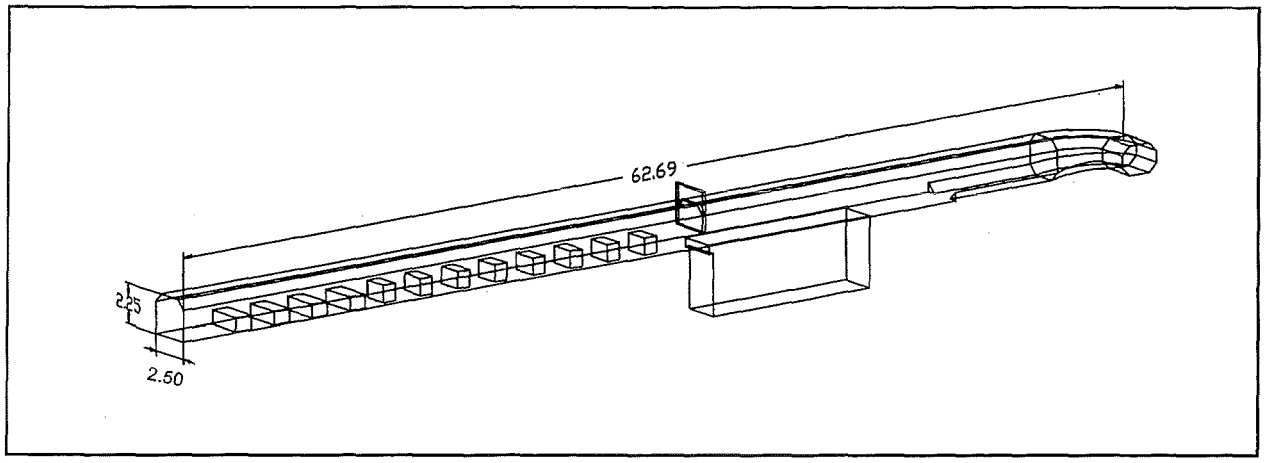

Fig. 4.24: Schematic view of RUT facility, consisting of first channel (equipped with obstacles), large cavity, and second channel leading to exit. All dimensions are shown on same scale (Autocad plot).

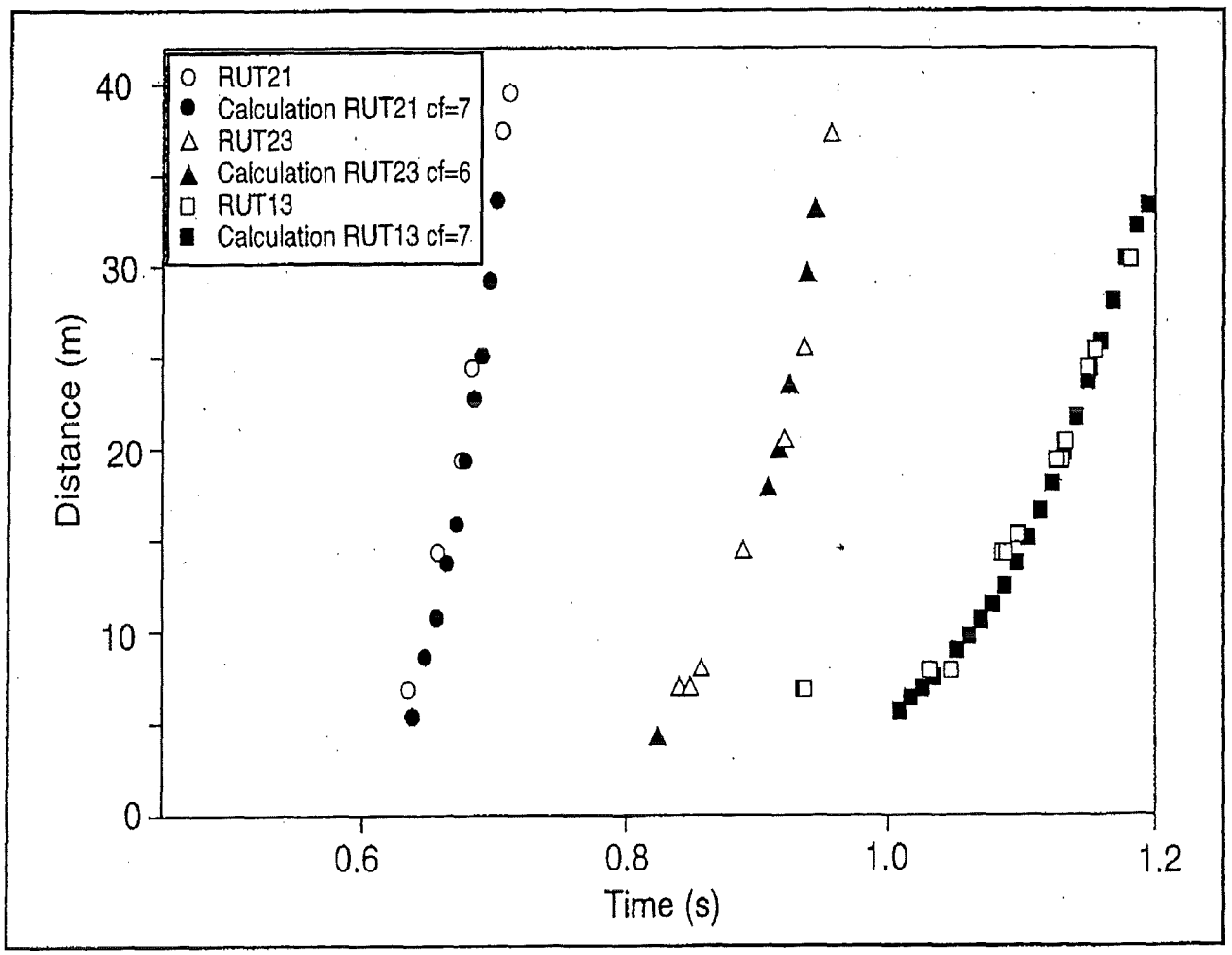

Fig. 4.25: Comparison of measured and calculated flame front trajectories in the first channel of the RUT facility (0 - 34 m).

Table 4.1 Experimental conditions of simulated RUT-tests and resulting Eddy-break-up coefficient c_f giving the best agreement with measured data.

Test	p_0 (bar)	T_o (K)	H_2 (%)	H_2O (%)	S_1 (m^2)	S_2 (m^2)	BR	v_{max} (m/s)	Optimum c_f value
13	1	280	11.0	-	2.0	0	30	210	7
17	1	280	11.0	-	5.6	2.5	30	440	6
19	1	280	12.5	-	5.6	2.5	0	35	9
21	1	280	12.5	-	5.6	2.5	60	650	7
23	1	28	11.2	-	5.6	2.5	60	340	6
stm2	1	370	14.7(dry)	14.7	5.6	2.5	30	680	10
stm7	1	370	17.5(dry)	25.7	5.6	2.5	30	680	10

In test 19 without obstacles the optimum c_f-value differed noticeably from tests 13, 17, 21 and 23. The most likely reason is that the calculated turbulence level is too low for two reasons:

- the κ-ε model does not include turbulence generation at the walls
- small obstacles in the channel (crane, instrumentation and cable piping) are not included in the geometrical COM3D model.

Then the turbulent time scale κ/ε in the eddy-break-up reaction rate $\overline{\omega}$:

$$\overline{\omega} = - c_f \frac{\varepsilon}{k} \min (y, 1 - y) \qquad (4.1)$$

becomes too small and must be compensated by an increased c_f value (y = fuel mass fraction). In experiments with large obstacles (BR= 30 and 60 %) the turbulence generation from walls and secondary small flow resistances is negligible compared to that from the large obstacles.

A comparison of the measured and calculated pressure histories in the RUT facility (**Fig. 4.26**) shows good agreement for the integral combustion development and local pressure loads. All major peaks in the experiments can be identified in the calculation, showing that the simulation captures, the essential wave propagation phenomena in the complex 3-d enclosure. At later times the calculated pressures exceed the test data because the late venting of the facility was not simulated.

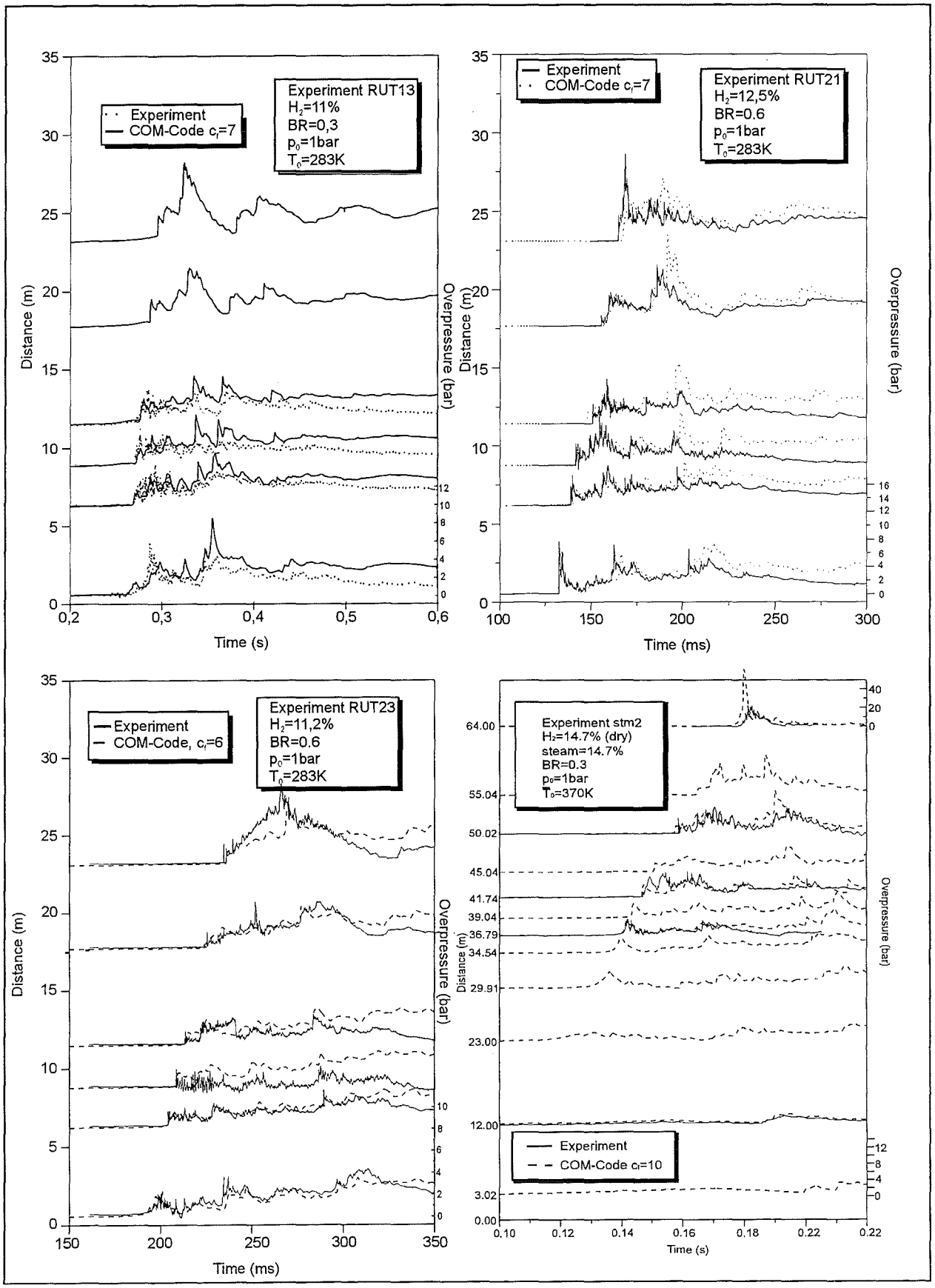

Fig. 4.26: Numerical simulation of large scale RUT - experiments with hydrogen - air and hydrogen - air - steam mixtures.

For simulation of the H_2-air-steam test a relatively high c_f-value (=10) was needed to obtain acceptable agreement. This is very likely due to the fact that the heating tubes and other additional equipment, which was installed for heating the RUT facility to about 100°C, were neglected in the COM3D geometry model. This results in too low calculated turbulence generation and requires an artificially high c_f-value for compensation, similar to test 19.

In summary the observed c_f-variation can be interpreted in terms of model approximations. It appears important that the dominant turbulence generation processes are captured in order to obtain reliable results from an eddy-break-up combustion model. For instance in large empty rooms it may be necessary to include wall functions in the turbulence model.

The described work allows now to calculate premixed turbulent combustion in severe accidents with a semi-empirical approach. Complex 3-d geometries with up to about 1 million mesh points can be handled on a dedicated Cray-J916 multiprocessor machine.

4.4 ERCO-code validation

Seven RUT experiments on turbulent H_2-air deflagration were simulated in 2-d geometry using the ERCO-code [4]. The hydrogen concentration ranged from 11.0 to 14.0 % H_2 in air. Different blockage ratios (30 and 60%) and flow geometries were investigated.

A set of standard computational parameters were defined and the effect of parameter variations on the important results, like e.g. terminal flame speed in the first channel were investigated (**Table 4.2**).

The calculations were performed on a Cray J904, the same machine type as used for the COM3D simulations.

Table 4.2 ERCO parameters used for 2-d RUT simulations

Parameter/Model	Standard value	Variations
- wall turbulence model	none	none
- space resolution ($\Delta X,\Delta Y$)	10 cm	5 cm
- initial flame shape	circular (25 cm radius)	plane over RUT cross section
- initial velocities	zero	-
- initial turbulence (u')	0.02 m/s	0.5 m/s
- turbulent burning law	$s_t=s_l+u'$	$s_t=s_l+2u'$
- flame buoyancy	modelled	not modelled
- geometry model	only first channel	first channel plus cavity

The parameter variations showed a number of important effects on the computational results:

- Finer space resolution (5 cm compared to 10 cm) leads to larger turbulence generation (u'_{max} = 28 m/s vs. 19 m/s), faster burning rates and higher flame speeds (900 m/s vs. 680 m/s) at the end of the first channel. Convergence could not be reached with the feasible grid resolution.
- The spherical initial flame shape produces higher flame speeds than the planar configuration (800 m/s vs. 550 m/s). The spherical case is more relevant to the experiment.
- The faster turbulent burning law leads to faster flame acceleration, but the effect is not very pronounced (970 m/s vs. 800 m/s). Nevertheless the burning law must be evaluated and chosen carefully.
- Neglecting of the (actually existing) flame buoyancy can strongly influence the initial slow combustion phase. The final flame velocities in the RUT tests were nearly equal (both about 800 m/s).

Fig. 4.27 compares measured and calculated flame trajectories for different RUT experiments. Some three-dimensional results from COM3D are included. The best predictions with the ERCO code are observed for the experiments with 12,5% H_2, possibly because the burning law was adjusted to this mixture and not varied with the H_2 concentration.

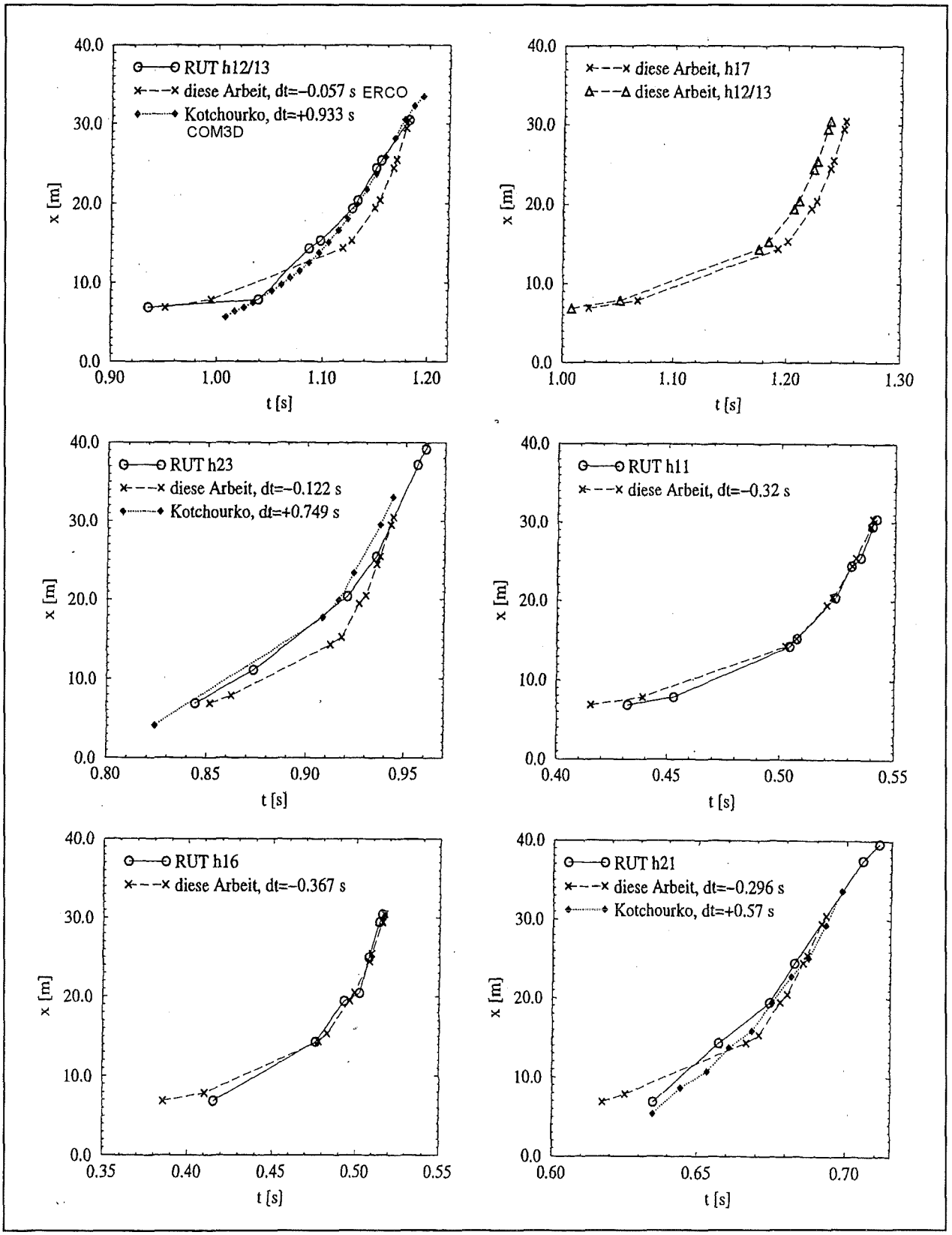

Fig. 4.27: Comparison of measured flame trajectories in large scale RUT - experiments with ERCO and COM3D predictions.

Fig. 4.28 shows the corresponding flame velocities. The flame velocities at the end of the first channel (34 m) tend to be above the experimental values. ERCO predicts generally a continuing flame acceleration up to the channel end, whereas most of the experiments showed a choked-flame regime. The ERCO flame velocities correspond closely to the sound velocity in the burned gas. The flame propagates in the ERCO calculation as a CJ-deflagration.

Despite of these differences the general agreement in the flame behaviour is good, considering that the computational parameters were fixed for all simulations. No DDT was observed in the computations, probably due to insufficient grid resolution which smears out local hot spots in compressed gas regions. The current H_2-air chemical kinetics can be extended to H_2-air-steam systems.

4.5 GASFLOW validation

4.5.1 FZK-tube tests

In support of the premixed H2-air turbulent deflagration experiments in the FZK-tube for the EG project FI4S-CT95-0001, we have performed three calculations. The geometry and conditions for these tests are described in [7].

The FZK-tube geometry was modeled two-dimensionally in cyclindrical geometry with 360 and 10 computational cells in z and r coordinate directions, respectively, or 3,600 total computational control volumes. The cell size in the z-direction was uniform with a size of 3.3333 cm., while in the r-direction, the first 8 cells were 1.83 cm and the last two cells were 1.68 cm. This allowed us to exactly model the array of blockages with walls every 50 cm in the axial direction. The global one-step chemical kinetics model coupled with the k-ε turbulence model was used in these calculations. The turbulence model was applied in its standard form without any adjustment of parameters. Calculations were performed for blockage ratios of 30, 60, and 90% for hydrogen volume fractions of 10, 12 and 15%. The following table puts the calculated turbulent flame velocities into the evaluated test matrix of these combustion tests

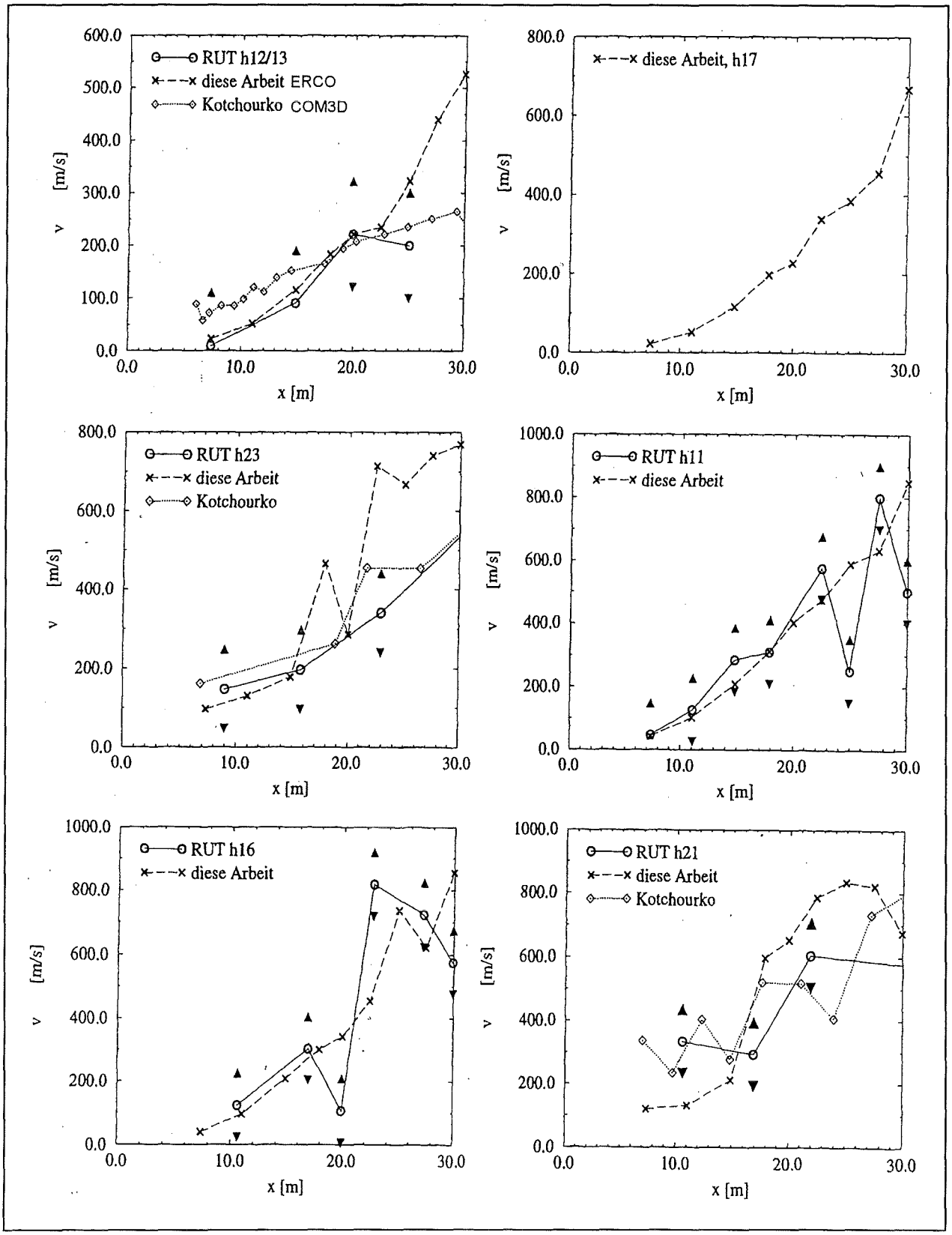

Fig. 4.28: Comparison of measured flame velocities in large scale RUT - experiments with ERCO and COM3D predictions. The black triangles show uncertainties in the measured flame speeds (± 100 m/s)

Table:4.3: Maximum turbulent flame velocity results from GASFLOW simulation of different tests in the FZK combustion tube

H_2 Vol %	Test/Calc	Blockage Percentage		
		30	60	90
10	FZK -Tube	-	-	-
	GASFLOW	45 m/s	-	-
12	FZK-Tube	-	524 m/s	361 m/s
	GASFLOW	300 m/s	500 m/s	200 m/s
15	FZK-Tube	1141 m/s	611 m/s	428 m/s
	GASFLOW	1000-1300 m/s	625 m/s	370 m/s

The GASFLOW results give a good picture of the dependence of hydrogen volume fraction and blockage fraction with respect to the flame velocities. In the very fine mesh that was applied the global one-step chemical kinetics model coupled with the k-ε turbulence model in GASFLOW does indeed predict the results quite well. An example of the calculated flame propagation for the 60% blockage test with 15Vol% hydrogen is given in **Fig.4.29**.

4.5.2 Experiment RUT-23

We then used the same one-step chemical kinetics model to calculate the turbulent combustion in the premixed H_2-air deflagration experiment RUT-23 with 11.25 Vol% hydrogen in dry air. The Russian RUT facility is a large concrete building having a length of 70 m and total volume of 480 m^3 [8].

We have modeled the RUT facility in cartesian geometry with 429 computational cells in the length direction, 40 cells in the height direction and 16 cells in the depth direction giving a total of 274,560 fluid volumes. More than half of these cells are blocked out by obstacles or regions to represent the actual geometry. These cells

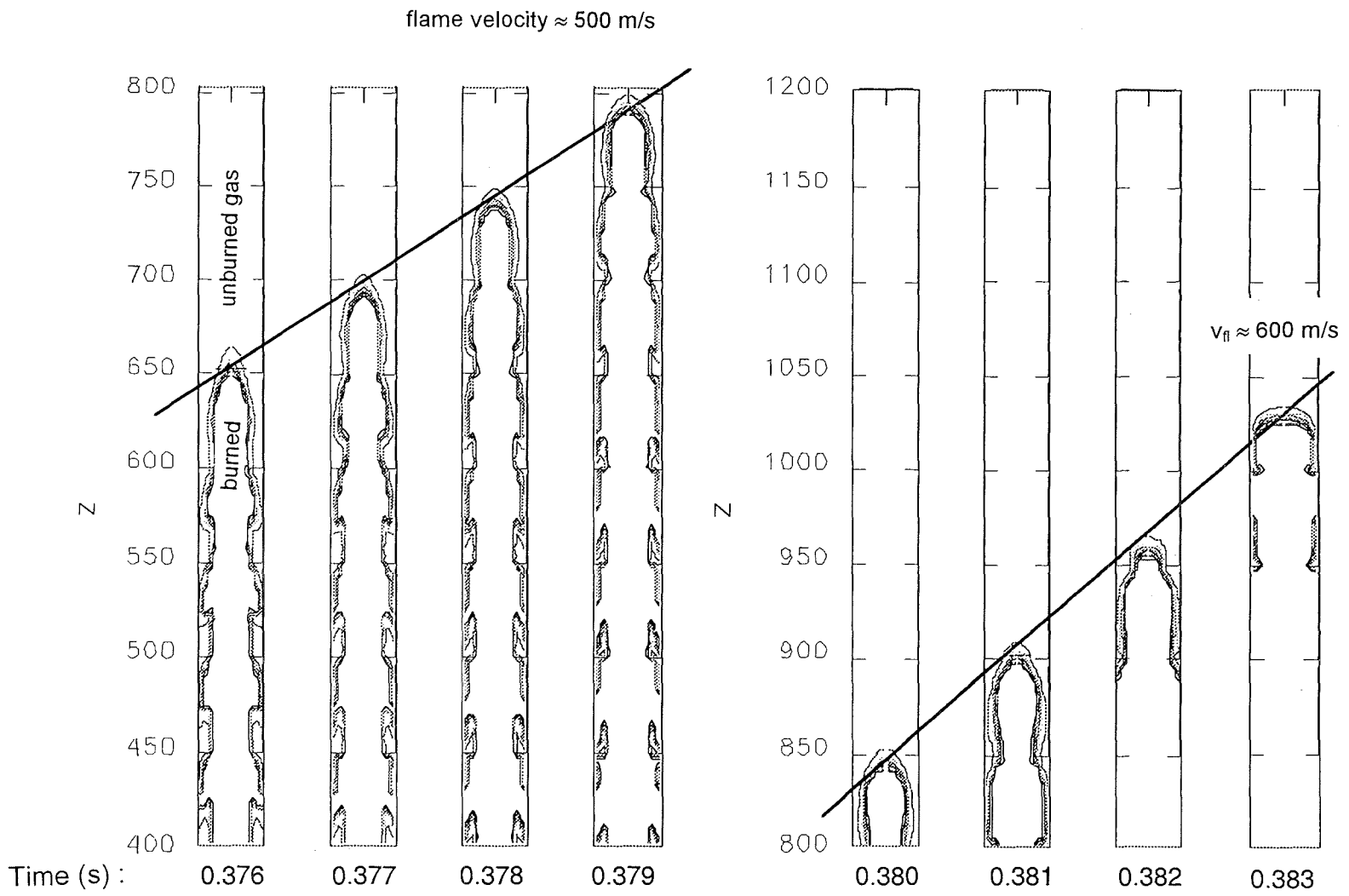

Fig.4.29: GASFLOW simulation of the FZK combustion tube: Experiment with 60 % blockage and 15 vol % H_2. Shown are hydrogen concentration contour fields.

lead to an average control volume size around 4 liters. We have performed two calculations using (1) the one-step chemical kinetics coupled with the algebraic turbulence model and (2) the one-step chemical kinetics with the k-ε model.

The simulation with the k-ε model produces maximum flame speeds before the flame expands into the canyon of 80 m/s. This is significantly below the measured peak value of 320 m/s. With the algebraic turbulence model the flame speed increases by roughly 50% to 120 m/s but is still too low compared to the measured data. The accuracy of this prediction which was made without any adjustment of the turbulence parameters is not acceptable. It is necessary to examine the spatial resolution issues and probably also necessary to develop better chemical kinetics models with more coupling to the turbulence modeling.

5. DETONATION CRITERIA

For the implementation of igniter systems as a hydrogen mitigation measure it is necessary to determine if an ignition event can lead to a deflagration-to-detonation-transition (DDT) or not. The direct numerical simulation on containment scale is currently not possible because very small time and space scales have to be resolved. The alternative is to derive DDT-criteria which allow a decision on the basis of the calculated gas distribution during the accident progression. The idea of a minimum scale requirement for DDT was developed at Kurchatov Institute and investigated during the last years in joint FZK-KI test-series on different scales, mixtures and geometries. The following criteria was proposed

$$D \geq 7\lambda \text{ for DDT} \qquad (5.1)$$

where D is the characteristic „size" of the mixture and λ the average detonation cell width in the reacting cloud. A minimum scale is required for a successful DDT, which depends on the chemical sensitivity of the mixture, characterised by λ.

Because a variety of geometrical configurations can be found in containment buildings, work in 1996 investigated how the characteristic size D depends on the shape of the confining geometry. The available literature data on DDT experiments were sorted into few different geometry classes and analysed systematically [9]. The

following results were obtained, assuming that a certain mixture fills the room completely.

5.1 DDT in room geometry

A typical room geometry with the linear dimensions is shown in **Fig. 5.1**. The width of the room width perpendicular to the page plane is denoted W. The room length is L and the room height is H.

Case I: Regular compartment geometry with L≈H≈W, (BR < 0.5, d < 0.5H). The arithmetical average of the room dimensions results in good representation of the experimental data

$$D = (L+H+W)/3 \qquad (5.2)$$

A very similar and equally suitable value is obtained from the geometrical average $D = (L \bullet H \bullet W)^{1/3}$.

Case 2: Flat compartment geometry, L≈H>> W (BR < 0.5, d < 0.5 H)
In a flat room the smallest dimension W has no noticeable influence on the maximum possible size of the mixture and the average of the other two dimensions is an appropriate measure for the characteristic size

$$D = (L+H)/2 \qquad (5.3)$$

5.2 DDT in channel geometry

The geometrical designations for a typical channel geometry is given in **Fig. 5.2**. W is again the dimension in vertical direction, S is the obstacle spacing.

Case 1: S≈H (BR<0.5, d >0.5H)
The following rules are proposed for estimating the maximum macroscopic size D of sensitised mixture if the obstacle spacing is similar to the channel diameter

$$D = 2.5\ S \qquad (5.4)$$

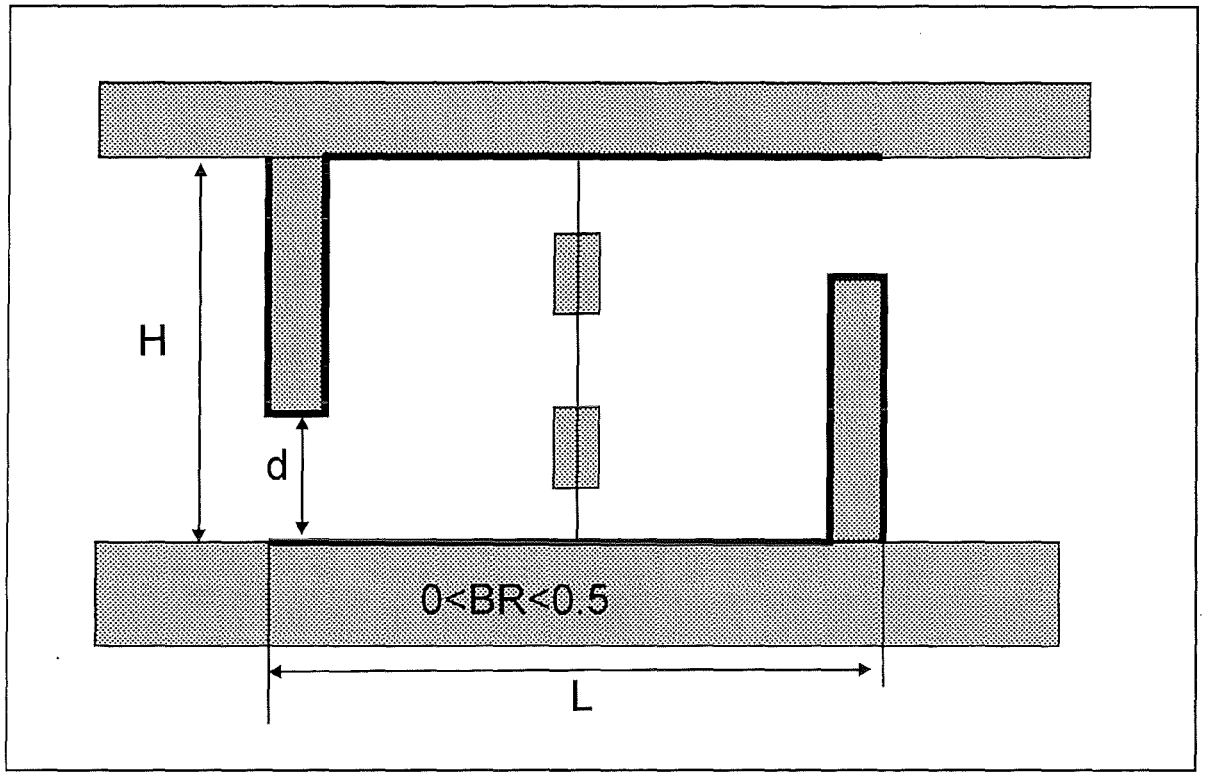

Fig.5.1: Typical room geometry with height H, length L, opening d and blockage ratio BR [9].

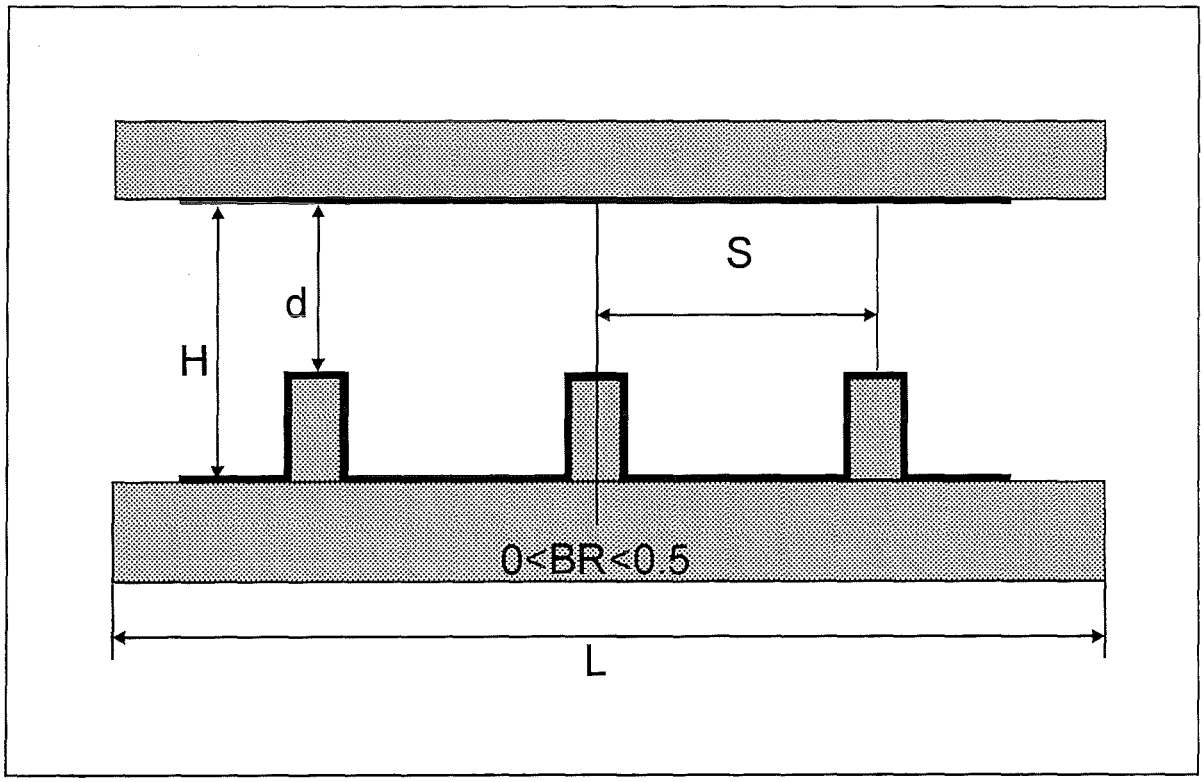

Fig.5.2: Typical channel geometry with height H, length L, opening d, blockage ratio BR and obstacle spacing S [9].

Case 2: S << H or S >> H (BR < 0.5, d > 0.5 H)

If the obstacle spacing is either much smaller of much larger than the channel (or tube) diameter a good measure is

$$D = 2.5\ H \qquad (5.5)$$

Figure 5.3 summarises all investigated experiments, when D is determined according to the above relations.

The mixture properties (λ) and the geometrical size (D) of each experiment is plotted in the form D/λ vs. D. The theoretical line very well separates the region in which DDT was observed ($D/\lambda > 7$) from the deflagration regime ($D/\lambda < 7$).

This criterion is valid for DDT in confined geometry, where the initial explosion wave develops from an approximately planar wave. The minimum scale requirement in this case seems to be $D \geq 7\lambda$.

In unconfined geometries only a spherical initiation wave can develop. It was shown that in this case the scale requirement is more severe: $D \geq 3 \bullet 7\lambda$ [9]. Turbulent jet initiation experiments without reflections in the flow path could be correlated well with this relation. For containment analysis the relation $D \geq 7\lambda$ is more relevant and more demanding.

5.3 Detonation cell size data.

The above DDT criteria require knowledge of λ-values as function of mixture composition, pressure and temperature. Cell size data for containment analysis were generated by fitting available measurements and by performing new theoretical calculations.

5.3.1 Fitting of experimental data

Measured cell size data were collected from the original literature sources and compared [9]. The data generally agree within a factor of two. A special fit program was developed and used to describe the experimental data basis with the least square deviation. Different statistical weights were given to the data according to the respective accuracy limits. Different analytical fit functions were applied to the data

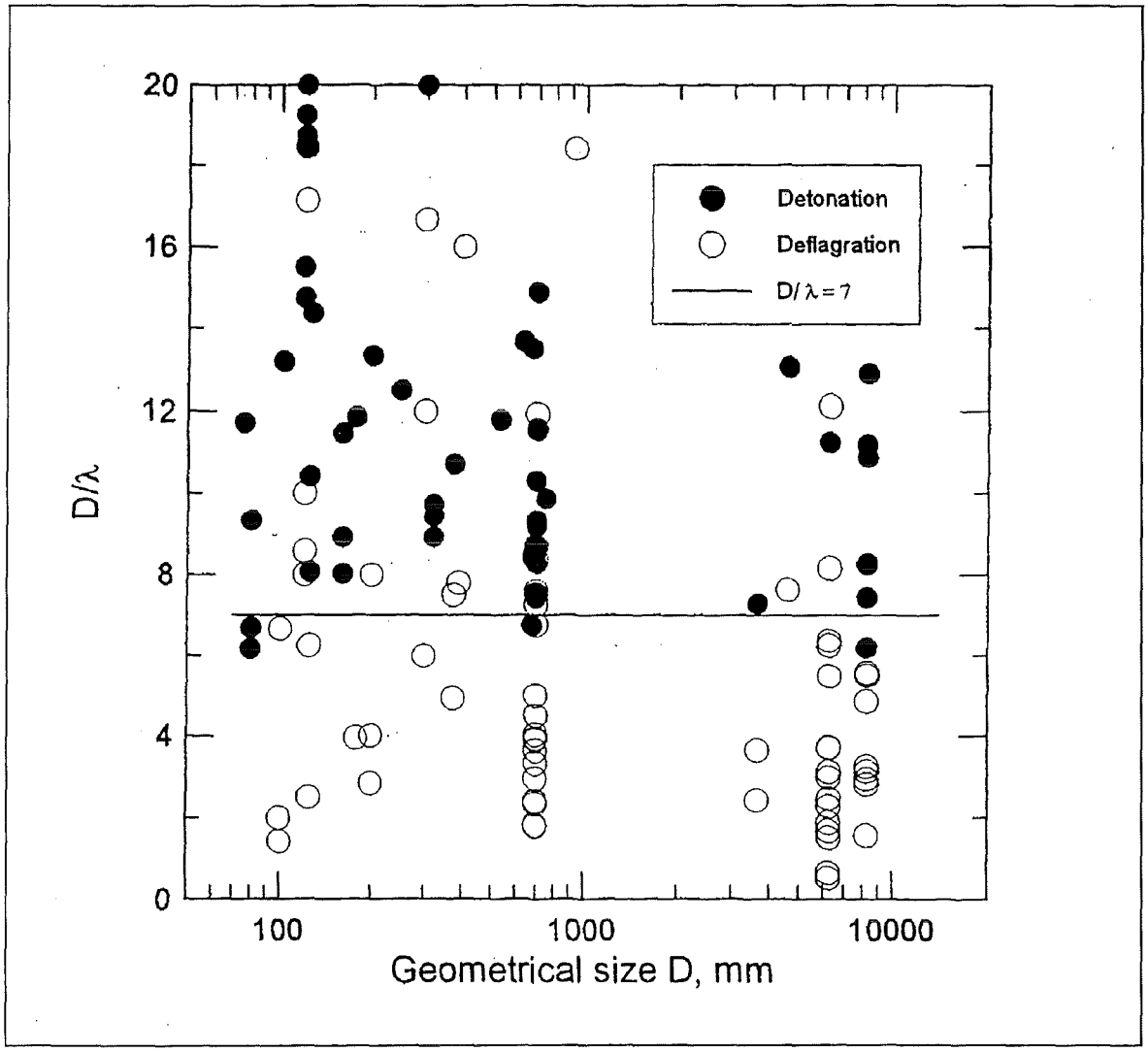

Fig.5.3: Summary of data analysis for DDT criterion. The theoretical line separates very well the region in which DDT was observed ($D/\lambda > 7$) from the deflagration regime ($D/\lambda < 7$). The data cover 2 orders of magnitude in the geometrical size of the reacting gas. The criterion may be used in severe accident containment analysis to predict the possibility of a deflagration - detonation transition.

and compared. The best functions gave mean deviations of a factor 1.5 which is within the experimental uncertainties.

A special approximation was made for 375 K, which is needed for analysis of the RUT tests with steam. **Figure 5.4** shows as an example predicted detonation cell sizes from this fit function for 1 bar. The effect of pressure is currently under investigation.

5.3.2 Theoretical predictions

The computer code DILIM was used to calculate detonation cell sizes for hydrogen-air mixtures at elevated temperatures with nitrogen or steam dilution [10]. The code solves the one-dimensional Euler equations together with detailed chemistry (42 elementary reactions). Wall losses of momentum and energy are also included. The theoretical model was evaluated against high temperature measurements in the range of 0.5-3 bar, 370-650 K, 0-50% H_2, and 0-30% steam. Predicted and measured cell sizes agree within a factor of about two, which is equal to the experimental uncertainties.

Detonation cell size calculations with nitrogen dilution were performed for the following conditions:

p_0 = 1-2 bar, T_0 = 300-600 K, H_2 = 10-30 %, O_2 = 9.5-17 %, N_2 = 60-78 %.

The results are supplied in the form of a small computer program which allows fast retrieval of the λ-data for specified conditions. Hot and nitrogen enriched mixtures were observed in GASFLOW simulations for the EPR, when hydrogen burned out only partially due to oxygen limitations. As an example **Fig. 5.5** shows calculated results at 600 K and 1 bar pressure. The hot mixtures are quite reactive, λ varies from 0.6 to 2.7 cm for the shown parameter range. N_2 dilution does not decrease the chemical sensitivity significantly.

Calculation were also performed for H_2-air-steam mixtures in the range from 300 to 600 K and 1-2 bar. It was found that the dilution of H_2-air with steam is more effective than N_2 with respect to suppressing detonation. **Fig. 5.5** shows results for the same conditions (600 K, 1 bar). With steam much larger detonation cell sizes are predicted

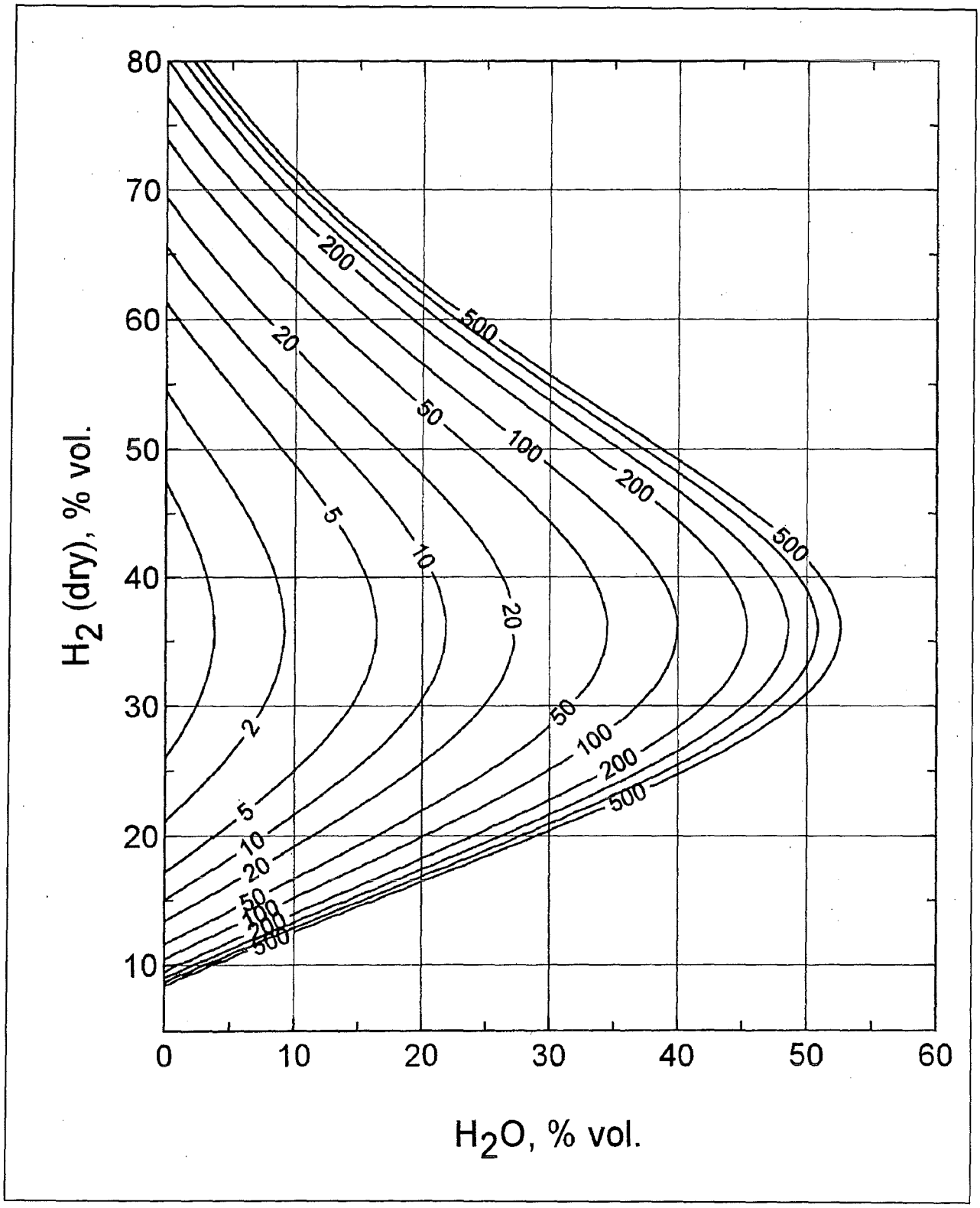

Fig.5.4: Predicted detonation cell width (cm) of hydrogen - air - steam mixtures at 375 K and 1 bar, based on a systematic fit of the available experimental data [9].

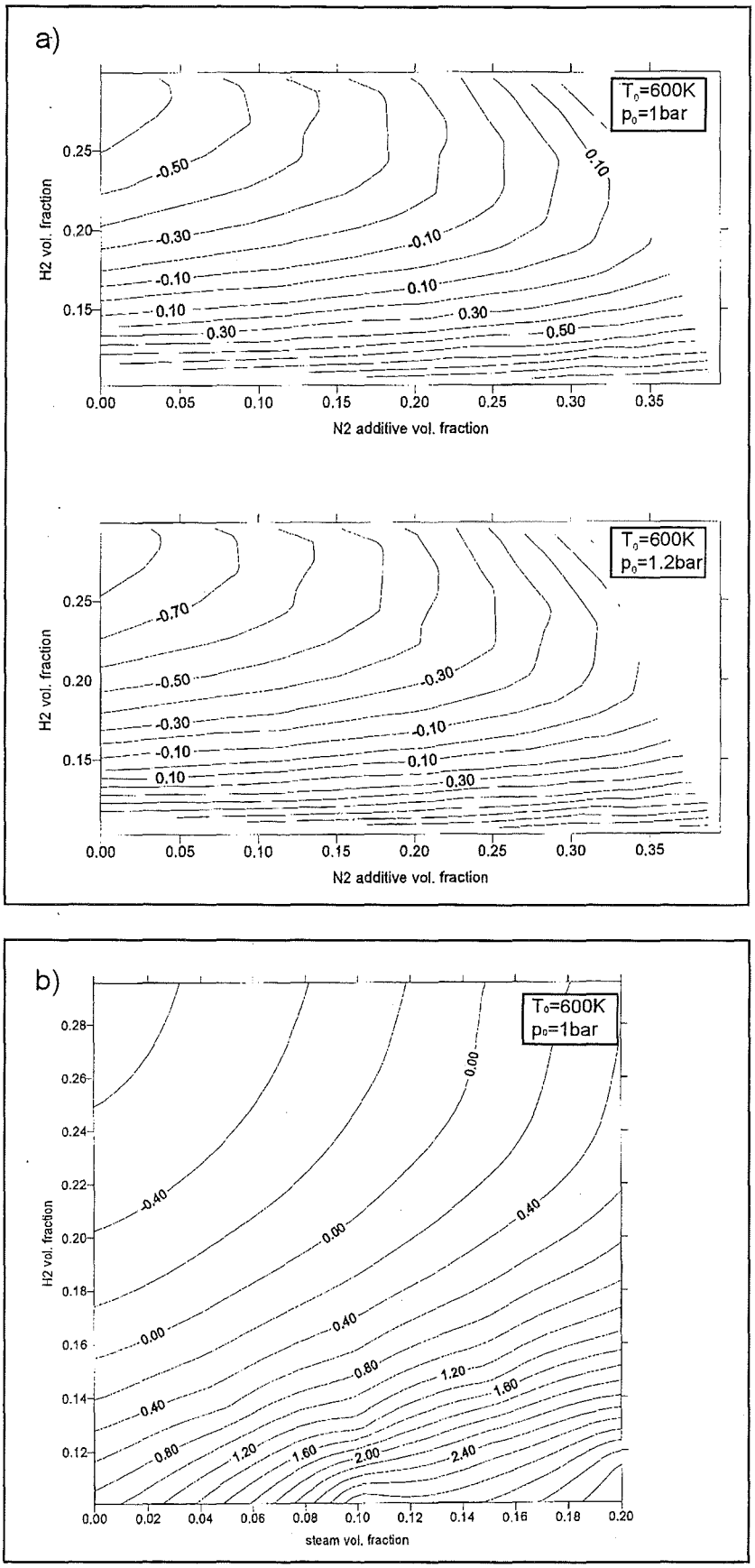

Fig.5.5: Calculated detonation cell sizes for 600 K and 1 bar

a) H_2 - air with additional N_2

b) H_2 - air with steam.

Plotparameter is ln (λ/cm). Steam is more effective in suppressing detonations than nitrogen.

than with N_2. An important difference is the higher heat capacity of steam (tri-atomic molecule) which acts as an inert heat sink.

The effect of the initial pressure on the calculated cell size was found to be negligible.

6.1 DETONATION

6.1 Heat release in DET3D

In the 3-d detonation code DET3D the chemical reaction is modelled by one single global reaction

$$2\,H_2+O_2 \rightarrow 2\,H_2O+Q \qquad (6.1)$$

where the heat release Q is taken from detailed chemistry models. The Q value is an input parameter for the code which contains all chemistry information. This simplified treatment is valid as long as the induction length of the mixture is small compared to the grid size. The chemical reaction is then a subgrid phenomenon.

The existing function $Q(x_{H2})$ was extended to include the effect of steam in the following way:

1. Lean H_2-air-steam mixtures ($x_{H2,\,dry} < 0.3$):

   x_{H2} = hydrogen mol fraction

$$Q(x_{H2}) = \left[220 + 36\frac{(0.3 - x_{H2})}{0.2}\right] \text{ kJ/mol} \qquad (6.2)$$

With 10 water vapor concentration:

$$\frac{\Delta Q}{Q} = 0.272\,x_{H2} - 0.043 \qquad (6.3)$$

With 20 water vapor concentration:

$$\frac{\Delta Q}{Q} = 0.272\,x_{H2} - 0.068 \qquad (6.4)$$

With 30 % water vapor concentration:

$$\frac{\Delta Q}{Q} = 0.272\, x_{H2} - 0.069 \qquad (6.5)$$

2. Rich H_2-air-steam mixtures ($x_{H2,\,dry} > 0.3$):

$$Q(x_{H2}) = \left[220 + 23\frac{(x_{H2} - 0.3)}{0.4}\right] \text{ kJ/mol} \qquad (6.6)$$

With 10 water vapor concentration:

$$\frac{\Delta Q}{Q} = 0.02\, x_{H2} - 0.058 \qquad (6.7)$$

With 20 water vapor concentration:

$$\frac{\Delta Q}{Q} = 0.154\, x_{H2} - 0.147 \qquad (6.8)$$

With 30 % water vapor concentration:

$$\frac{\Delta Q}{Q} = 0.172\, x_{H2} - 0.169 \qquad (6.9)$$

Fig. 6.1 compares calculated detonation velocities from the DET3D code with „exact" STANJAN results which are based on detailed chemistry. The agreement is better than 2 %. The improved fit for Q (x_{H2}, x_{H2O}) allows now detonation calculations for all relevant H_2-air-steam mixtures.

6.2 Missile generation by local detonations

Fast combustion processes during severe accidents can threaten the containment or safety related systems by generation of fast missiles. No quantitative results on obtainable missile velocities are available. The investigation of the missile problem started in 1995 with small-scale experiments and model development [11]. The work was completed in 1996 with necessary drag coefficient calculations and several 2-d containment simulations for local detonations to derive upper limits for missile velocities.

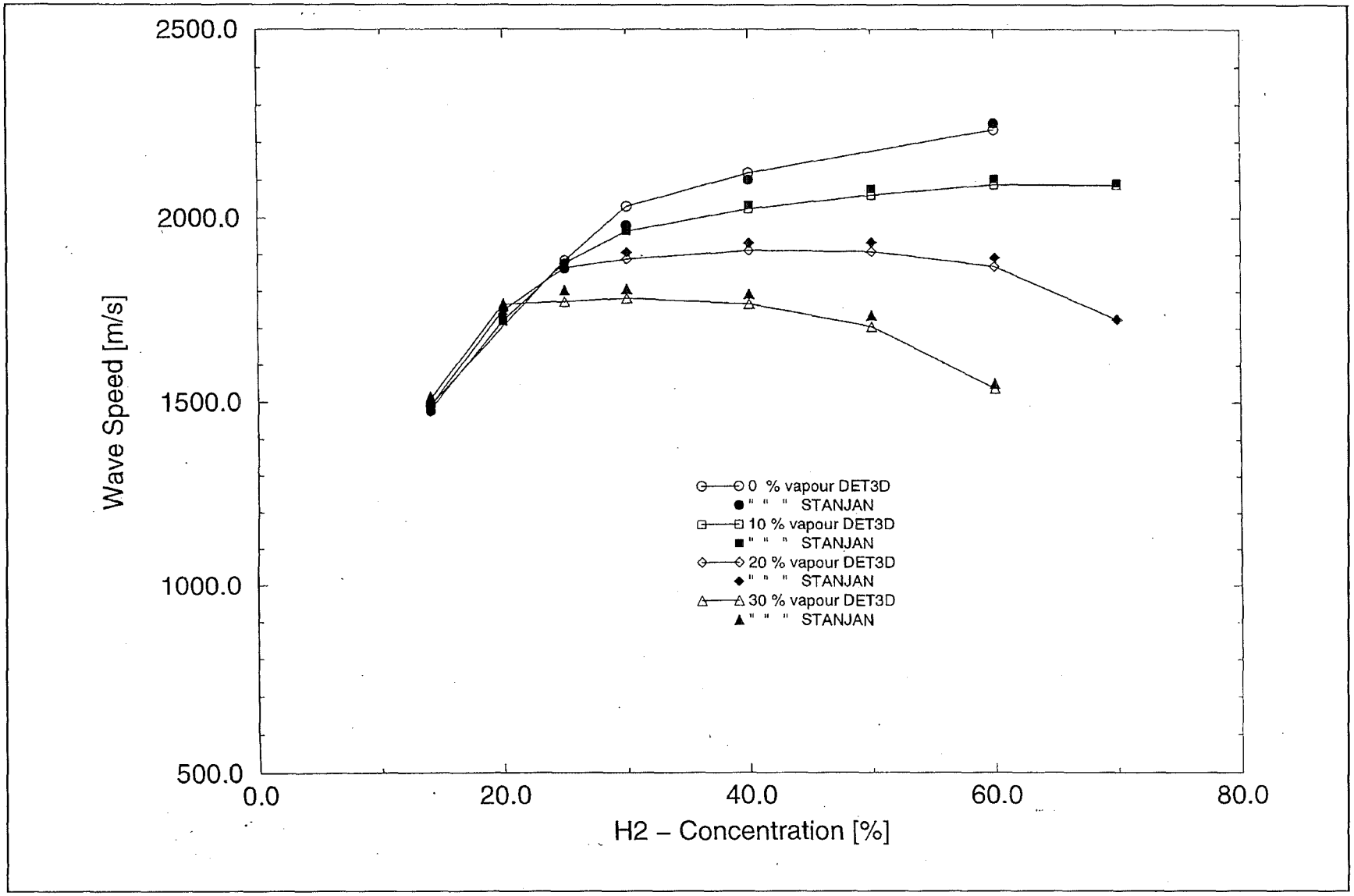

Fig.6.1: Comparison of calculated detonation velocities from DET3D with simplified chemistry model to STANJAN results with detailed chemistry. The deviations are less than 2 %. DET3D can be used for H_2-air-steam mixtures.

6.2.1 Drag coefficient calculations

A computer code was written in 1995 to describe the motion of a missile in a 3-d containment geometry when subjected to a gas flow [12]. The analysis is restricted to the case that the missile is much smaller than characteristic size of the gas flow, so that the flow pattern is not significantly influenced by the missile. The code requires drag coefficients as input, however most of the published data concern completely different conditions and cannot be used for the current applications in severe accidents. Drag coefficients were therefore calculated for different missile shapes, missile orientations, flow Mach numbers M, and specific heat ratios γ.

The drag coefficients are derived from direct numerical simulation of the stationary flow around the missile by integrating the pressure over the missile surface. Inviscid gas and ideal equation of state were used. The grid resolution necessary to exclude numerical effects was found to be about 16 nodes across the flow exposed missile surface. Additional validation of the method was obtained by comparing calculated stagnation point pressures with known analytical solutions. Deviations existed only in the third digit. The flow properties were chosen to be characteristic for fast Deflagration or detonation waves in H_2-air mixtures. 2-d simulations were performed for (infinitely) long missiles, and full 3-d calculations for finite bodies like cube and sphere.

Fig. 6.2 shows an example for the calculated pressure distribution around an infinite missile. The drag coefficient c_d is found by integrating the calculated stationary pressure distribution p(A) over the missile surface A:

$$\text{drag force} = c_d \, S \, \tfrac{1}{2} \, \rho \, (v - u)^2 = \iint_A p(A) \, d(A) \qquad (6.10)$$

with

S = flow cross section of missile (m^2)

ρ = flow density (kg/m^3)

u = flow velocity (m/s)

v = missile velocity(m/s).

Fig.6.2: Calculated pressure distribution around infinte square bar missile, 2-d calculation. Mach number of incident flow M = 1.2, ratio of heat capacities γ = 1.4, pressure of incident flow 1.0 MPa. Pressure range is from 0.36 MPa (black) to 2.41 MPa (white). The drag coefficient can be evaluated from the missile surface pressures.

The drag coefficients were determined via Eq. 6.10 as function of missile shape, orientation, Mach number and specific heat ratio γ. **Fig 6.3** summarises the results for γ = 1.4. The value of γ had only a weak influence on the calculated drag coefficients, its effect may be omitted in hydrogen-air combustion situations.

Results from **Fig. 6.3** may be used in a detailed or averaged form. The drag coefficients for cube and sphere bracket the values for elongated missile shapes.

6.2.2 Wall missiles

The first missile calculations indicated that free missiles dragged by gas flow require a relatively large scale combustion before containment threatening velocities are obtained [11]. Another mechanism for generating missiles consists of breaking a wall by a high dynamic combustion load and by accelerating the fragments with the outflowing gas. In this case the missile motion has a large effect on the gasflow and the drag coefficient model is not applicable.

The code BO2 was modified to treat simplified 2-d cases in which a missile of rectangular shape can move along one axis without rotation. The analysis is valid only for cases in which the velocity of the missile is much smaller than the sound speed of the ambient gas. In this case the interaction of the gas flow with the missile surface represents a quasi-stationary boundary condition for the missile motion. The missile acceleration a (t) results from integration of the actual pressure over the missile surface:

$$\text{Force on missile} \equiv F(t) = \iint_A p(t)\, dA \approx \Delta p(t)\, wh \qquad (6.11)$$

with

w = missile width (m)

h = missile height (m)

d = missile thickness (m)

$$a(t) = \frac{F(t)}{m} = \frac{\Delta p(t) wh}{\rho\, whd} = \frac{\Delta p(t)}{\rho\, d} \qquad (6.12)$$

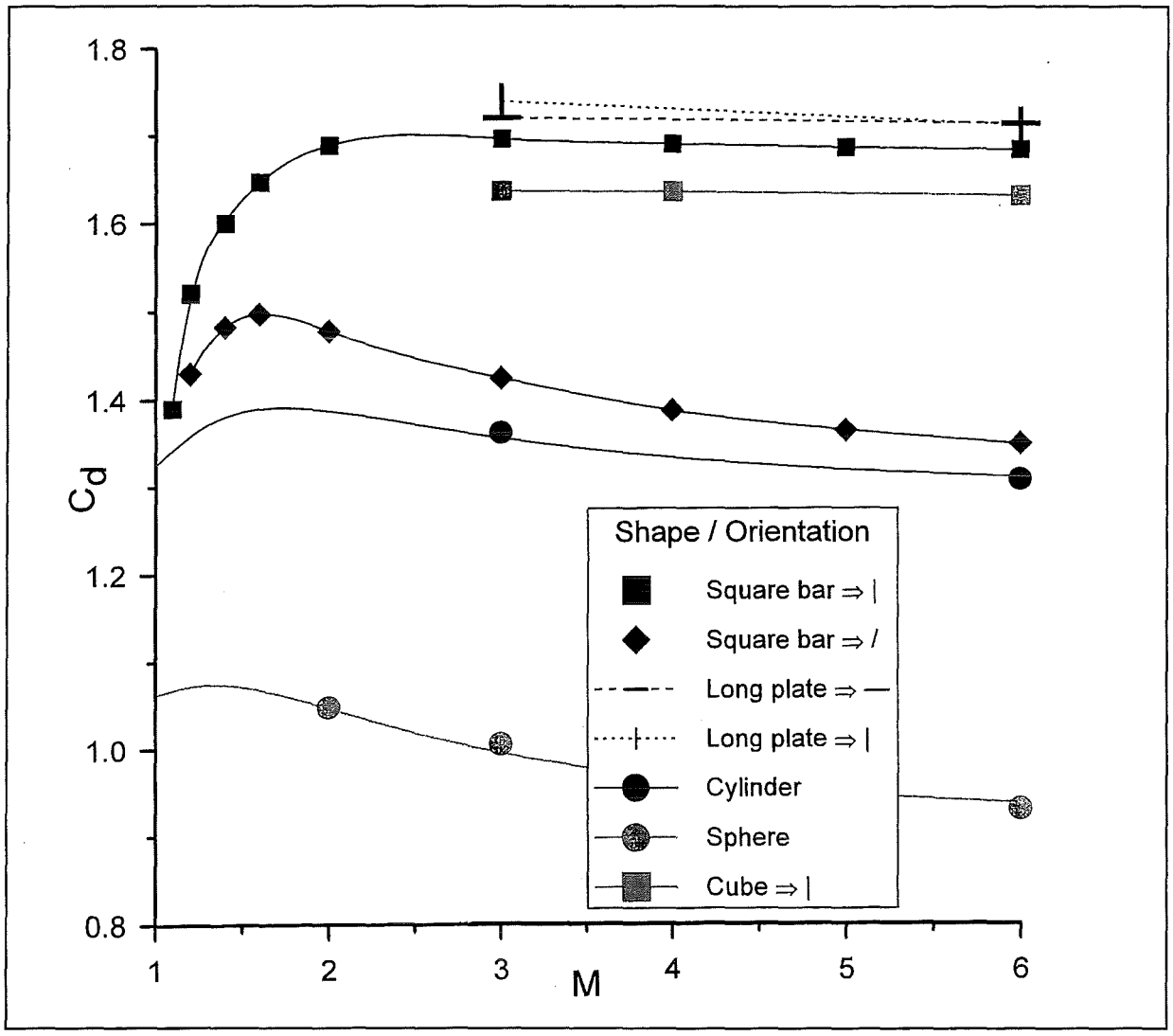

Fig.6.3: Summary of calculated drag coefficients for different missile shapes, missile orientation and flow Mach number (γ =1.4).

Note that only the thickness of the missile in flow direction (d) enters into the missile acceleration, the other missile dimensions cancel. A 2-d treatment is therefore sufficient.

The described model was applied to the case of a local detonation in a closed compartment. It is assumed that the initial reflection of the detonation wave fractures a wall and that part of this wall moves under the influence of the existing pressure differences according to Eq. 6.12. The rest of the wall is treated as immobile. The fracture process itself is not modelled, the missile can move freely from the beginning.

A two-compartment situation was analysed, one being filled with a detonable mixture, the other with air (**Fig. 6.4**). The central part of the wall separating the two compartments was regarded as missile. The mixture was ignited opposite to the center of the missile. The missile mass, initial position, thickness and the thickness of the inner wall were varied in five calculations. The values of these parameters and the main results are given in **Fig. 6.5**. A mesh size of 1 cm was used in the calculations. Only half of the volume was modelled because of the symmetry of the problem, resulting in a total of about 340.000 nodes.

Calculated flow field parameters for missile case no 1 are summarised in **Fig. 6.6**. The detonation wave reaches the wall 5.05 ms after ignition (first frame). The other frames show flow field properties shortly before the missile collides with the right hand wall of the second compartment. The characteristics of the missile motion are shown in **Fig. 6.7**. Most of the acceleration occurs within the first meter of the missile's flight path because thereafter large lateral cross sections exist for the venting flow and because back pressure on the back side of the missile increases rapidly.

The described scoping calculations have clearly shown that confined rapid combustions can in principle accelerate missiles to significant velocities and impulses. Because the terminal velocity is independent of the missile area the damage potential (impulse) of a missile increases with its area. Scaling relationships were derived to scale the cases of **Fig. 6.5** to other geometries and mixtures.

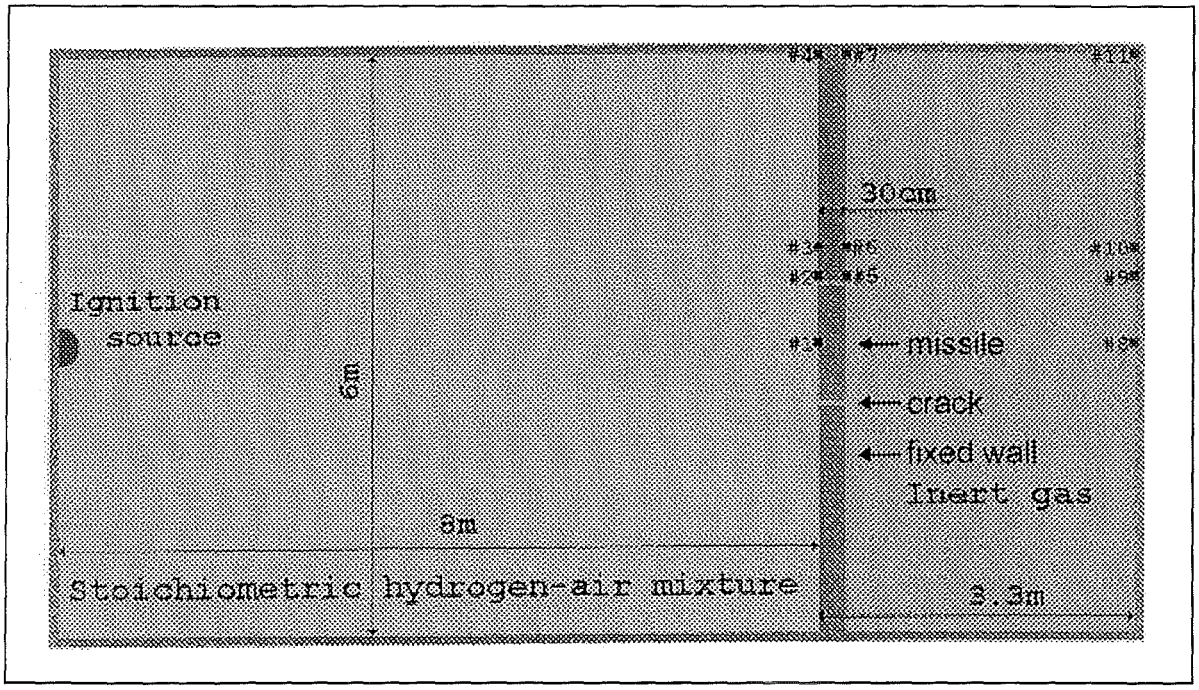

Fig.6.4: Investigated two - compartment geometry with missile in the separating wall. Dark squares mark locations of pressure transducers. Properties of reactive mixture: p_0 = 1 bar, T_0 = 275 K, 30 % H_2 in air. Geometry of calculation no.1.

Test	№ 1	№ 2	№ 3	№ 4	№ 5
Missile mass, kg	80	200	200	200	500
Wall thickness, mm	300	600	600	600	600
Missile thickness, mm	300	600	100	100	600
Distance, mm	3000	2700	3200	2700	2700
Drift time, ms	11.19	18.70	21.30	19.51	32.40
Average speed, m/s	268.09	144.36	150.21	138.38	83.33
Final speed, m/s	313.14	204.95	194.86	171.94	111.87
Maximal speed, m/s	313.14	205.50	203.25	179.94	115.61

Fig.6.5: Calculational parameters and main results of five missile simulations for the two - compartment geometry shown above.

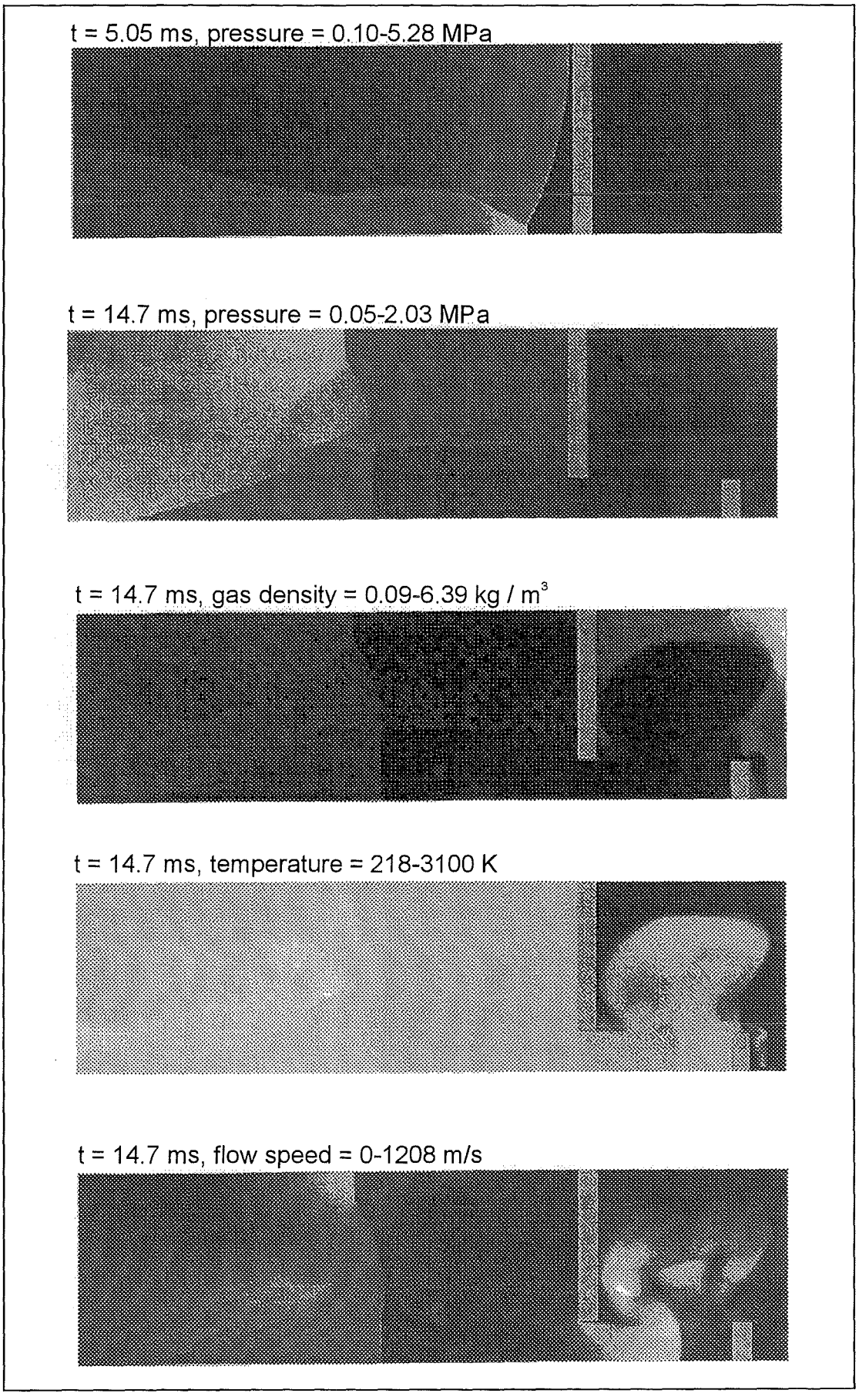

Fig.6.6: Calculated flow field parameters for missile case 1. Black = lowest value, white = highest value of given property [12].

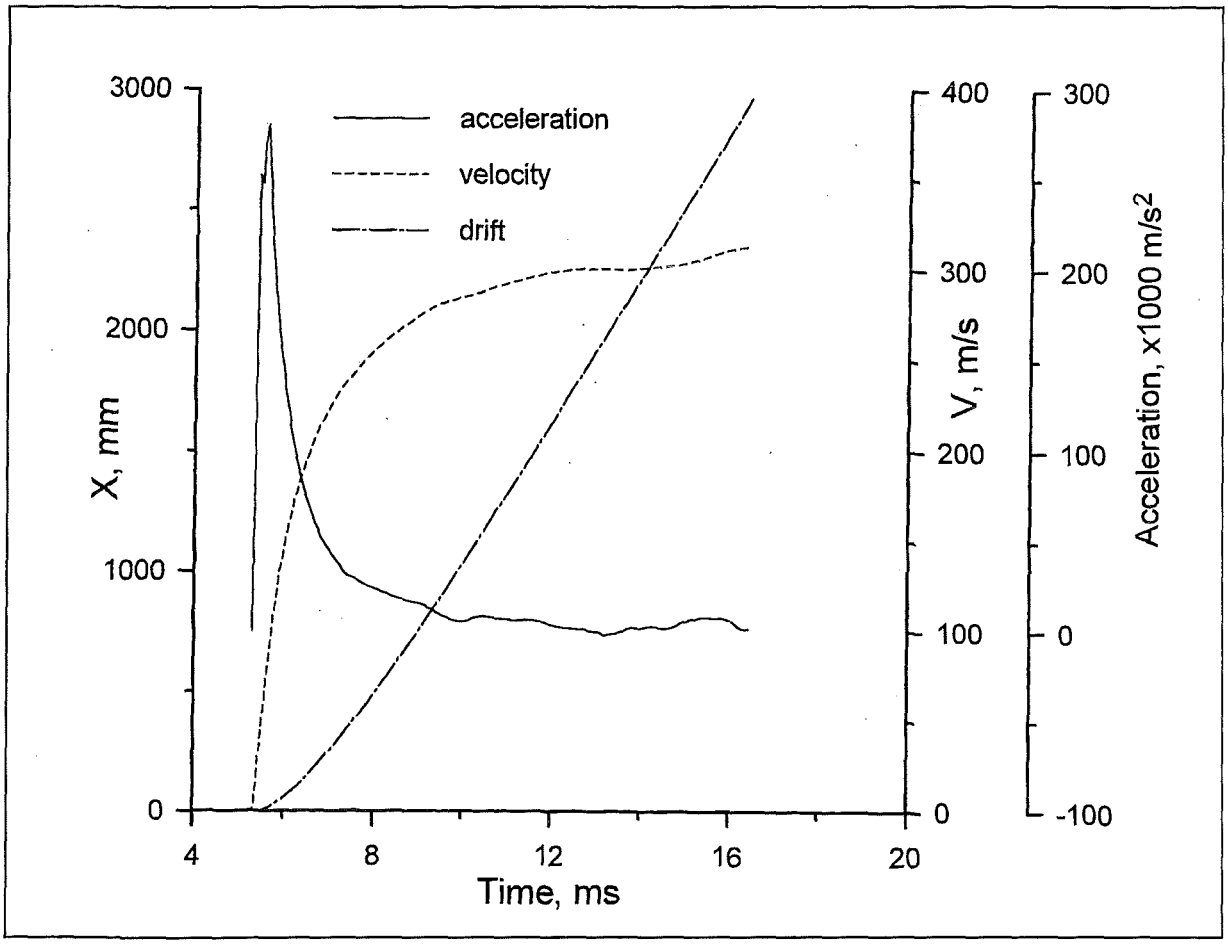

Fig.6.7: Calculated missile acceleration, velocity and drift for case 1. Most of the acceleration occurs within the first meter of the missile's flight path [12].

The calculated velocities from this simplified model are not upper limits. They may be exceeded by additional effects, like e.g. 3-d wave focusing, or complete collapse of a wall, in which case a less effective vent flow would occur and a longer driving pressure would exist. The main conclusion from the described simulations is that local explosions must be avoided in severe accidents at any case. The missile investigations were completed in 1996, no further work is planed. The developed two codes, one for the free flying missile and one for the wall missile, will be implemented at FZK in 1997.

7. MITIGATION WITH CO_2

Dilution of the accident atmosphere with CO_2 is one possible mitigation measure against energetic hydrogen combustion in core-melt accidents. It is well known that CO_2-additions generally inhibit H_2-air combustion processes. However, before implementation of such a measure can be considered, a complete understanding of the important combustion related consequences should be reached. Since only a limited and incoherent data base exists on the effects of CO_2 addition, a detailed and consistent research program was performed at the Russian Academy of Sciences investigating the fundamental reaction phenomena in CO_2 containing H_2-air mixtures [13].

The following sections present the main results of this program. The combustion phenomena are discussed in the order of increasing reactiveness.

7.1 Flammability limits

Most of the experimental work has been carried out at an initial pressure of 1 bar. To obtain data for severe accident conditions the pressure influence on the flammability limit of H_2-air-CO_2 mixtures was measured in constant-volume bomb experiments. The ignition was considered unsuccessful when a spark energy of 2 Joules did not cause a noticeable pressure increase in the bomb.

The results are compared in **Fig. 7.1** to earlier experiments at 1 bar. The data agree well on the lean side, for the rich side a small 2 % difference in the CO_2-concentration was obtained. It is apparent that the pressure rise from 1 to 5 bar diminishes the limiting CO_2-concentration by about 6 % (from 57.6 % to 51.2 % CO_2

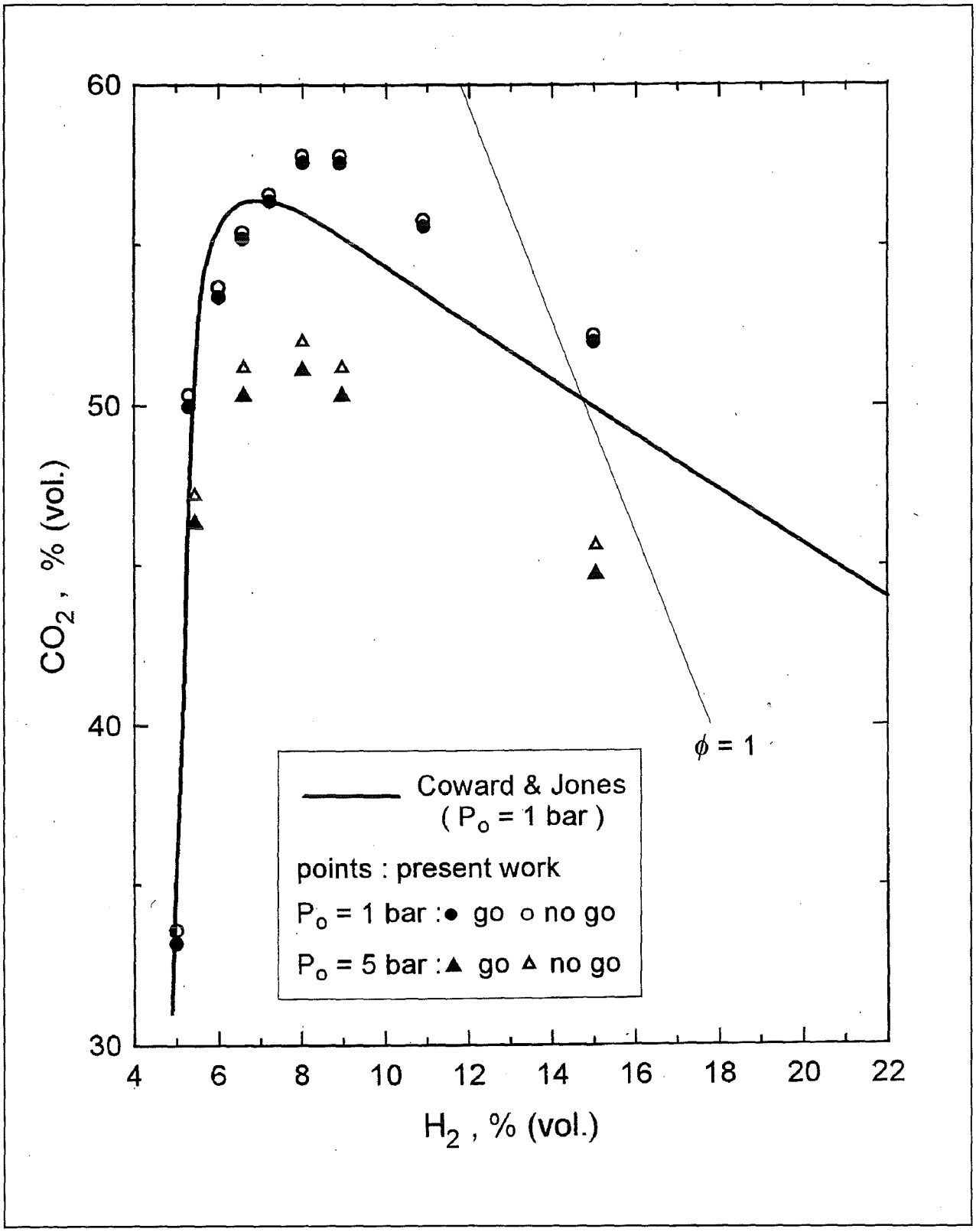

Fig.7.1: New measured data for the influence of initial pressure on the flammability limit of H_2 - air - CO_2 mixtures [13]. CO_2 quenches more effectively at higher pressures which could be beneficial in reactor applications

at about 8 % H_2). CO_2 quenches more effectively at higher pressures. This could be a beneficial effect for reactor applications.

7.2 Laminar premixed burning velocity

After a successful ignition the flame kernel will initially grow as a laminar flame. The fundamental property of interest for this phase is the burning velocity S_u of the mixture, which is connected to the flame velocity S_b through the expansion ratio $E = \rho_{unburned}/\rho_{burned}$.

$$S_u = S_b/E \tag{7.1}$$

The flame velocity S_b was calculated from measured flame kernel radii r(t):

$$S_b = dr/dt \tag{7.2}$$

An explosion bomb of 20 cm diameter, equipped with a high-speed Schlieren system was used in the experiments to measure r(t).

This method is suitable for lean and slowly burning mixtures. The burning velocities of more reactive H_2-air-CO_2 mixtures were obtained from a mathematical processing of measured pressure-time records. This method was also preferred for tests at higher initial temperatures and pressures (T_o and p_o up to 200 °C and 5 bar).

Fig. 7.2 shows Schlieren records from a smooth, rapidly burning flame and from a lean, slowly burning flame kernel with a district cellular surface. A mass/thermal diffusion instability causing locally different gas compositions and burning velocities is the reason for the cellular structure.

The second mixture in Fig. 7.2 is very close to the flammability limit, + 1 % CO_2 or - 0.5% H_2 will lead to quenching. These are the first pictures from H_2-air-CO_2 flames in the literature.

A one-dimensional computational model was developed for the prediction of laminar, freely propagating spherical flames in H_2-air-CO_2 mixtures. The model takes into account a detailed reaction scheme with 72 elementary reactions. In specific cases a reduced scheme with 26 reactions was used. In this approximation CO_2 is treated as an inert component. The time-dependent conservation equations for total mass,

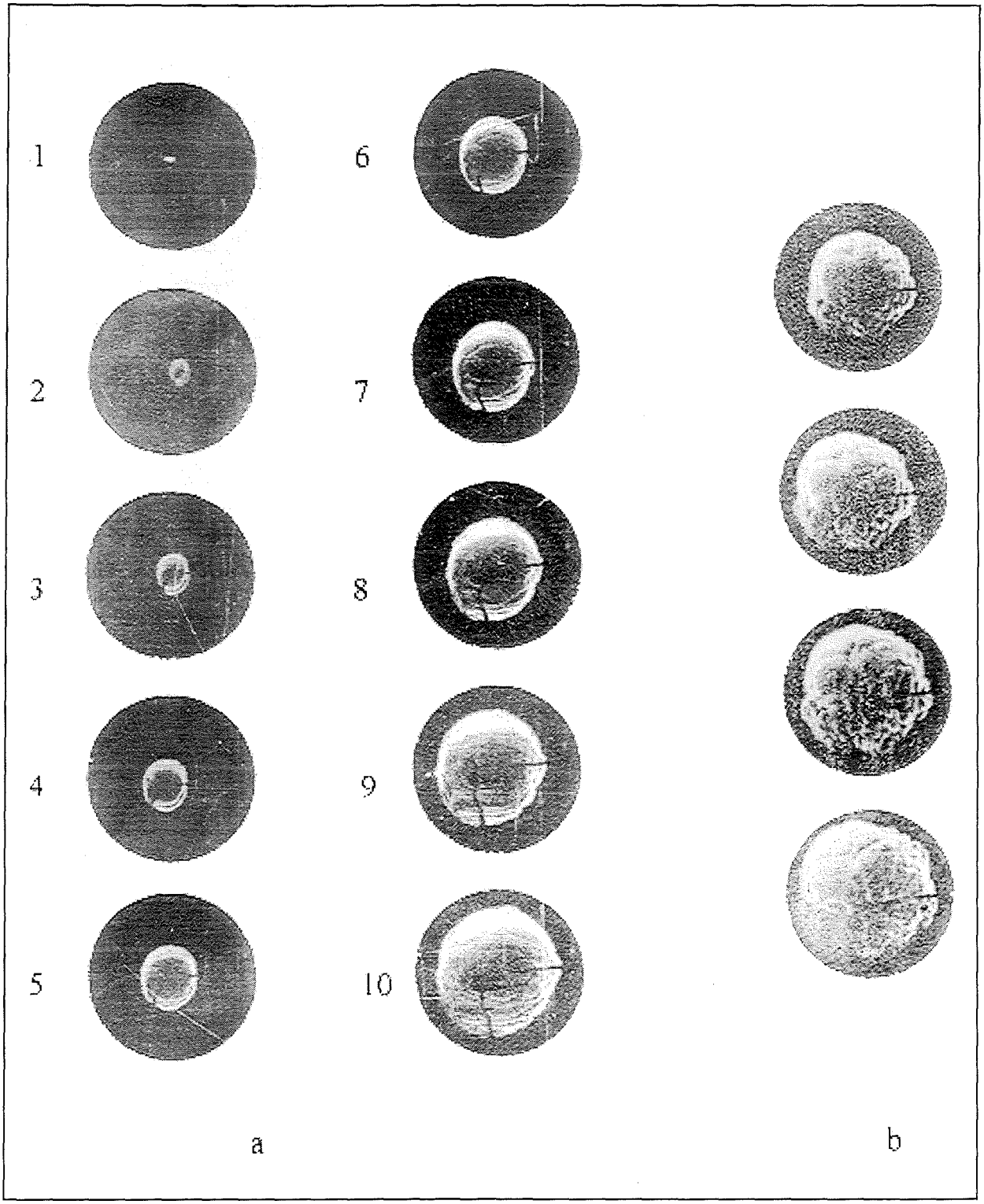

Fig.7.2: Schlieren photographs of flame kernels in H_2 - air - CO_2 mixtures at 298 K [13].
a) fast burning mixture with smooth surface, 21.2 % H_2, 15 % CO_2, p_0 = 1 bar, Δt = 1 ms;
b) lean, slowly burning mixture with cellular flame surface, 11.2 % H_2, 20 % CO_2, p_0 = 3 bar, Δt = 10 ms.

species fractions and energy are numerically integrated to calculate the steady-state flame speed. The mixture is ignited with 10 mJ energy, corresponding to the experimental spark energy. The flame zone is resolved with ≥ 40 nodes.

Fig. 7.3 shows the measured and calculated effect of the CO_2 addition on the laminar burning velocities. The experimental data derived from the pressure record p(t) and those derived from the visual flame radius r(t) agree well with the model calculations. Three different equivalence ratios (Φ = 0.21, 0.26, 0.39) are diluted with CO_2 up to the quenching limit. The relative influence of the CO_2 dilution is expressed in the lower part of the figure as the ratio S_u/S_{uo}, where S_{uo} is the burning velocity of the undiluted mixture (% CO_2 = 0). The used S_{uo} values for normalisation are also given. In a relative sense, CO_2 additions are more effective in lean H_2-air mixtures, than in near stoichiometric mixtures. To reduce e.g. the burning velocity by a factor of two, 5 % CO_2 are needed for Φ = 0.21, but 20 % for Φ = 1.

The effect of the initial pressure was also investigated. The dependence is only weak, generally reducing S_u by a factor of 2 in going from 1 to 5 bar initial pressure. Detailed calculations are presented in [13].

The burning velocity increases strongly with increasing initial temperature. The numerical calculations gave the following temperature dependence

$$S_u(T)=S_{uo}(T/T_o)^{\alpha} \qquad (7.3)$$

where $\alpha \approx 3$

S_{uo} = burning velocity at 298 K.

In the region of 300-500 K Eq. 7.3 results in about a factor of 2 increase in S_u for 100 K temperature increase. The temperature effect is important for the ex-vessel hydrogen generation when hot CO_2 is generated by core-concrete interaction.

The newly generated data base and the theoretical model now allow to determine the laminar burning velocity of H_2-air-CO_2 mixtures for practically all accident relevant temperatures and pressures. S_u is a fundamental mixture property which is also needed for turbulent burning models.

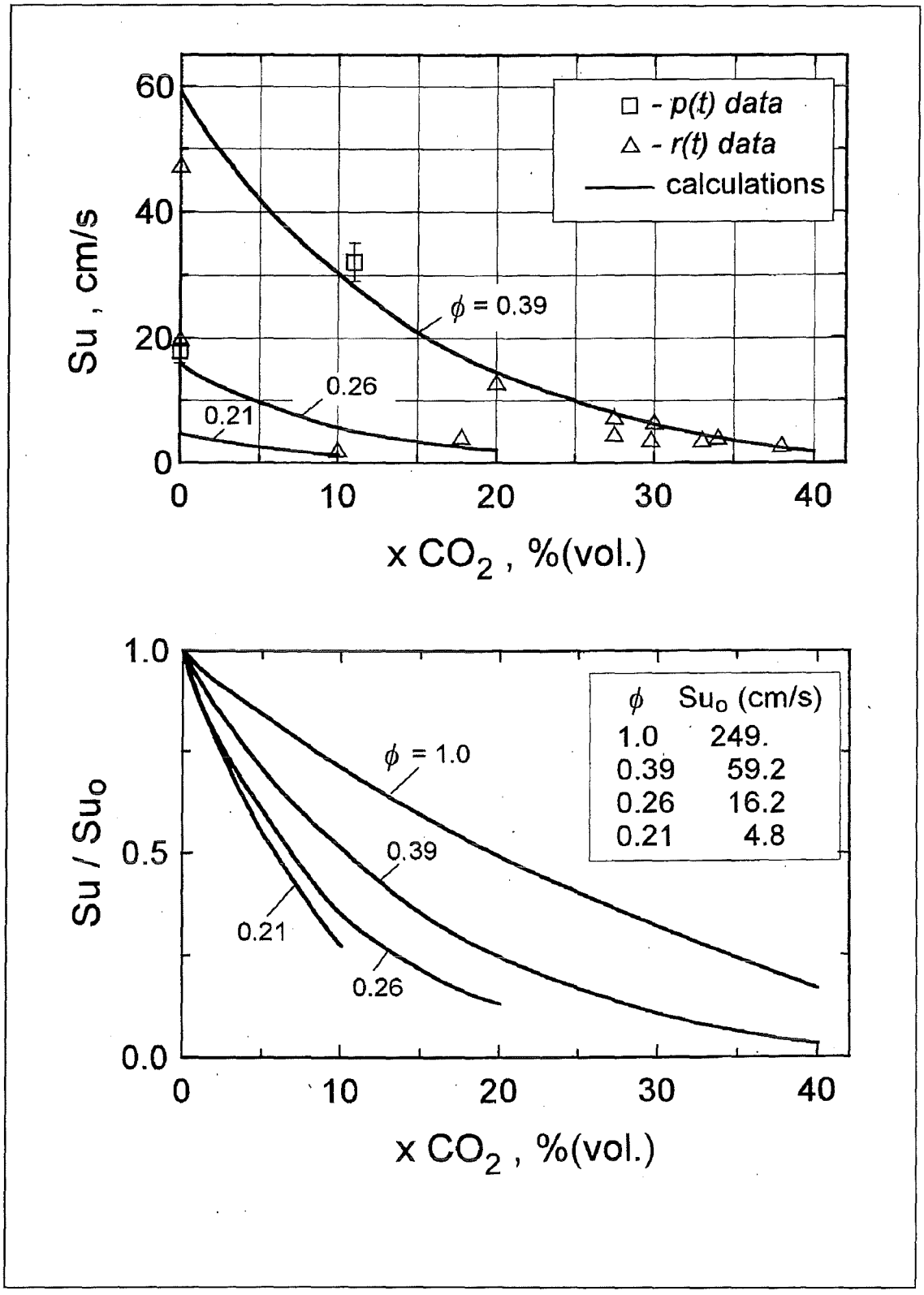

Fig.7.3: Measured and calculated influence of CO_2 dilution on the laminar burning velocity S_u in H_2 - air - CO_2 mixtures (p_0 = 1 bar, T_0=298 K, S_{u_0} = burning velocity without CO_2, Φ = fuel equivalence ratio). CO_2 dilution is more effective in lean mixtures than in near - stoichiometric mixtures.

7.3 Turbulent premixed burning velocity

Turbulence in the flow field can increase the combustion rate on the molecular level by turbulent diffusion and on the macroscopic level by flame folding. Turbulent deflagration is the most important combustion regime because fast turbulent flames can develop spontaneously if the gas composition and geometrical configuration are appropriate. The main goal of CO_2-mitigation is to suppress high flame speeds in this regime.

Experiments were carried out on the turbulent combustion of H_2-air-CO_2 mixtures in a spherical explosion bomb, which was equipped with fans to produce known levels of isotropic turbulence. The turbulence intensity u' ranged up to 8 m/s. The inhomogenity of the turbulence intensity was less than 20 %. Experiments were performed for 3 equivalence ratios (0.21, 0.26, 0.39), CO_2 concentrations up to 36 %, and pressures up to 5 bar. The results for Φ = 0.39 are summarised in **Fig. 7.4**. The data were measured at room temperature.

The turbulent burning velocity of a given mixture is significantly larger than the laminar velocity due to the increased mass transport rate and flame surface (e.g. a factor of 6 in pure H_2-air for u'=8m/s). After reaching a maximum value the turbulent burning velocity S_T decreases in CO_2-containing mixtures with further increasing turbulence.

The extinction limits (%CO_2) were close to those observed in the laminar burning tests. Variation of the initial pressure from 1 to 5 bar did not affect S_T within the measurement scatter. The Schlieren photographs show a very fuzzy, irregular flame shape. The surface is no longer closed and smooth, but rather consists of many apparently individual flamelets.

7.4 Self-ignition delay times

Fast turbulent flames produce precursor shocks which can cause the formation of hot spots in confined geometries. Self-ignition can then occur in these hot spots and lead to deflagration or even detonation, if certain conditions are met. The self-ignition delay time τ_i (or induction time) is therefore the most useful quantity of a

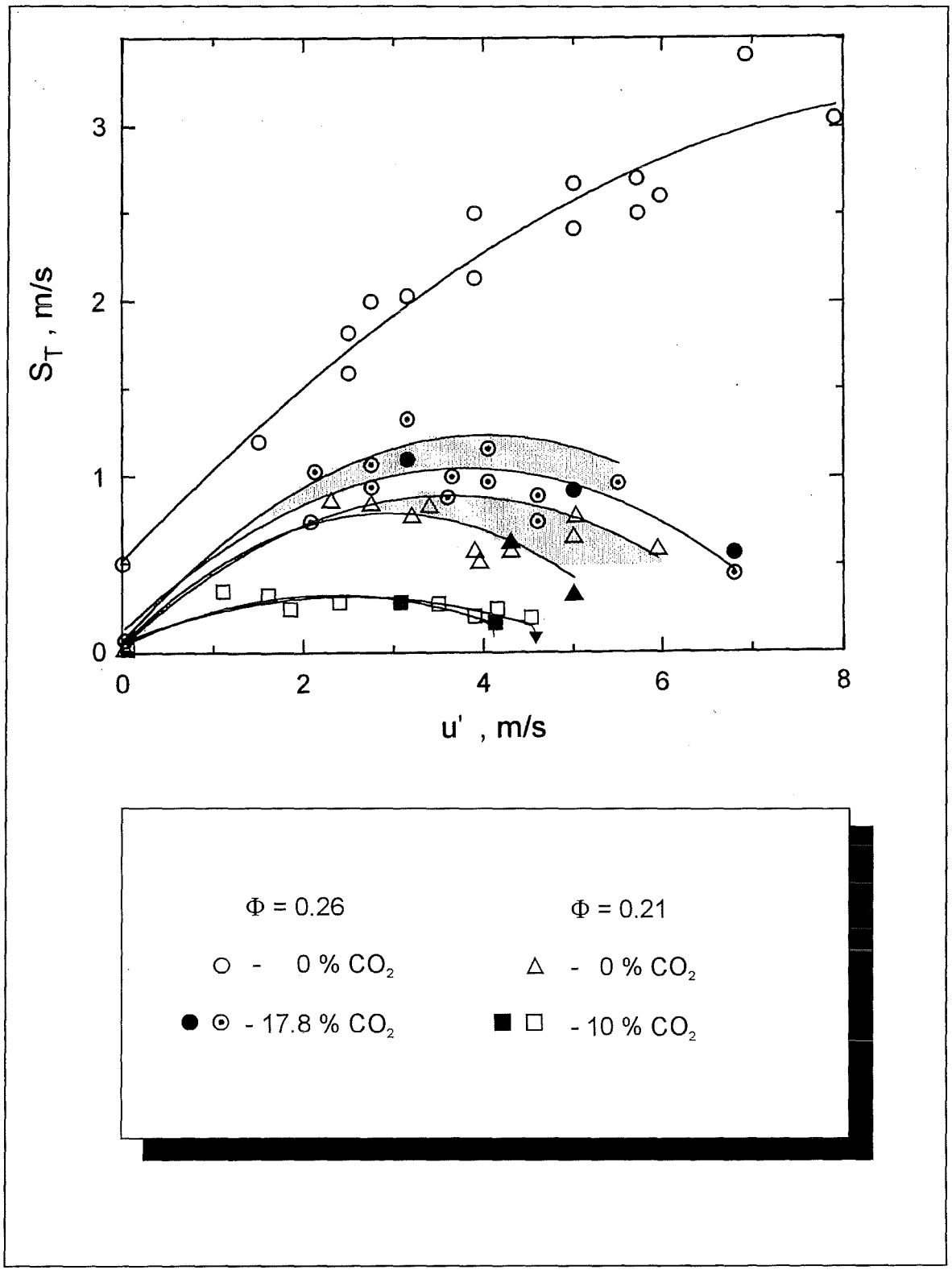

Fig.7.4: Measured turbulent burning velocities in H_2 - air - CO_2 mixtures at 298 K [13]. Open points p_0 = 1 bar, solid points p_0 = 5 bar. Pressure has a negligeable effect on the turbulent burning velocity. Extinction was observed at nearly the same CO_2 - concentrations as in the laminar tests.

mixture to judge its potential for transition into detonation. The influence of CO_2 on this property was therefore investigated experimentally and theoretically.

A computer code IDD was written to calculate the self-ignition delay times for H_2-air-CO_2 mixtures in a wide range of parameters (p_o = 1-15 bar, T_o = 800-1200 K, 10-20 % H_2, 5-20 % CO_2). The code integrates the rate equations of a detailed chemical reaction model (72 elementary reactions). τ_i is defined as the time after which the maximum heat release is reached:

$$\tau_i \equiv t \Big|_{\left(\frac{\delta T}{\delta t}\right)_{max}} \qquad (7.4)$$

Fig. 7.5 shows calculated induction times for a 15% H_2-mixture with 5 and 20 % CO_2, respectively. The inhibiting effect of CO_2 becomes noteworthy above 900 K in the shown Ω-zone. Compared to pure H_2-air mixtures, the addition of 20% CO_2 increases τ by roughly a factor of 2, which is not very significant.

Two modes of self-ignition can be distinguished in H_2-air mixtures

- mild or spotty self-ignition, characterised by a slow pressure rise and formation of numerous, distributed ignition centers, and
- strong ignition with a sharp, detonation-like pressure rise.

The ignition process depends on the pressure and temperature. The first ignition mode is connected to the slow thermal explosion mode of radical production, and the second one to the fast chain branching regime in the detailed kinetics of the H_2-O_2-reaction.

Experiments were made in a shock tube to investigate the influence of CO_2 on the mild and strong ignition regimes. The pressure and temperature development behind a reflected shock wave was measured with pressure transducers and photodiodes. The initial pressure and temperature in the reflected shock was evaluated from shock tube theory (700-1350 K, 8-44 bar).

The results of the experiments with 15% H_2-mixtures are summarised in **Fig. 7.6**. The solid curve is the calculated boundary between the mild and the strong regime

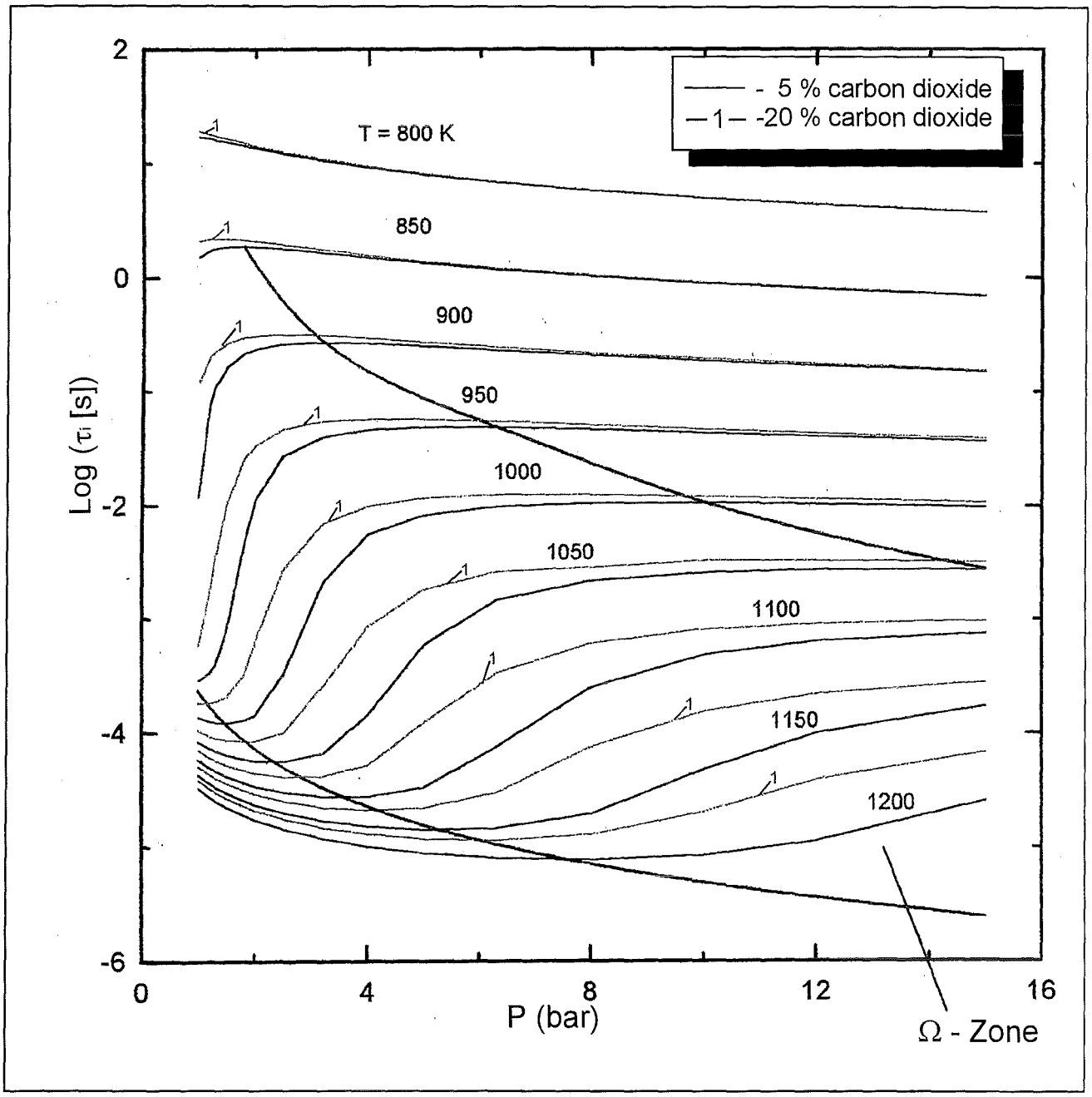

Fig.7.5: Calculated induction times τ_i for 15 % H_2 - air - CO_2 mixtures using a detailed chemistry model. The addition of 20 % CO_2 increases τ_i by roughly a factor of 2 compared to a pure 15 % H_2 - air mixture.

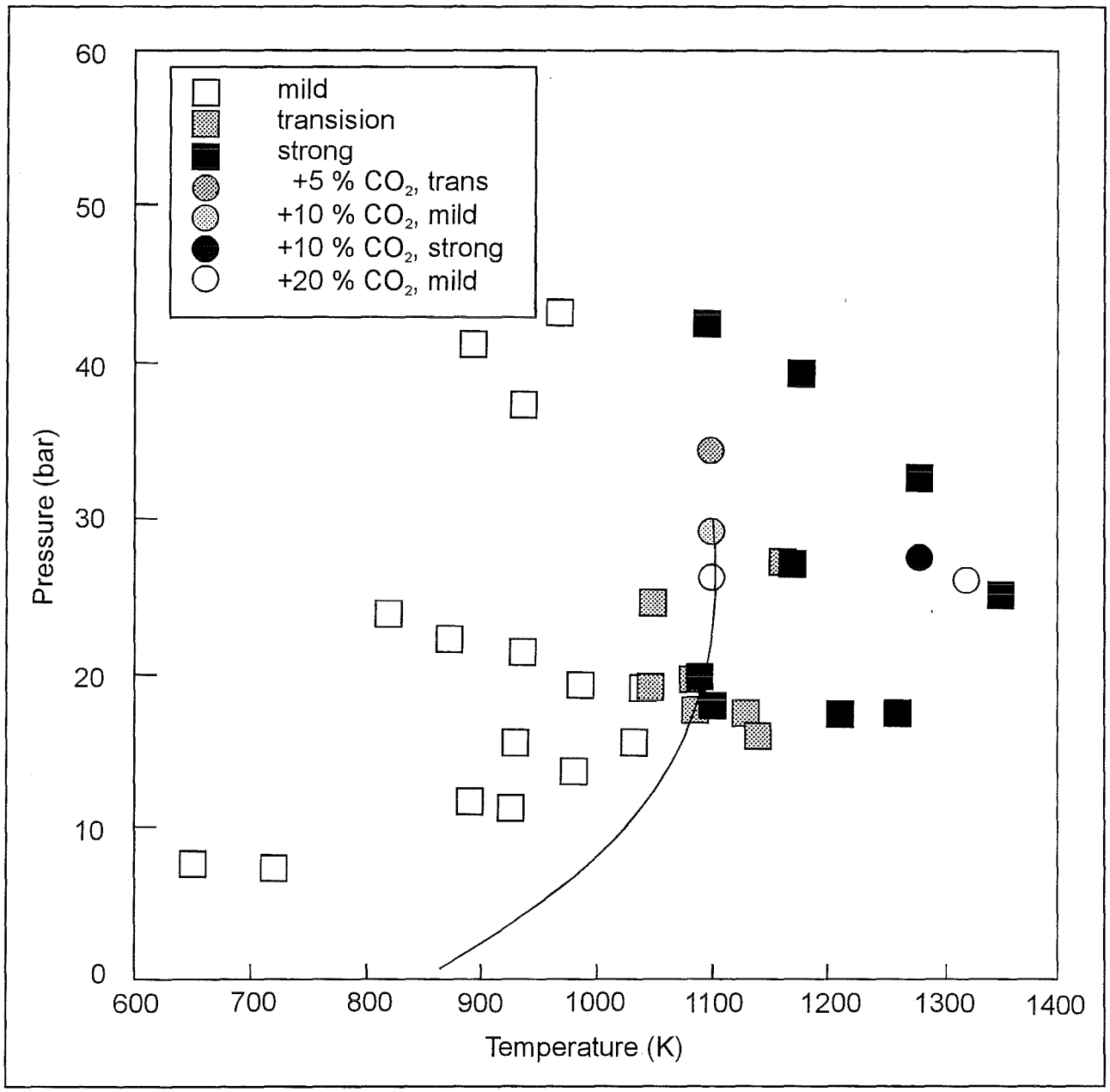

Fig.7.6: Influence of CO_2 on the self - ignition in H_2 - air - CO_2 mixtures. Points = experiments, line = theory, 20 % CO_2 are needed for a significant delay in self - ignition.

of self-ignition without CO_2. It agrees well with the measurements for 15% H_2-air (squares) which gave a transition temperature of 1100 ± 50 K for p_o> 10 bar.

The transition boundary is not influenced by 5 % or 10 % CO_2, only 20 % CO_2 produce a significant shift to higher temperatures.

7.5 Detonability limits

In case of a strong ignition, which can e.g. result from focusing of a pressure wave in a confing structure, a detonation may proceed into the unburned gas away from the ignition location. The stable propagation of such detonation wave requires certain geometrical sizes. In a tube geometry e.g., the wave will fail if the tube diameter is below a certain limiting value (d_{im}), because the losses are too high and no stable transverse shock wave system can be established. The limiting tube diameter d_{im} can therefore be used to quantify the detonability of gas mixtures. The value of d_{lim} represents roughly the minimum characteristic size necessary for detonation propagation in an extended channel or tube like geometry.

The numerical model described in [10] was used to calculate limiting tube diameters for H_2-air-CO_2 systems. The predictions of this model agree very well with earlier detonation experiments in H_2-air and with the limited data in H_2-air-CO_2 mixtures [13]. Pressures of 1, 3, and 5 bar, initial temperatures of 298, 400 and 500 k, different equivalence ratios and CO_2 concentrations were investigated in a large member of calculations.

Fig. 7.7 presents the results for moderately elevated temperatures and pressures, which are representative for global containment conditions in a severe accident, far away e.g. from H_2 or CO_2 sources (core-concrete interaction). For the interpretation of these results it is helpful to use the relation

$$d_{lim} = \lambda/\pi \qquad (7.5)$$

which is based on the fact that the detonation cell size of the limiting single head spin detonation in a tube is equal to the tube circumference. Fig.7.7 shows that the CO_2 concentration necessary to suppress a stable detonation propagation, increases with the tube diameter (17 % CO_2 in a 2 cm tube, 38 % CO_2 in a 1 m tube).

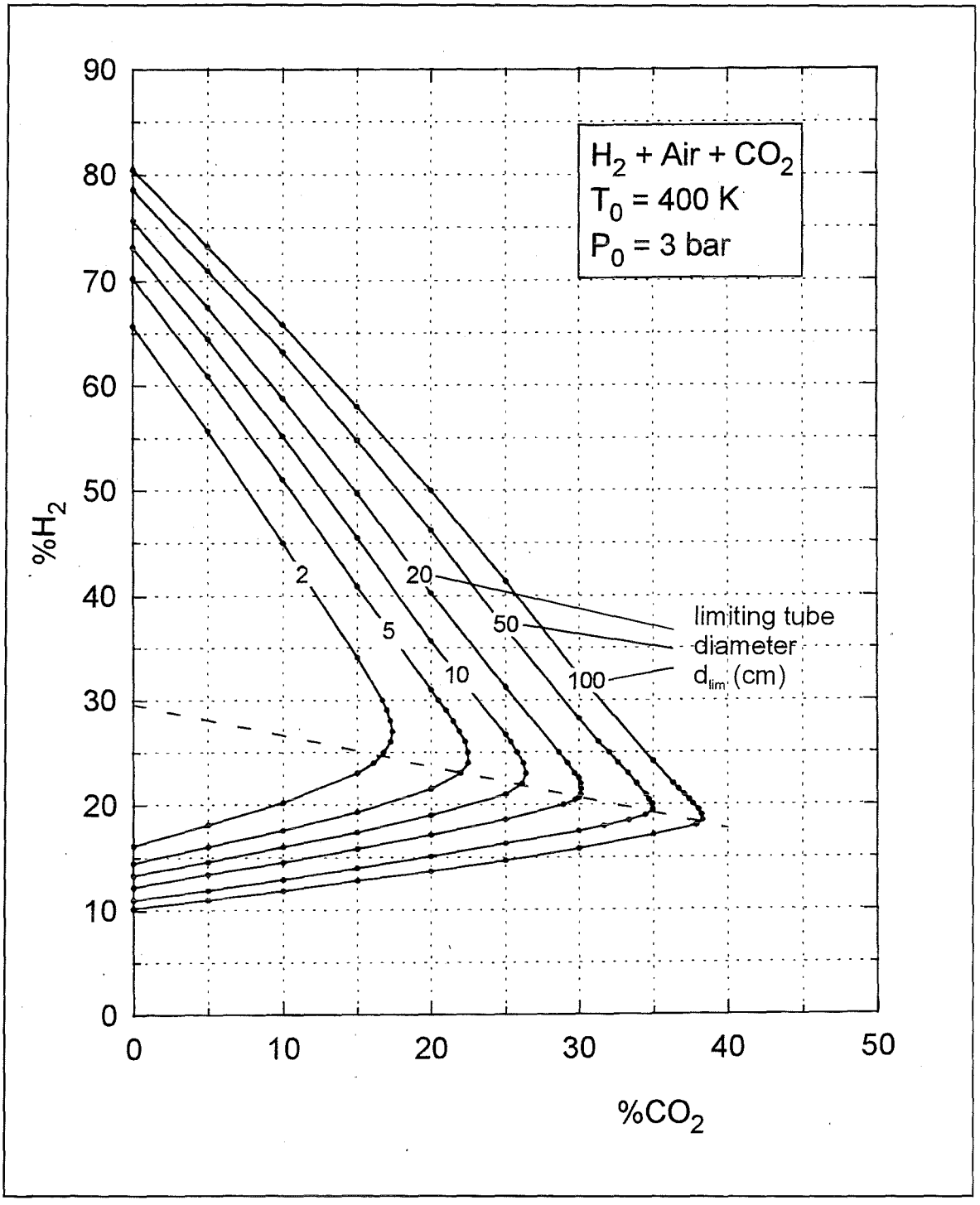

Fig.7.7: Calculated detonability diagram for H_2 - air - CO_2 mixtures at 400 K initial temperature and 3 bar initial pressure, representing global containment conditions in severe accidents. Significant CO_2 concentrations are needed on large scale to suppress detonations (> 30 %).

The shown range in d_{lim} covers the situations of interest for more accidents because d_{lim}=1m corresponds to a detonation cell size of about 3.1 m. According to the DDT criterion described in Section 5, a volume of $V \approx (7\lambda)^3 \approx (7 \bullet 3{,}1\ m)^3 \approx 10.000\ m^3$ would be necessary for starting a detonation in such an insensitive mixture.

The calculations showed that rising temperature widens the detonability range for a given d_{lim} significantly.

7.6 Conclusions on CO_2 effects

The effects of CO_2 on the suppression of deflagration and detonation in H_2-air-CO_2 mixtures can be summarised with the help of **Fig. 7.8**. The value of d_{lim}=1 m is a realistic limit for containment situations.

The lower flammability limit with CO_2 is the same as with steam. This is due to the preferential hydrogen distribution in the lean regime which drives the flame propagation alive. The H-diffusion is very similar in a steam or CO_2 containing atmosphere.

To suppress detonations and fast deflagrations between 30 and 50 % CO_2 are necessary (ø = 1). Smaller amounts of CO_2 dampen all explosion phenomena because the high heat capacity of CO_2 lowers the final combustion temperature. The induction times with CO_2 become longer. CO_2 certainly helps, but as long as burning is possible the same governing phenomena exist as without CO_2.

The CO_2-concentrations necessary to quench laminar and turbulent flames are close to the required steam concentrations. CO_2 is not more effective than steam, both being triatomic molecules.

A significant disadvantage of introducing CO_2 into an accident atmosphere is the pressure increase in the containment. In case of a combustion a higher pressure will exist in the containment than without CO_2 addition.

The main conclusion from the view point of combustion processes is that CO_2 only brings a significant mitigation effect if flames can be safely quenched. If one takes advantage of the presence of steam this will require more than 50% in steam + CO_2 concentration, which is not trivial to reach in a multicompartment containment in the

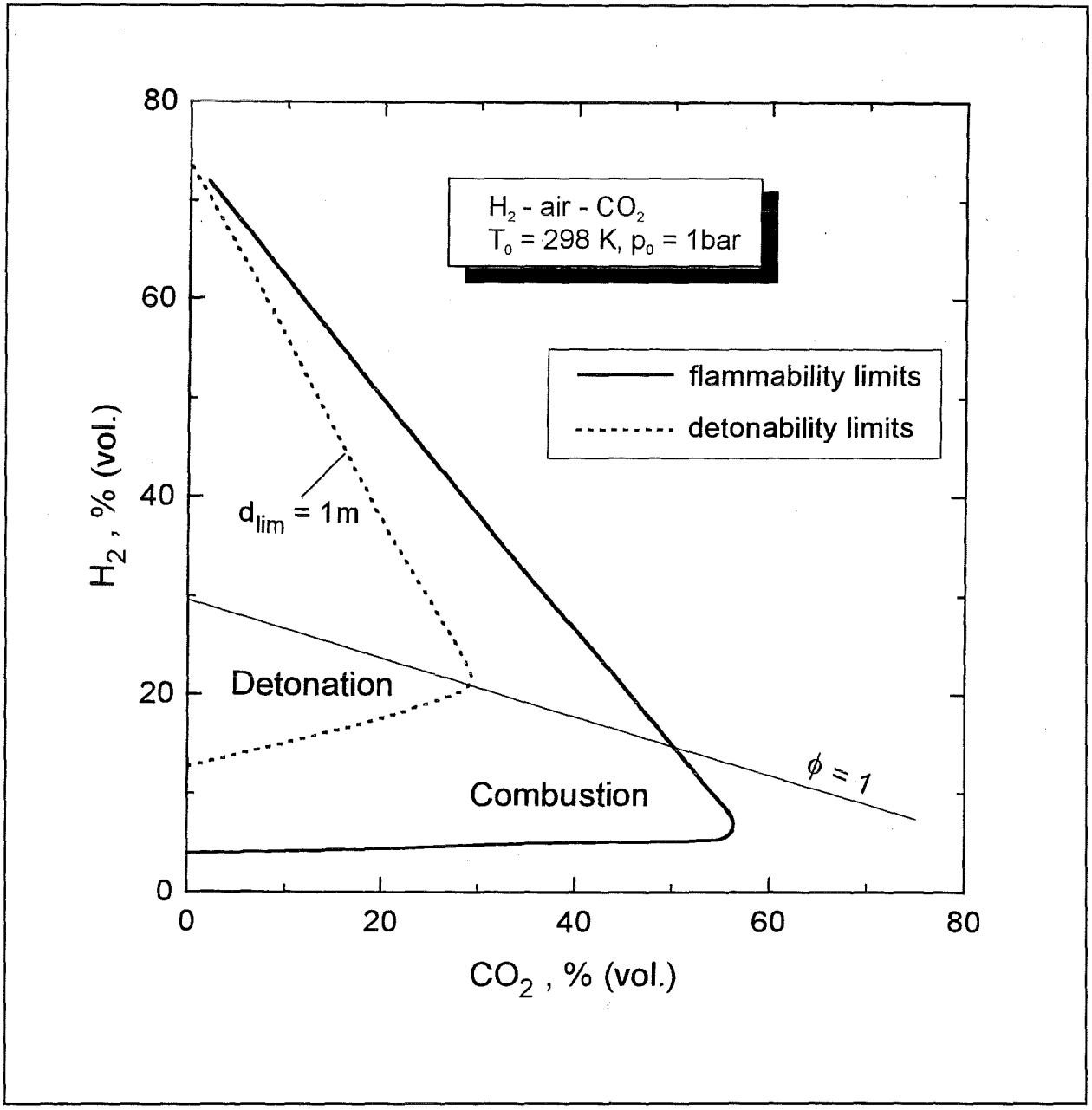

Fig.7.8: Effect of CO_2 on the suppression of detonation and deflagration in H_2 - air mixtures. Between 30 and 50 % CO_2 are needed.

available relatively short time span (≈30 min). The effectiveness of a CO_2-injection system to reach inertization in a nuclear containment can only be reliably demonstrated with a careful 3-d analysis.

8. EPR APPLICATIONS

The described models and criteria were applied to the EPR to investigate the effectiveness of spark igniters in „dry scenarios", where the in-vessel produced gases (H_2, steam) are released to the containment via the IRWST [14].

8.1 The GASFLOW model

The EPR geometry was modelled with a 3-d cylindrical mesh consisting of about 12000 computational cells. 180 degree symmetry was assumed. **Fig. 8.1** shows one horizontal and six vertical cuts through the geometry model. All major components of the primary system are included.

The containment was subdivided into six control volumina (rooms 1-6 in Fig. 8.1). In each volume the characteristic size of the H_2-air-steam cloud and its average composition was evaluated during the H_2-release (**Fig. 8.2**). At any given time the characteristic size D, the average H_2, and steam concentrations $\overline{x_{H2}}$ and $\overline{x_{H2O}}$ are calculated to

$$D = (\Sigma \Delta V_i)^{1/3} \tag{8.1}$$

where ΔV_i = GASFLOW cell with burnable mixture, e.g. 4-75 % H_2 in dry mixture.

$$\bar{x}_{H2} = \Sigma x_{H2,i} \cdot \Delta V_i \; / \; \Sigma \Delta V_i \tag{8.2}$$

$$\bar{x}_{H2O} = \Sigma x_{H2O,i} \cdot \Delta V_i \; / \; \Sigma \Delta V_i \tag{8.3}$$

where $x_{H2,\,i}$ = local H_2-concentration in cell i, which is part of the reactive cloud volume

$x_{H2O,\,i}$ = corresponding steam concentration in cell i.

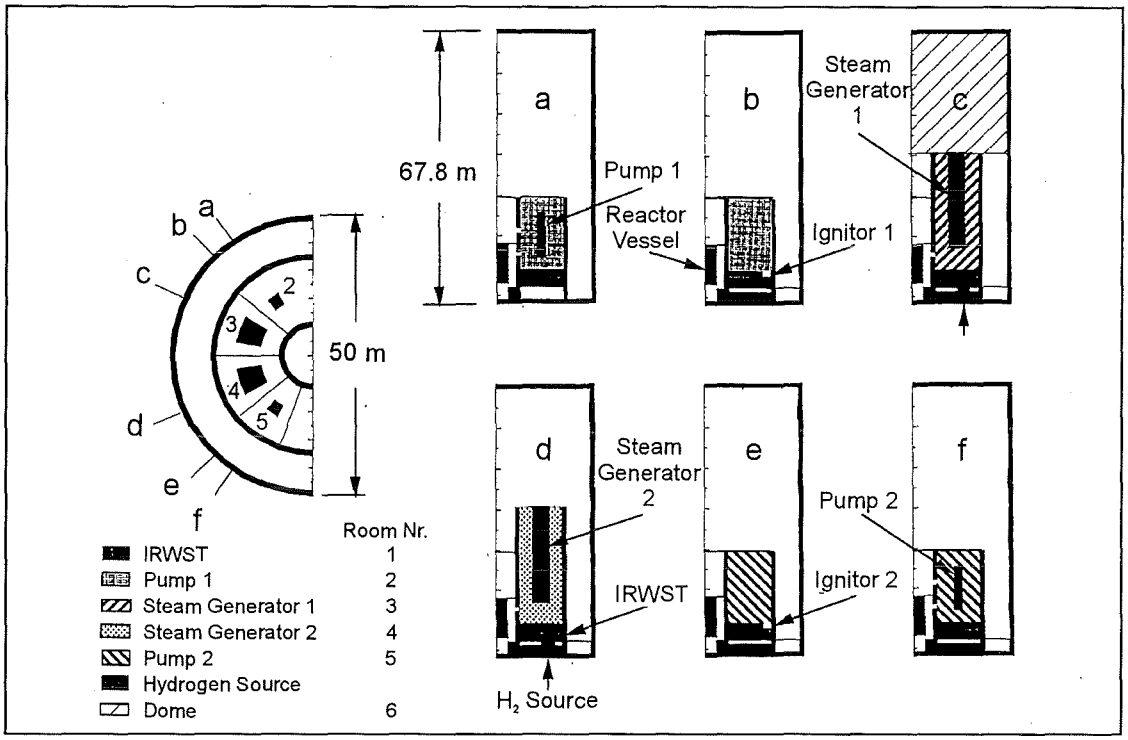

Fig. 8.1: 3 - d GASFLOW geometry model for the EPR with about 12000 computational cells.

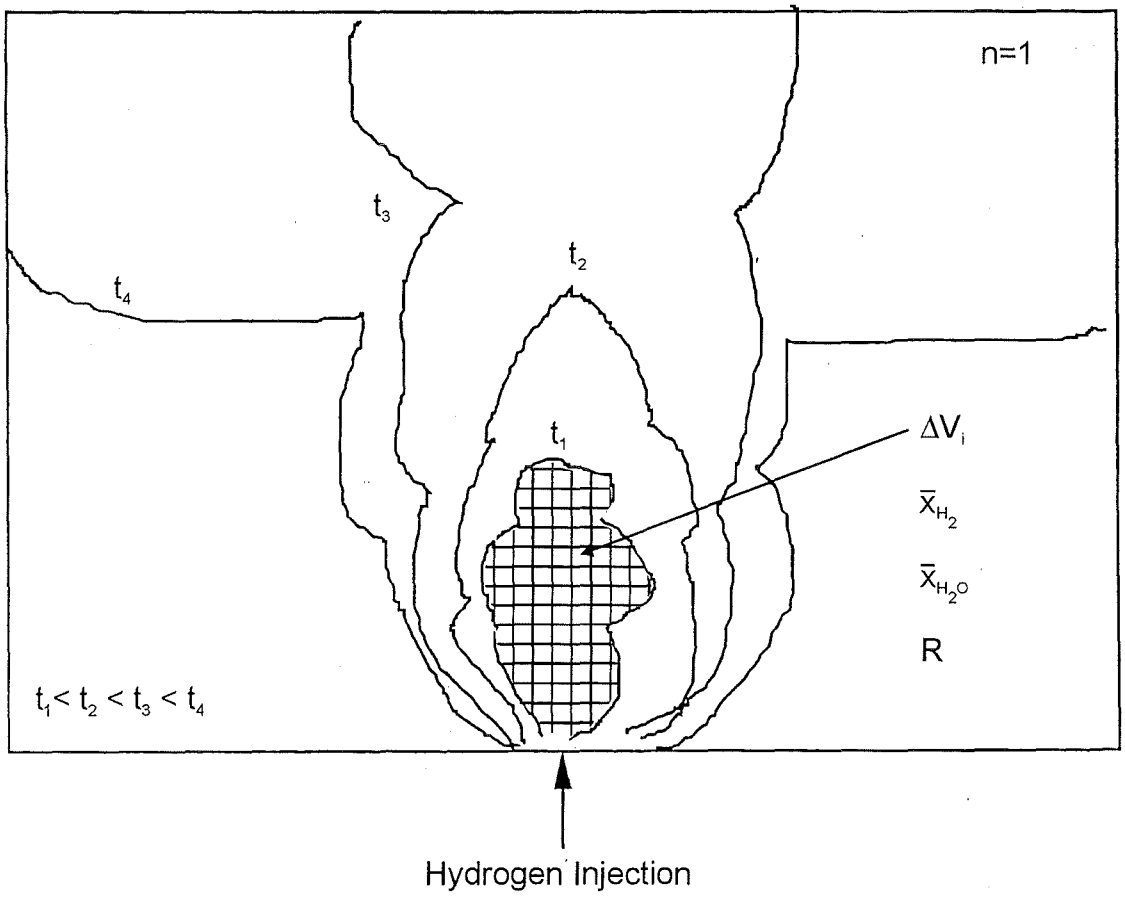

Fig. 8.2: Evaluation of characteristic properties of H_2 - air - steam cloud during the H_2 - release process. Computed cloud size and average composition are used to evaluate the DDT potential according to the 7λ - criterion.

The detonation cell size of the average cloud mixture is then evaluated from the known relation

$$\lambda = f(x_{H2}, x_{H2O}, p, T) \qquad (8.4)$$

The DDT potential is calculated according to the 7λ criterion described in section 5:

$$R = \frac{D}{7\lambda} \quad \begin{cases} > 1 & DDT\ possible \\ < 1 & DDT\ not\ possible \end{cases} \qquad (8.5)$$

The DDT index R is evaluated in each room n of the containment (n=1...6) as function of time.

8.2 Analysis without mitigation

A quite conservative dry release scenario was investigated to fully explore the limits of the deliberate ignition concept for dry hydrogen sources. Release rates of up to 2 kg H_2/s were used (**Fig. 8.3**). The first release phase up to 2000 s is the result of a MAAP calculation for the EPR in-vessel H_2-production. The same release history was added between 2000 and 4000 s to roughly represent an ex-vessel phase. The total released H_2-mass is about 1200 kg.

First a transport analysis without deliberate ignition was performed to understand the time and space dependent evolution of burnable H_2-mixtures. **Fig. 8.4** shows the computed DDT index R as defined in Equ. 8.5.

During the first release phase up to 2000 s, detonable mixtures only develop in the compartments close to the H_2-source location, namely in the IRWST and pump room 1. The second release of 600 kg H_2 drives all compartments into the detonable regime. A global detonation could not be excluded after 3000 seconds.

It is important to note that the time needed to change from the deflagration regime (R < 1) to the potential detonation regime (R > 1) can be relatively short. The large dome volume makes the transition in about 100 s in this test calculation. This demonstrates the need for a fast reacting H_2-control system, recombines alone may not be sufficient for high dry release rates.

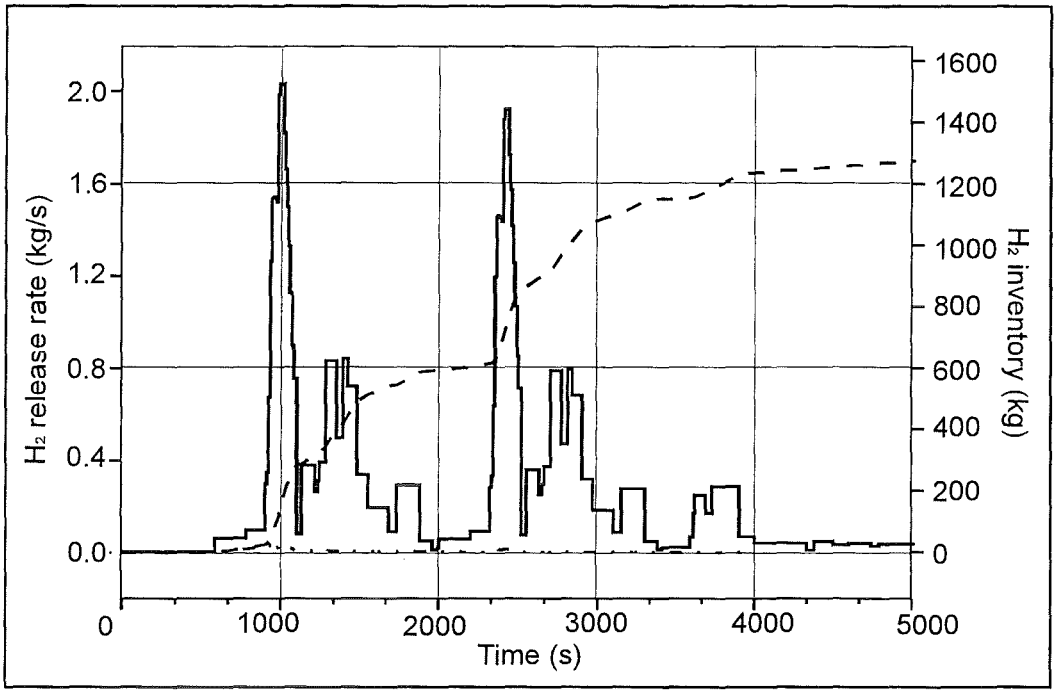

Fig. 8.3 : Assumed conservative H_2 - release rate into EPR during dry release scenario (in - vessel and ex - vessel phase about 600 kg H_2 each)

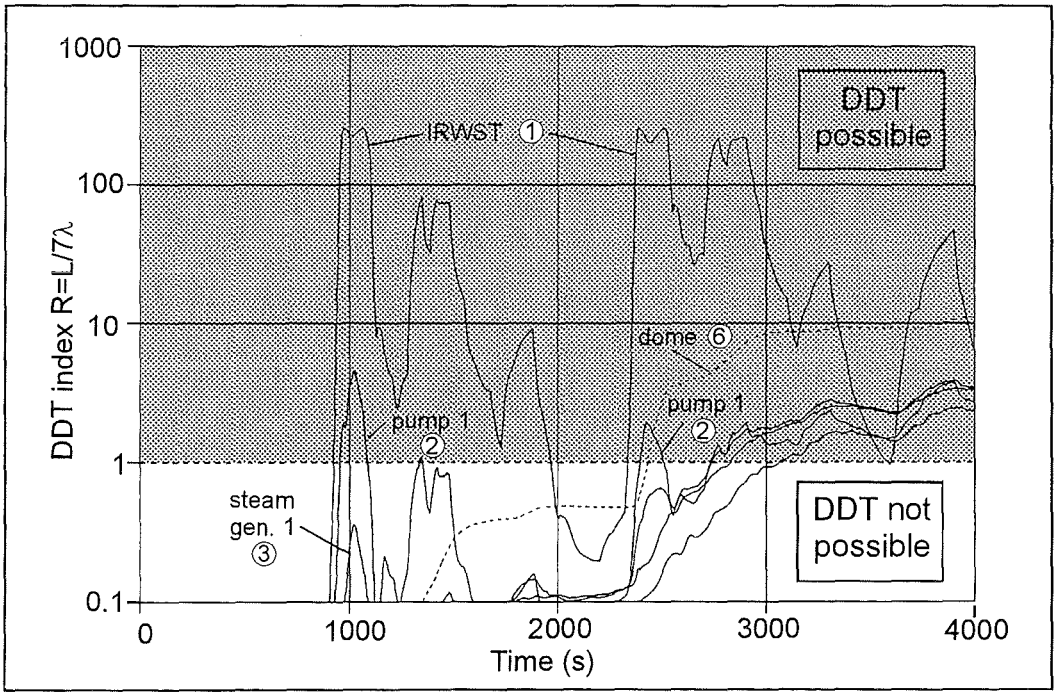

Fig. 8.4 : Computed detonation potential for six rooms of the EPR containment, according to the 7λ - criterion (detonation possible for R > 1).

The described GASFLOW models allowed for the first time a mechanistic 3d prediction and a quantitative measure for the possibility of local detonations in a H_2 release scenario.

8.3 Analysis with spark igniters

The described release sequence was analysed with spark igniters at different positions in the IRWST and with different spark frequencies (1 and 10 Hz). The computations showed that it is possible to control severe dry release scenarios with appropriately positioned spark igniters (**Fig. 8.5**). The first large scale burn-out of the release compartment (the IRWST) could be triggered early enough before DDT possibilities had developed. Very effective H_2-removal was predicted for the whole release duration without damaging pressure loads.

Fig. 8.5 shows the lower EPR geometry with two spark igniters located about 3 m above the two hydrogen sources. The dark surface below the two igniters represents the calculated 200 K isosurface of the burning H_2-flame at 922 s. During high hydrogen release rates the flame in the IRWST becomes oxygen limited. Unburned H_2 leaves the IRWST and ignites above the left hand opening to the containment.

The current model verification in GASFLOW covers the sequence of events up to the first burn-out where either the detonation regime (R>1) or the deflagration regime (R < 1) is entered. For slow deflagrations (R<<1) the current global reaction model of GASFLOW appears adequate. For the intermediate regime of fast deflagrations it is intended to derive a flame acceleration criterion which will allow to introduce a branching point in the GASFLOW analysis concerning the transition from slow to fast turbulent deflagration.

9. INCA PROGRAM DEVELOPMENT

The development of a next generation program for INtegral Containment Analysis was started at FZK (INCA code).

The main objective of the work is development, testing and application of 3-d adaptive grid techniques to full scale containment analysis. Such a method would

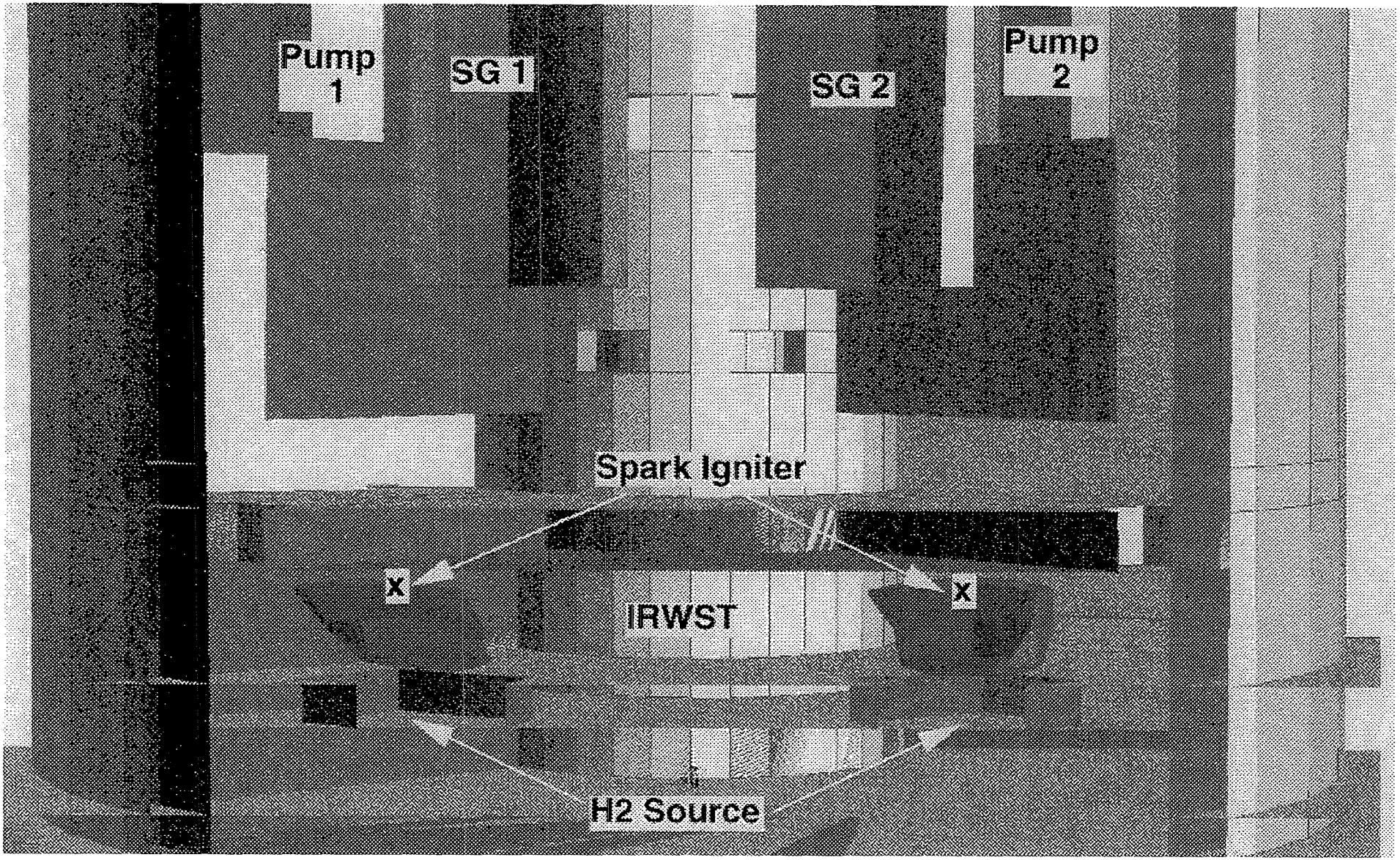

Fig. 8.5: Lower EPR 3 - d containment geometry with spark igniter positions leading to early H_2 - ignition without pressure development (case 3 - C2 at 922s)

allow much improved space and time resolution in local areas of the computational domain, automatically adjusted to the evolution of the flow field or the flame motion.

The INCA-code structure is depicted in **Fig. 9.1**. The important characteristics of the new program are

- adaptive grid for local resolution of the computational domain (equidistant cartesian, 3-d),
- modular structure with clearly defined interfaces between the main modules for distribution, deflagration, and detonation,
- graphical user interface for input of geometry and initial conditions,
- vectorization and parallelization capabilities,
- automatic switching between distribution and different combustion regimes, reversible scheme.

Currently COM3D and DET3D exist as stand-alone codes. The program V3D is under development. The hydrodynamics and turbulence part has been completed and will be validated against theoretical and experimental results (Riemann problem, FZK turbulence tests).

For the generation of a 3-d adaptive Eulerian grid a C++ library of Lawrence Livermore National Laboratory (LLNL) is used. The library together with a LLNL test problem was successfully implemented at FZK. The next step will be replacement of the LLNL-problem with the DET3D code.

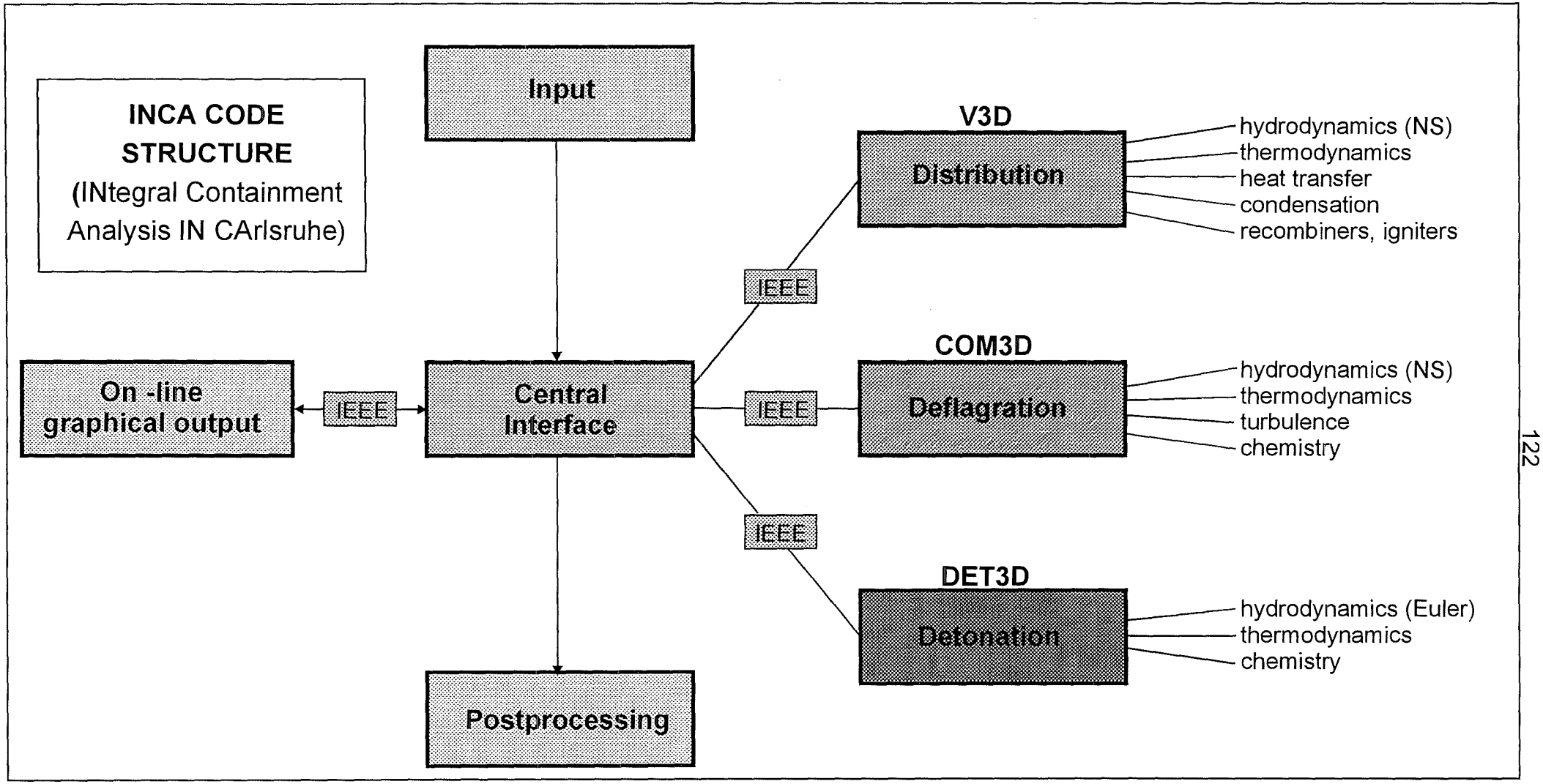

Fig. 9.1 : Structure of FZK next generation program for integral containment analysis (INCA - Code)

REFERENCES

[1] A. Miassoedov,
„Ein Modell zur Beschreibung der Wasserstofferzeugung durch Kernflutung bei Kernschmelzunfällen",
Dissertation, Universität Karlsruhe (1996)

[2] P. Royl, W. Breitung, L. Seyffarth, J. R. Travis, H. Wilkening
"Simulation of Hydrogen Transport with Mitigation Using the 3D Field Code GASFLOW "
To be published at Second International Conference on Advanced Reactor safety, June 1-4, 1997, Orlando, Florida

[3] E. A. Haytcher, P. Royl, J. R. Travis, H. Wilkening
" Theoretical Investigations with GASFLOW "
3. Fortschrittsbericht FZK/EVU/Siemens Zusammenarbeit, Seite 95, März 1996

[4] V. Moser;
„Simulation der Explosion magerer Wasserstoff-Luft-Gemische in großskaligen Geometrien",
Dissertation RWTH Aachen, Institut für Techn. Mechanik (1996)

[5] I.D. Matsukov, M.S. Kuznetsov, V.I. Alekseev, S.B. Dorofeev;
" Experimental study of turbulent flame propagation and flame-vortex interaction for turbulent combustion modelling", report Russian Research Center "Kurchatov Institute" (November 1996)

[6] B.E. Gelfand, S. P. Medvedev, O.V. Popov;
"Turbulent deflagration phenomena in hydrogen - fog - air mixtures", Internal report to FZK from Russian Academy of Sciences, Moscow (November 1996)

[7] A. Veser
„Numerische Simulation von H_2-Luft-Verbrennungsexperimenten"
Diplomarbeit chem. ing., Forschungszentrum Karlsruhe and Univesität Karlsruhe, 1996

[8] W. Breitung, A. Veser
"Specifications for Premixed H_2-air turbulent deflagration experiment RUT-23", Benchmark tests for EG project FI4S-CT95-0001, 1996

[9] S.B. Dorofeev, A.A. Efimenko, A.V. Bezmelnitsyn
"Analysis and evaluation of DDT criteria for severe accident conditions",
report Russian Research Center" Kurchatov Institute", Moscow (Nov. 1996)

[10] A.M. Bartenev, B.E. Gelfand, O.E. Popov,
"Evaluation of hydrogen containing mixture detonability for accident relevant conditions", Report Russian Academy of Sciences, Moscow (Nov. 1996)

[11] W. Breitung, G. Engel, E. Hesselschwerdt, A. Kotchourko, H. Massier, R. Redlinger, H. Wilkening, J. Wolff, A. Veser,
„Untersuchungen zu H_2-Verbrennungsvorgängen" PSF Jahresbericht 1995 (R. Hüper Ed.), Report FZKA 5780 (1996) p.73

[12] A.A. Efimenko, A.V. Denkevits, S.B. Dorofeev
"Computer code for missile problem evaluation", Report Russian Research Center „Kurchatov Institute", Moscow (Nov. 1995)

[13] B.E. Gelfand, O.E. Popov, S.V. Khomik
"Laminar and turbulent flame propagation in hydrogen-air-CO_2 mixtures at accident relevant pressure-temperature conditions", Report Russian Academy of Sciences, Moscow (Nov. 1996)

[14] W. Breitung, S.B. Dorofeev, J.R. Travis
"A mechanistic approach to safe igniter implementation for hydrogen mitigation", OECD Workshop "On the Implementation of Hydrogen Mitigation Techniques", Winnipeg, Manitoba, Canada, May 13-15, 1996

PUBLICATIONS

[1] W. Breitung, P. Royl, J. R. Travis, H. Wilkening,
„ Analysen zur Wasserstoffverteilung in DWR-Anlagen"
Atomwirtschaft 41 (Juni 1996) 411

[2] W. Breitung, G. Keßler
" Calculation of hydrogen detonation loads for future
reactor containment designs", Festschrift zu Prof. Eibl's 60. Geburtstag
(März 1996), p.131, K. Hilsdorf, G. Kobler (Eds.) Institut für Massivbau und
Baustofftechnologie, Universität Karlsruhe, 76128 Karlsruhe

[3] W. Breitung, H. Massier, M. Möschke, R. Redlinger,
A. Veser, P. Galon, M. Lepareux,
" Hydrogen-air detonation experiments in complex
geometry and their analysis with different codes",
Proc. of FISA-95-EU research on severe accidents (1996), G. van Goethem,
W. Balz, E. Della Loggia (Eds.), EU Report EUR 16896 EN, p. 498

[4] W.Breitung, A. Kotchourko,
„ Numerische Simulation von turbulenten Wasserstoff-
Verbrennungen bei schweren Kernreaktorunfällen",
FZK-Nachrichten Heft 2/3, 1996, p.175

[5] W. Breitung, S. B. Dorofeev, J. R. Travis,
" A mechanistic approach to safe igniter implementation
for hydrogen mitigation", OECD Workshop on the
Implementation of Hydrogen Mitigation Techniques,
Winnipeg, Canada, May 13-15, 1996

[6] S.B. Dorofeev, V. P. Sidorov, A. E. Dvoinishnikov, W. Breitung
" Deflagration to detonation transition in large confied volumes
of lean hydrogen-air mixtures". Combustion and Flame 104
(1996) 95-110

[7] W. Breitung, G. Engel, E. Hesselschwerdt, A. Kotchourko,
H.Massier, R. Redlinger, , H. Wilkening, J. Wolff, A. Veser
„Untersuchungen zu Wasserstoff-Verbrennungsvorgängen",
3. Fortschrittsbericht zu FZK/EVU/ Siemens Zusammenarbeit
März 1996, p. 36-35

[8] A. Veser, „ Numerische Simulation von H_2-Luft-Verbrennungs-
experimenten", Diplomarbeit, FZK und Lehrstuhl
für Feuerungstechnik der Uni Karlsruhe, January 1996

[9] P. Royl, J. R. Travis, "Simulation of hydrogen transport with mitigation using the 3D field code GASFLOW", to be published in Procs. 2nd International
Conference on Advanced Reactor Safety, June 1-4, 1997, Orlando, Florida, USA
[10] E. A. Haytcher, G. Necker, P. Royl, J. Spore, J. R. Travis, H. Wilkening, "Theoretical investigations with GASFLOW", Annual Report 1996, 4. Fortschrittsbericht Zusammenarbeit FZK/EVU/Siemens, March 1997

[11] W. Breitung, P. Royl, J. R. Travis, H. Wilkening, L. Seyffarth, "GASFLOW Analysen zur Wasserstoffverteilung im Sicherheitsbehälter nach Kühlmittelverluststörfällen im Kernkraftwerk Biblis A", PSF-Report 32 58, February 1997

[12] P. Royl, E. A. Haytcher, J. R. Travis, H. Wilkening, "3D-Simulationen von Wasserstoffverteilung und -verbrennung im Sicherheitsbehälter eines Druckwasserreaktors," FZK-Nachrichten Heft 2/3, 1996, p. 192

[13] P. Royl, J. R. Travis, E. A. Haytcher, H. Wilkening, "Analysis of mitigating measures during steam/hydrogen distributions in nuclear reactor containments with the 3D field code GASFLOW," OECD/NEA
CSNI Workshop on the Implementation of Hydrogen Mitigation Techniques, Winnipeg, Canada, May 13-15, 1996.

[14] E. A. Haytcher, P. Royl, J. R. Travis, H. Wilkening, "Theoretical investigations with GASFLOW," Annual Report 1995, 3. Fortschrittsbericht Zusammenarbeit FZK/EVU/Siemens, März 1996 p. 66

[15] W. Rehm, P. Royl, W. Breitung, M. Carcassi, F. Fineschi, M. Heitsch, R. Reinders, K. Freudenstein, "Combustion Phenomena in Nuclear Reactor Containments," Procs FISA 95-EU Research on Severe Accidents, G. van Goethem, W. Balz, E. Della Loggia (Eds), Eu Report, EUR 16896EN, p. 330

[16] Gelfand, B.; Popov, O.; Kusharin, A.; Agafonov, G.; Breitung W. " High-temperature self-ignition and detonation of H2-air mixtures with NOx additives"; Proceedings, 15th Int. Colloqium on "The Dynamics of Explosions and Reactive Systems", University of Colorado, Boulder/Colorado, USA, July 31 Aug. 4, 1996, pp.473-475

[17] Alekseev, V.I.; Dorofeev, V.P.; Dvoinishnikov, E. A.; Breitung, W. " Experimental study on the transmission of gaseous detonation to less sensitive mixtures ;Proceedings of 15th Int. Colloqiuum on "The Dynamics of Explosions and Reactive Systems", University of Colorado, Boulder/Colorado, USA, July 31- Aug. 4, 1996, pp.13-16

[18] Dorofeev, S. B.; Kochurko, A. S. ; Sidorov, V.P.; Bezmelnitsin, A. V.; Breitung W.; "Experimental and numerical studies of the pressure field generated by DDT events",
Shock Waves 1996 5, p. 375-379

[19] Breitung, W.; Dorofeev, S. B.; Efimenko, A.A.; Kochurko, A.S.; Redlinger, R.; Sidorov, V.P.
" Large scale confined hydrogen-air detonation experiments and their numerical simulation"; Proc. of the 20th Int. Symp. On Shock Waves, California Inst. Of Technology, Pasadena, CA, USA, Juli 23-28, 1995
B. Sturtevant, J. Shepherd (Eds), Vol. 2, p. 1101-1106, World Scientific Publ. CO., Singapore 1996

[20] W. Breitung, "Proceedings of the Hydrogen Seminar 1996", FZK, December 2-5, 1996

[21] J. Spore, J.R. Travis, P. Royl, G. Necker, " Version 2.1.0.0 of GASFLOW" Los Alamos Report LA-UR-97-865, January 1997

PRESENTATIONS

[1] W. Breitung, " Results on hydrogen mitigation research at Forschungszentrum Karlsruhe", GPR-RSK Workshop on Severe Accident Issues for Future Pressurised Water Reactors, Munich, January 10-11, 1996

[2] W. Breitung, E. A. Haytcher, R. Redlinger, P. Royl, J. R. Travis, H. Wilkening, "Results obtained in 1995 and future activities on hydrogen transport and mitigation", Project Council Nuclear Safety, January 18, 1996

[3] W. Breitung, " Neue Ergebnisse zur H_2-Verbrennung aus FZK-PSF Programm", EVU-Siemens- FZK Contract, Meeting of H_2-Working Group, FZK, February 2, 1996

[4] W. Breitung, A.S. Kotchourko, A. Veser, " Numerical simulation of turbulent hydrogen-air combustion experiments", European Research Conference on" Mathematical Methods for Industrial Problems", Mt. St. Odile, France, February 16-21, 1996

[5] A.S. Kotchourko " Validation and application of a turbulent combustion code", European Research Conference on " Mathematical Methods for Industrial Problems", Mt. St. Odile, France, February 16-21, 1996

[6] W. Breitung, " Neue Ergebnisse zum Wasserstoff-Verhalten", EVU-Siemens-FZK Vertrag, 7th Meeting of Project Committee, FZK, February 29, 1996

[7] P. Royl, " Hydrogen Behavior: GASFLOW Development and Validation at FZK", WG-3 Meeting Accident Behavior, FZK, March 11, 1997

[8] W. Breitung, "Hydrogen combustion research at FZK", CEA-FZK Cooperation on Severe Accidents, Meeting on Containment Accident Behaviour, FZK, March 20, 1996

[9] W. Breitung, "Simulation of hydrogen control methods at FZK", Meeting on Combustion and Inertization for the Borssele Nuclear Power Plant, Ministry of Social Affairs and Employment, Den Haag, Netherlands, March 28, 1996

[10] S. Dorofeev, V. Sidorov, W. Breitung, J. Vendel, "First results of large scale hydrogen air-steam experiments in the RUT facility", US-NRC CSARP Meeting, Bethesda, MD, USA, May 6-10, 1996

[11] P. Royl, W. Breitung, J. R. Travis, "Hydrogen Combustion and Mitigation Research at Forschungszentrum Karlsruhe". US-NRC CSARP Meeting,Bethesda, MD, May 6-10, 1996

[12] P. Royl, "Status of GASFLOW development and future cooperation in the frame of the FZK/LANL GASFLOW cooperation agreement", Vortrag Los Alamos, NM, USA, May 17, 1996

[13] W. Breitung, „Versuchsergebnisse und analytische Studien zur Absicherung des Dualen Konzepts", 137th Meeting of RSK-LWR Committee, Bonn, June 30, 1996

[14] P. Royl, "GASFLOW Aktivitäten zum EPR", Siemens/EVU/FZK-Vertrag, FZK, Juli 24, 1996

[15] W.Breitung, "Hydrogen research and program planning 1996", EVU-Siemens-FZK Vertrag, AG Wasserstoffverhalten, FZK, July 24,1996

[16] W. Breitung , "Results on hydrogen mitigation research at Forschungszentrum Karlsruhe", 17th Meeting of EU Study Project on Development of a Common Safety Approach in EU Countries for Large Evolutionary PWR's, FZK, September 23-25, 1996

[17] W. Breitung, "Ergebnisse des Bereichs Wasserstoff", 8th Meeting of PSF Project Committee, EVU-Siemens-FZK Contract, FZK, October 10, 1996

[18] J. R. Travis, P. Royl, " Simulation of hydrogen transport and combustion in multi-compartment geometries with the CFD code GASFLOW", Fakultätsseminar Institut für Energietechnik TU-Dresden October 25, 1996

[19] J. Gauvain, P. Royl. "Simulation of Hydrogen Distribution", Joint CEA/FZK Seminar on EPR related R&D, FZK, November 7-8, 1996

[20] P. Royl, "Overview of the GASFLOW code and interesting validation experiments for MISTRA", Mistra Workshop on Advanced Containment Thermohydraulics, Saclay, France, Nov. 12, 1996

[21] W. Breitung, " Current tools for hydrogen combustion simulations", CEA/FZK - Seminar on EPR related severe accident research, Forschungszentrum Karlsruhe, November 7-8, 1996

[22] P. Royl, "Validation of GASFLOW recombiner and igniter models and application to Biblis A", Hydrogen Seminar FZK, December 2-5, 1996

[23] J. R. Travis, " Recent development and experiments with GASFLOW", Hydrogen Seminar FZK, December 2-5, 1996

[24] J. Spore, "GASFLOW II Development and Verification at LANL", Hydrogen Seminar FZK December 2-5, 1996

[25] W. Breitung, "Status of hydrogen mitigation modelling at FZK", Information exchange KfA Jülich/FZK on severe accidents, FZK, December 12, 1996

[26] W. Breitung, "Hydrogen behaviour and control in severe accidents," 8th Meeting of PSF Project Council, January 21, 1997

[27] P. Royl, J. R. Travis, " Further GASFLOW development: Validation of mitigation models",8th Meeting of PSF, Project Council, FZK, January 21, 1997

[28] W. Breitung P. Royl, "Arbeitsvorschlag Konvoi und Biblis A GASFLOW Analysen", Badenwerk/VGB Projektarge Scheibenhardt, January 28, 1996

[29] P. Royl, "Wasserstoffausbreitung und -verbrennung Arbeiten zu Altanlagen", Presentation ILA IRS, February 3, 1996

[30] W. Breitung, " Investigations on hydrogen behaviour and control in core-melt accidents", Presentation to Chinese Nuclear Power Safety Delegation, FZK, February 5, 1997

[31] P. Royl, "GASFLOW Untersuchungen zur Wasserstoffverteilung ohne und mit Gegenmaßnahmen", EVU-Siemens-FZK- Vertrag, AG Wasserstoff-verhalten, FZK, February 20, 1997